Stony Brook University

Thalamocortical Input to the Primary Visual Cortex

A Dissertation Presented

by

Michelle Kloc

to

The Graduate School

in Partial Fulfillment of the

Requirements

for the Degree of

Doctor of Philosophy

in

Neuroscience

Stony Brook University

December 2014

Stony Brook University

The Graduate School

Michelle Kloc

We, the dissertation committee for the above candidate for the

Doctor of Philosophy degree, hereby recommend

acceptance of this dissertation.

Arianna Maffei – Dissertation Advisor
Associate Professor, Department in Neurobiology and Behavior

Gary G. Matthews - Chairperson of Defense
Professor, Department in Neurobiology and Behavior

Alfredo Fontanini – Committee Member
Assistant Professor, Department of Neurobiology and Behavior

Lonnie Wollmuth – Committee Member
Professor, Department of Neurobiology and Behavior

Fereshteh S. Nugent – Committee Member
Assistant Professor, Department of Pharmacology
Uniformed Services University of the Health Sciences

This dissertation is accepted by the Graduate School

Charles Taber
Dean of the Graduate School

Abstract of the Dissertation

Thalamocortical Input to the Primary Visual Cortex

by

Michelle Kloc

Doctor of Philosophy

in

Neuroscience

Stony Brook University

2014

The lateral geniculate nucleus (LGN) is the region of the thalamus that innervates and relays sensory information to the primary visual cortex (V1). Thalamocortical (TC) input from the LGN drives the activity of V1, and underlies the health and function of the visual system. However, little is known about the synaptic properties of this input. LGN inputs innervate two layers, layer 4 (L4) and layer 6 (L6). This input has been examined functionally and anatomically, but the synaptic mechanisms of this input are poorly understood. The anatomy of the projection from the LGN to V1 encumbers the preparation of an acute thalamocortical slice, thus direct electrophysiological investigations of TC synapses onto V1 neurons have not been done. In this study, I use optogenetics to selectively activate TC terminals in an acute slice preparation containing V1 and recorded postsynaptic currents from V1 neurons to investigate TC synaptic properties. I show that TC inputs to V1 have layer-specific synaptic properties, organization, and experience dependence. I have shown that TC inputs to L4, which receives the largest LGN projection, have target cell-type specific properties which are mediated by distinct pre-and postsynaptic mechanisms. Finally, I have shown a novel mechanism of feedback from the V1 circuit onto TC synapses, which is mediated by presynaptic $GABA_A$ receptors on TC terminals. Taken together, these results outline mechanisms for TC activation of the V1 circuit.

Table of Contents

List of Figures

Acknowledgments

I would like to thank my advisor Arianna Maffei, for the exceptional guidance and mentorship, and superhuman patience that have been the rock of my graduate career and defined half of a decade of my life. My graduate career has been an incredible experience, for which I am extremely grateful.

I would like to thank my graduate committee for their support, feedback, suggestions, and guidance of my graduate thesis work: Dr. Gary Matthews, Dr. Alfredo Fontanini, Dr. Lonnie Wollmuth, and Dr. Fereshteh Nugent.

I would like to thank Lang Wang for extensive contributions to this work, discussed in Chapter II (Wang et al., 2013) and Chapter IV (Wang et al., In preparation); as well as the mentorship, guidance, patience, and friendship that have spanned our mutual experience in the lab together.

I would like to thank my fellow past and present lab members, Yury Garkun, Melissa Haley, Trevor Griffen, Melinda Lee, Alan Wei and Roberta Tatti for their support, assistance, advice, and friendship; which has made this thesis possible.

I would also like to thank the laboratories that have contributed to my scientific education and the progress and completion of this thesis: the Ge lab, the Evinger lab, the Levine lab, the Wollmuth lab, and the Kritzer lab.

Finally, I would like to thank my family for their never-ending love, support, and encouragement – without which, I really can't do anything at all.

Financial support: NIH/R01 EY019885; NIH/RO1 DC 013779; The Whitehall Foundation.

Chapter I: Introduction

The primary visual cortex (V1) is the area of the brain responsible for encoding specific properties of visual stimuli; such as direction of motion and orientation. In order to encode these properties, incoming visual stimuli are translated into electrical signals (i.e. action potentials), which are processed by V1 neurons.

Visual stimuli are transformed into transmittable electrochemical signals by the photoreceptors in the retina. These signals are transmitted by retinal ganglion cells to the visual portion of the thalamus, the lateral geniculate nucleus (LGN), and then relayed to V1 (Fig. 1.1 A). The circuit receiving LGN inputs in V1 is organized in 6 layers (Fig 1.1 B) containing excitatory and inhibitory neurons which are highly interconnected within and between layers. While the anatomical distribution of LGN afferents in V1 has been well studied, little is known about the neuronal targets and synaptic properties of the inputs from LGN onto V1.

Before the introduction of optogenetics as an investigatory tool, the complex anatomy of axonal pathway from the LGN to V1 encumbered the preparation of an acute slice for whole cell patch clamp electrophysiology, the ideal preparation to investigate in detail the synaptic properties of an input (MacLean et al., 2006). For decades, our understanding of the synaptic connection between the LGN and V1 has been extrapolated from anatomical reconstructions and recordings from intact anesthetized animals. Anatomical studies lack the capability to measure synaptic currents; and recordings from intact anesthetized animals lack sufficient resolution to determine synaptic properties. As a result, the mechanisms of LGN to V1 synaptic transmission are poorly understood. Recordings from anesthetized animals aimed at investigating ocular dominance column segregation suggest that LGN inputs to V1 directly activate only excitatory neurons, and that recruitment of inhibitory neurons is entirely disynaptic (indirect; Hensch, 2005). However,

in other primary sensory cortices such as somatosensory (S1) and auditory (A1) cortices, normal and healthy circuit function relies on the feedforward activation of both excitatory and inhibitory neurons by thalamic afferents (Cruikshank et al., 2007; Schiff and Reyes, 2012). The results obtained from recordings in vivo would therefore suggest that thalamocortical (TC) activation of V1 would differ significantly from other sensory cortices. However, more recent studies showed that inhibitory neurons can be driven by visual stimuli with a similar delay as excitatory neurons (Hirsch et al., 2003; Swadlow 1989; 2002), and that excitatory and putative inhibitory neurons have cell-type specific tuning properties (Cardin et al., 2007). This suggests that LGN afferents may directly drive both excitatory and inhibitory neurons also in V1.

Here, I will provide experimental evidence to characterize the neuronal targets of LGN inputs and their synaptic properties in V1. In Chapter II, I will show that TC inputs have layer specific synaptic properties, organization, and sensitivity to changes in visual experience. In Chapter III, I will show that TC inputs to the main input layer of cortex, layer 4 (L4), have target-specific synaptic properties. In Chapter IV, I will provide evidence for a novel mechanism for local inhibitory feedback from V1 onto LGN afferents. Lastly, in Chapter V I will outline the future directions of this work.

Investigating the organization, dynamics and specific receptor composition of LGN inputs onto V1 neurons is crucial to understating how the cortical circuit is activated by incoming visual stimuli. This study also has important implications for our understating of TC systems in general. The work I present here shows that TC inputs onto V1 present many similarities, but also significant differences with TC inputs onto other cortical circuits. This suggests that while some of the properties are general to all TC systems, the differences between them may respond to the different demands of the specific sensory modalities.

The Visual Pathway and the Lateral Geniculate Nucleus

Visual perception relies on the transmission and interpretation of visual stimuli. Photoreception occurs in the retina, where visual stimuli are detected and converted into electrical and chemical signals by photoreceptor cells. There are two types of photoreceptor cells, rods and cones. Cones are responsible for color vision in bright light, while rods are sensitive to contrast in dim light. Visual information is transmitted from the photoreceptor cells to bipolar cells, and then to the ascending retinal ganglion cells (RGCs). RGCs relay visual information to the lateral geniculate nucleus (LGN) of the thalamus. The LGN is divided into three areas: the dorsal LGN (dLGN), ventral LGN (vLGN), and intergeniculate leaflet (IGL). The dLGN is the largest division of the LGN, and relays visual information from the retina to the cortex.

The region of the environment perceived by one eye is known as the visual field. In many animals, the visual fields of each eye overlap by varying degrees. The region of overlap in the visual fields of the two eyes is known as the binocular visual field. The remainder of the visual field for each eye is known as the monocular visual field. Visual stimuli are perceived either in the monocular or binocular visual field, which corresponds to a monocular or binocular representation on the retina. RGCs carrying information from the monocular field of the retina cross hemispheres before reaching the LGN, while RGCs from the binocular zone do not cross to the opposite hemisphere. Therefore, the monocular region of the LGN is located contralateral to the eye that projects to it.

The LGN is retinotopically organized: the spatial organization of visual stimuli on the retina is preserved in the thalamus. The output of the LGN to V1 is mediated by LGN relay neurons, also known as thalamocortical projection neurons. LGN relay neurons project to and activate neurons of layers 4 and 6 of V1. Inputs from each of the two eyes are kept separate until they reach V1.

V1 is divided into two zones, the monocular (mV1) and binocular (bV1) zones. Inputs to mV1 and bV1 correspond to the retinal fields, but the boundary between these two areas is not distinct, and is instead organized as a gradient of overlapping LGN inputs.

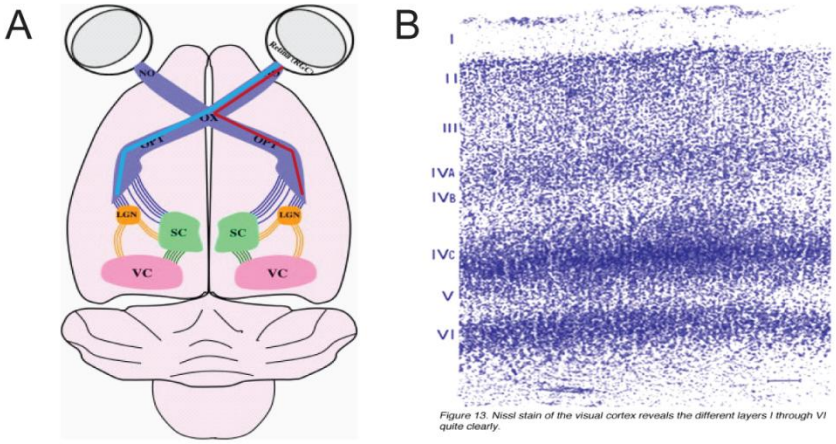

Figure 1.1: Connectivity of the visual system and primary visual cortex. A, The optic nerve projects from the retina to the LGN (and the super chiasmatic nucleus, SC), and from the LGN to the primary visual cortex (V1). The nerves that project to the LGN from the retina originate either from the monocular field and cross hemispheres at the optic chiasm (blue line) or the binocular zone, which stay in the ipsilateral hemisphere (red line). Adapted from Liu et al., 2011. B, Example Nissl stain of the layers of V1 in primary neocortex. Adapted from Schmolesky, 2007.

V1 Circuits

Visual information processing occurs across layers within computational units, known as local microcircuits (Douglas and Martin, 1991; 2004). V1 is composed of six layers of neurons interconnected within and between layers (Fig 1.1 B). The largest portion of LGN terminal fields innervate L4, and to a lesser extent L6. Activation of recurrent circuits by incoming visual stimuli is necessary to amplify the incoming signal and facilitate its propagation to the other layers (Da Costa and Martin, 2011; Li et al, 2013; Lee, 2013). Excitatory pyramidal neurons in L4 form synaptic contacts with pyramidal neurons in L2/3 and the dendrites of L2/3 neurons located in L1. L4 neurons also form a smaller number of synapses with L2/3 inhibitory neurons; and receive a large inhibitory input from L2/3 inhibitory neurons (primarily mediated by L2/3 somatostatin positive neurons). Pyramidal neurons in L2/3 make synaptic contacts with the apical dendrites of layer 5 (L5) pyramidal neurons, which in turn project out of V1. From L5 signals are transmitted to higher cortical areas, higher order thalamic nuclei, and subcortical areas.

Layer 4

Layer 4 is the main recipient of LGN afferents. Neurons in L4 are directly activated by incoming stimuli and mediate feedforward activation of V1. L4, like all of V1, is composed of approximately 80% excitatory neurons (spiny stellate and pyramidal neurons), and 20% GABAergic inhibitory neurons. Of the GABAergic population, 60% are parvalbumin expressing inhibitory neurons with basket-like morphology, 20-30% are somatostatin expressing inhibitory neurons with bipolar morphology, and the remainder are calretinin and calbindin expressing inhibitory neurons (Markram et al., 2004; Rudy et al., 2011). In rodents, L4 has no distinct subdivisions, thus LGN afferents are distributed throughout the thickness of the lamina.

LGN activation of L4 neurons is robust and efficient, but TC synapses only make up 6-10% of all synapses onto excitatory neurons in this layer (Fig 1.2 A; Ahmed et al, 1994; Da Costa and Martin, 2009). Electron micrographs also show that TC terminals are large and contain a large number of vesicles, suggesting that this synapse is powerful (Nahmani and Erisir, 2005). This is consistent with findings from recordings in anesthetized animals suggesting that TC transmission is mediated by a small number of strong synapses (Stratford et al., 1996). Despite this powerful input, intracortical amplification of TC signals is also necessary for normal cortical processing and function (Stratford et al, 1996; Da Costa and Martin, 2011).

TC inputs onto L4 inhibitory neurons in V1 are much less studied. In S1 and A1, TC afferents directly activate L4 fast spiking inhibitory (FS) neurons. This form of feedforward inhibition has been shown to be very important for healthy cortical function (Cruikshank et al., 2007; Schiff and Reyes, 2012). Anatomical studies in cat V1 have shown that inhibitory L4 basket cells receive approximately 15% of their total synapses from TC afferents (Fig 1.2 B; Ahmed et al., 1997, providing evidence that TC input onto inhibitory neurons may also be very powerful. The remainder of asymmetric (excitatory) synapses onto L4 basket cells originate from recurrent connections with L4 excitatory neurons, and inputs from L6 pyramidal neurons (Fig 1.2 B; Freund et al., 1985; Ahmed et al., 1997). The presence of functional TC inputs onto inhibitory neurons in V1 has also been suggested by results obtained from recordings in acutely anesthetized animals (Ferster and Lindstrom, 1983; Gabbott et al., 1988; Cardin et al., 2007). Whether TC inputs onto excitatory and inhibitory neurons in V1 have similar connectivity and synaptic properties is unknown.

Layer 6

Layer 6 receives a significant projection from the LGN, however its role in sensory processing is

poorly understood. Although TC inputs to L4 act as a driver, LGN inputs to L6 neurons are likely modulatory (Sherman 2007; 2012). TC input to L6 may operate as a coincidence detector (Usrey, Alonso, and Reid, 2000), or may provide an indirect amplification of thalamic input to layer 4 (Da Costa and Martin, 2009). In V1, excitatory neurons in L6 innervate L4, accounting for approximately 45% of synapses formed on both excitatory spiny stellate cells and inhibitory basket cells (Fig 1.2 A, B; Ahmed et al. 1994, 1997). Excitatory neurons in L6 also activate L6 FS neurons. Because FS neurons have axons that span across layers, feedforward activation of L6 may indirectly inhibit most of the cortex (Bortone et al., 2014).

Layer 6 not only receives TC inputs from the LGN, but also sends a corticothalamic projection to the LGN. The L6 corticothalamic input to LGN is large, nearly ten-fold greater than the TC input that L6 receives (Thomson, 2010). This differs from layer 5, which sends output to higher order thalamic nuclei as well as other subcortical structures. Visually driven feedback from L6 neurons alters both spatial and temporal characteristics of LGN relay cells (Stillito and Jones, 2002; Sherman and Guillery, 2002). Possible roles for L6 feedback to the LGN include gain control, tuning, feedback, receptive field control (specifically control the focus of thalamic mechanisms, in order to optimize the segmentation, such as synaptic zoning of sensory inputs to the neocortex) and integration of inputs in secondary signal processing (Stillito and Jones, 2002).

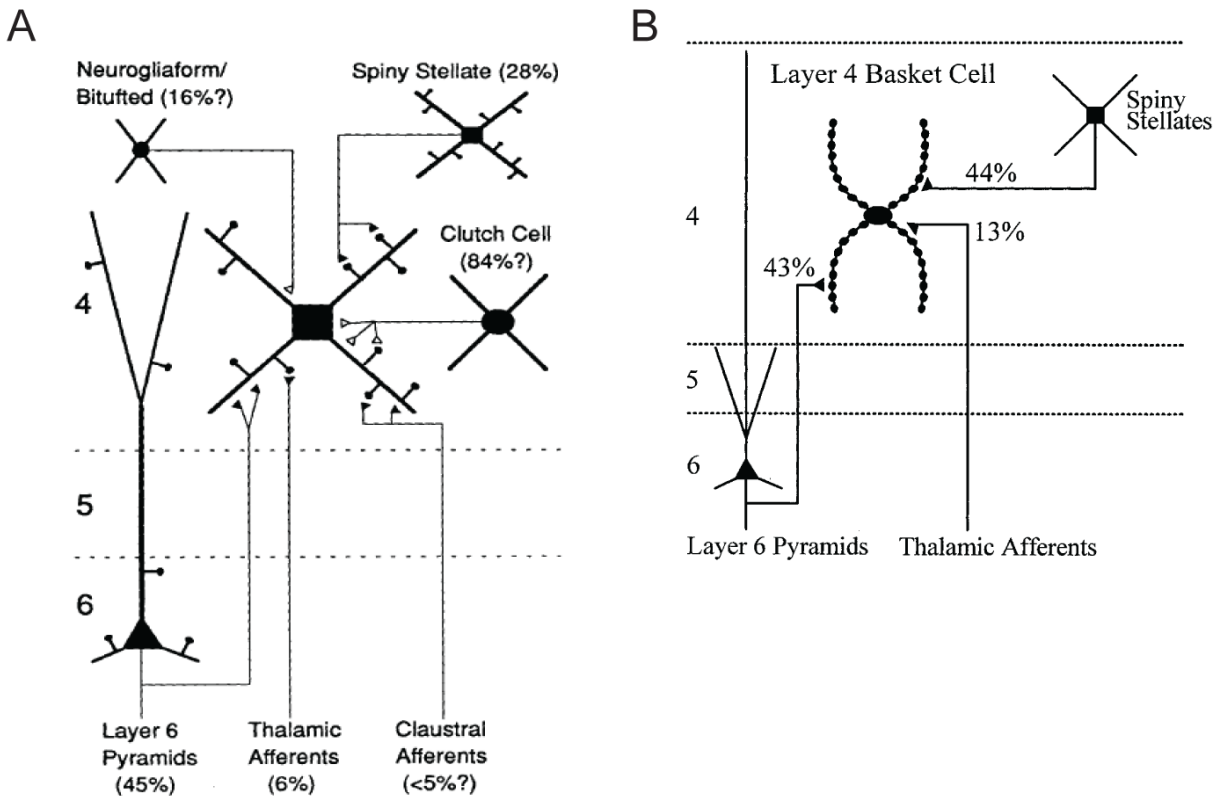

Figure 1.2: Anatomical synaptic inputs onto L4 neurons in V1. A, B, thalamocortical and intracortical innervation of L4 excitatory spiny stellate (A) and inhibitory basket neurons (B). Only 6-10% of synapses formed onto excitatory and inhibitory neurons in L4 are formed by TC relay neurons, and the majority of the remainder are formed by inputs from neurons in L4 and L6. Adapted from Ahmed et al., 1994 (A) and 1997 (B).

Receptive fields

Receptive fields (RFs) are an important feature of visual neurons. A RF, by definition, is the region of the visual field where a stimulus elicits an action potential from a given neuron (Fig 1.3 A). The RF of visual neurons show antagonistic center-surround motifs that can be either ON- or OFF-center; indicating that visual stimuli within the receptive field of a given neuron can either excite or inhibit that neuron if it falls within the center, and will have the opposite effect within the surround. In the RGCs and LGN neurons, center-surround RFs are circular in shape.

The receptive fields of L4 neurons differ from those of the RGCs and LGN relay cells. Instead of responding to just a flash of light (Fig 1.3 A), L4 neurons also respond to more complex stimuli. In the classic experiments by Hubel and Weisel, a moving bar of light was used to identify the RF properties of neurons in V1 (Fig 1.3 B). They identified two groups of cells based on their RFs: simple cells and complex cells (Hubel and Wiesel, 1959; 1962). In V1, neuronal RFs are ovoid in shape. The ON- and OFF- antagonistic center surround properties correspond to the RF properties of the incoming LGN relay cells.

RF properties are important for determining the tuning (the transformation of synaptic input to firing rate) of L4 neurons. When a neuron is tuned to a specific stimulus feature, it responds the strongest to a specific characteristic range of that feature (Fig 1.3 B). The stimulus feature can refer to location, direction, orientation, etc. of a visual stimulus. Complex neurons have larger receptive fields, and while they have a preferred range of orientations, do not exhibit the specific orientation preference observed in simple cells, and do not have clearly defined ON and OFF regions. LGN inputs primarily converge onto simple cells; and neurons in L4 are mostly simple cells (80-90%; Hubel and Wiesel, 1959; 1962).

Although excitatory neurons are tuned to be optimally activated by specific feature

characteristics, the range of feature characteristics that they will respond to is narrow. Interestingly, this is not the case for every neuron type (Contreras and Palmer, 2003). In vivo experiments have provided evidence that neuronal tuning properties differ between excitatory and inhibitory neurons (Cardin et al., 2007). When recording from awake animals, it was determined that excitatory neurons in L4 are narrowly tuned for a given stimulus, and only fire action potentials for a limited range of stimulus characteristics (Alonso and Swadlow, 2005; Cardin et al., 2007). Conversely, inhibitory neurons are more broadly tuned to incoming stimuli (Cardin et al., 2007), indicating that visual stimuli are more likely to activate the inhibitory network than the excitatory network. It is unclear whether these differences arise from properties of the neurons themselves, or whether TC inputs also contribute to this. The broad tuning of FS neurons is experience dependent. FS neuron tuning is narrow at eye opening, like that of excitatory neurons, but broadens after a period of visual experience (Kuhlman et al., 2011). This suggests that TC inputs may contribute to shaping the tuning properties of FS neurons. In this dissertation, we suggest that differences in RF properties may depend not only to intrinsic properties, but also to target cell-type specific differences in TC synapses. TC input is critical to the normal function of the cortex, and may affect how sensory information is encoded.

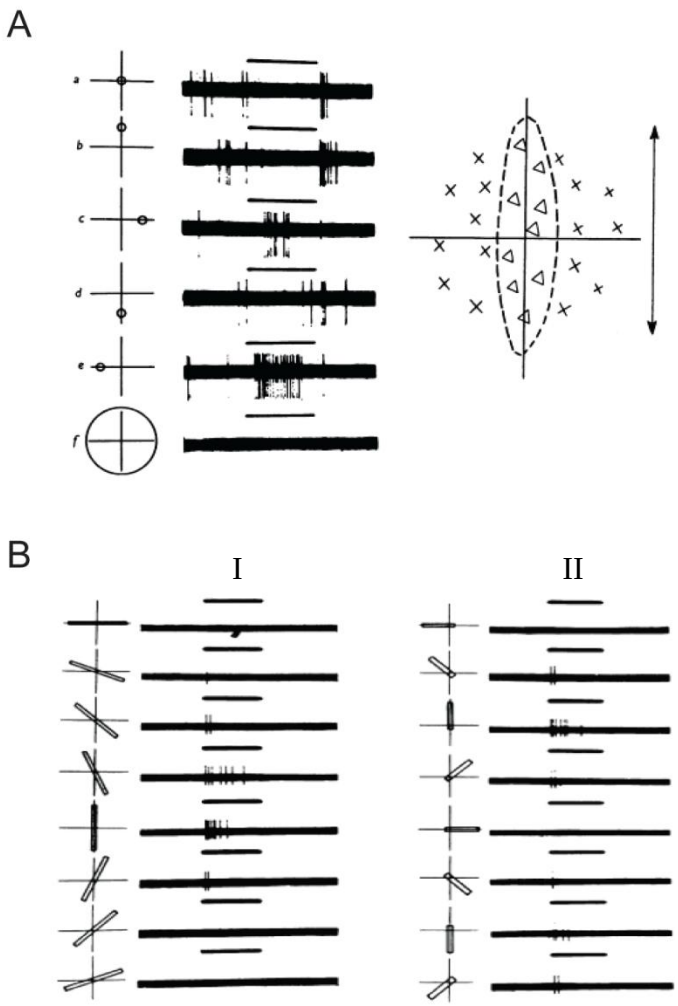

Figure 1.3: Receptive field properties of V1 neurons. A, Left, location of a point of bright light in the visual field. Center, the activity recorded from a unit in V1, which is elicited by the light stimulus on the left. Right, spatial representation of the area of the visual field that the recorded neuron responds to. The neuron recorded responds the strongest to stimuli in the center of the visual field, not in the periphery. B, Orientation selectivity of a unit recorded from V1. I and II, Left, a bar stimulus was presented in the center of the visual field in various orientations. I and II, Right, the response of the V1 neuron when the stimulus was presented. The horizontal line over each trace indicates when the stimulus was applied. The neuron responds the strongest when the visual stimulus (bar) was vertical. Adapted from Hubel and Wiesel, 1959.

Thalamocortical Input, Development, and Plasticity

Thalamocortical synapses are glutamatergic. On the postsynaptic membrane, glutamate binds to α-amino-3-hydroxy-5-methyl-4-isoxazolepropionic acid (AMPA) and N-methyl-D-aspartic acid (NMDA) receptors. AMPA and NMDA receptors have a variety of different subunits, which endow the receptors with specific properties. Generally, when AMPA receptors open, they pass a large fast current that is mediated by sodium and potassium ions. However, when AMPA receptors lack the GluA2 subunit, they can also pass calcium ions (Bowie, 2012). NMDA receptors pass a slow, prolonged current that is mediated by sodium, potassium and calcium. Different subunit compositions alter the probability that NMDA receptors will open. At membrane potentials that are lower than -40 mV, NMDA receptors are typically blocked by magnesium. However some subunits, such as GluN2C and GluN2D, have lower affinity for magnesium at hyperpolarized membrane potentials. Thus, as glutamate binds to and activates NMDA receptors that contain these subunits, it is more likely that these receptors will open even if the membrane potential of the neuron is lower than -40 mV (Paoletti et al., 2013).

Thalamocortical axons that project to primary sensory cortices form synapses early in development. During the second week of embryonic development, the thalamus and the cortex develop synchronously. In the visual system, this occurs between embryonic day (E) 12 and E14. Subsequently, between E13 and E18, they link to one another by forming reciprocal connections (Lopez-Bendito and Molnar, 2003). This connectivity is mediated via attractive and repulsive molecular cues and sculpted by spontaneous neuronal activity. Spontaneous activity is critical for axon guidance and organization. When spontaneous cortical activity is blocked, for example by chronic infusion of tetrodotoxin (TTX) into the cortex, the guidance of TC axons and formation of contacts with V1 neurons does not occur (Catalano, 1998).

By birth, TC axons have reached the cortex. Lamination of V1 and the subsequent TC innervation occur during an early postnatal developmental period. Starting at birth, postnatal day (P) 0, TC axons move into their classic innervation pattern of L4 and L6. This is complete by the end of the first postnatal week (Lopez-Bendito and Molnar, 2003). The next step following TC fiber innervation is the maturation of functional glutamatergic TC synapses with L4 neurons. During the second week of postnatal development, the number of AMPA receptors increases (Crair and Malenka, 1995), and the number of silent synapses (NMDA receptors only) decreases (Agmon and O'Dowd, 1992; Isaac et al., 1997). This means that more synapses become active and responsive to the activity driven by spontaneous retinal waves. During the first two weeks in development there is also a transition in subunit composition of NMDA receptors. NMDA receptors switch from predominantly consisting of GluN2B subunits, to a combination of GluN2A, GluN2B, and GluN2C (Sheng et al., 1994). TC inputs and cortical signaling are maturing together during this stage, and are essential to healthy cortical function.

Experience dependent plasticity

Thalamocortical development and patterning is mediated by molecular cues and spontaneous activity during embryonic and early postnatal development. Although innervation is complete, the circuit is not mature. During late postnatal development, circuit maturation is mediated by sensory experience. In V1, this occurs after eye opening. In rodents, eye opening occurs at postnatal day (P) 14. Cortical circuits are refined into their mature configuration in an experience dependent manner (Hensch, 2004) during specific windows of heightened sensitivity to changes in visual drive, the best studied of which is known as the critical period for visual cortical plasticity (Hensch, 2004).

The maturation of GABAergic inhibition is necessary to open, maintain, and close the critical

period for visual cortical plasticity (Fig 1.4 A; Hensch, 2005). Visual experience is necessary for the maturation of GABAergic inhibition in primary visual cortex (Chen et al., 2001; Morales et al., 2002). When GABAergic signaling occurs too early in development, by drug application or overexpression of BDNF, critical period plasticity occurs sooner (Fig 1.4 A; Huang et al., 1999; Hanover et al., 1999; Iwai et al., 2003). When GABAergic signaling is delayed, either by dark rearing or by transgenic deletion, critical period plasticity is delayed (Fig 1.4 A; Hensch et al., 1998; Mower, 1991). If sensory input is perturbed during the critical period, for example by monocular deprivation, there are profound and permanent effects on cortical circuit function (Fagiolini et al, 1994; Katz and Shatz, 1996).

Monocular deprivation (MD) leads to unbalanced activity from the two eyes. The effects of MD are loss of visual responsiveness to the deprived eye (Hubel and Wiesel, 1963; Fagiolini et al., 1994), reduced visual acuity (Prusky et al., 2000), and loss of tuning to stimulus properties (Crair et al., 1997; White et al., 2001); followed by a rapid shift of neural responses in favor of the open eye. These changes occur intracortically, very shortly after visual deprivation occurs. Short MD (3 days) during the critical period induces potentiation of inhibitory synapses from FS to pyramidal neurons (Maffei et al, 2006), and reduced neuronal responsiveness to visual stimuli (Frenkel and Bear, 2004). In addition, when MD is maintained for several days, TC axons withdraw from their targets (Fig 1.4 B; Antonini et al, 1999). These axons are still functional, and the experience-dependent shortening of TC axons does not affect the density of synapses on the remaining axon (Silver and Stryker, 1999). Unbalanced activity from the two eyes is necessary to induce this effect, as binocular deprivation and dark rearing do not result in these changes (Fagiolini et al., 1994; Hensch 2005). This process is also dependent on inhibition, and applying $GABA_A$ antagonists blocks the effects of monocular deprivation. Additionally,

inhibition shapes LGN axon branching of incoming afferents that are taking over the deprived area of cortex (Cabelli et al., 1995).

Whether TC axons are also plastic during this period is also controversial. Because of the delayed anatomical response and lack of adequate techniques, historically it was considered unlikely that TC synapses play an active role in the initial stages of cortical circuit refinement. However, more recent evidence from electron microscopy studies has shown that TC synapses are also plastic during postnatal development (Erisir and Dreusicke, 2005; Khibnik et al, 2010; Coleman et al, 2010). In fact, TC synapses may have an active role in circuit development by driving experience dependent plasticity during the critical period (Khibnik et al, 2010), via different patterns of firing (Linden et al, 2009). Furthermore, despite long standing theories that plasticity cannot be induced at TC synapses following the first postnatal week, long term potentiation (LTP) of glutamatergic synapses can be induced at TC synapses onto L4 neurons under circumstances of environmental enrichment in adult rats (Mainardi et al, 2010). Studies in A1 have shown that this is because the expression of LTP and LTD at TC synapses becomes gated with age by presynaptic adenosine receptors (Blundon et al., 2011; Chun et al., 2013).

These studies present a complex portrait of LGN inputs onto V1, which is slowly being pieced together through a variety of techniques. TC inputs from the LGN are not just a relay, but a vital part of the development and maintenance of healthy cortical circuits in V1. In order to understand the mechanisms underlying cortical plasticity and visual information processing, we must first understand the mechanisms underlying TC input to V1. In this thesis, I will show that TC inputs to V1 do in fact have layer specific properties of activation; and that TC inputs onto L4 neurons have cell-type specific mechanisms of activation. I will discuss a novel mechanism of corticothalamic feedback, via presynaptic $GABA_A$ receptors present on TC terminals. Finally,

I will show that TC synapses can express plasticity during later postnatal development, and outline the future directions of this work. Taken together, I will provide new evidence for the activation of V1 circuits via TC inputs.

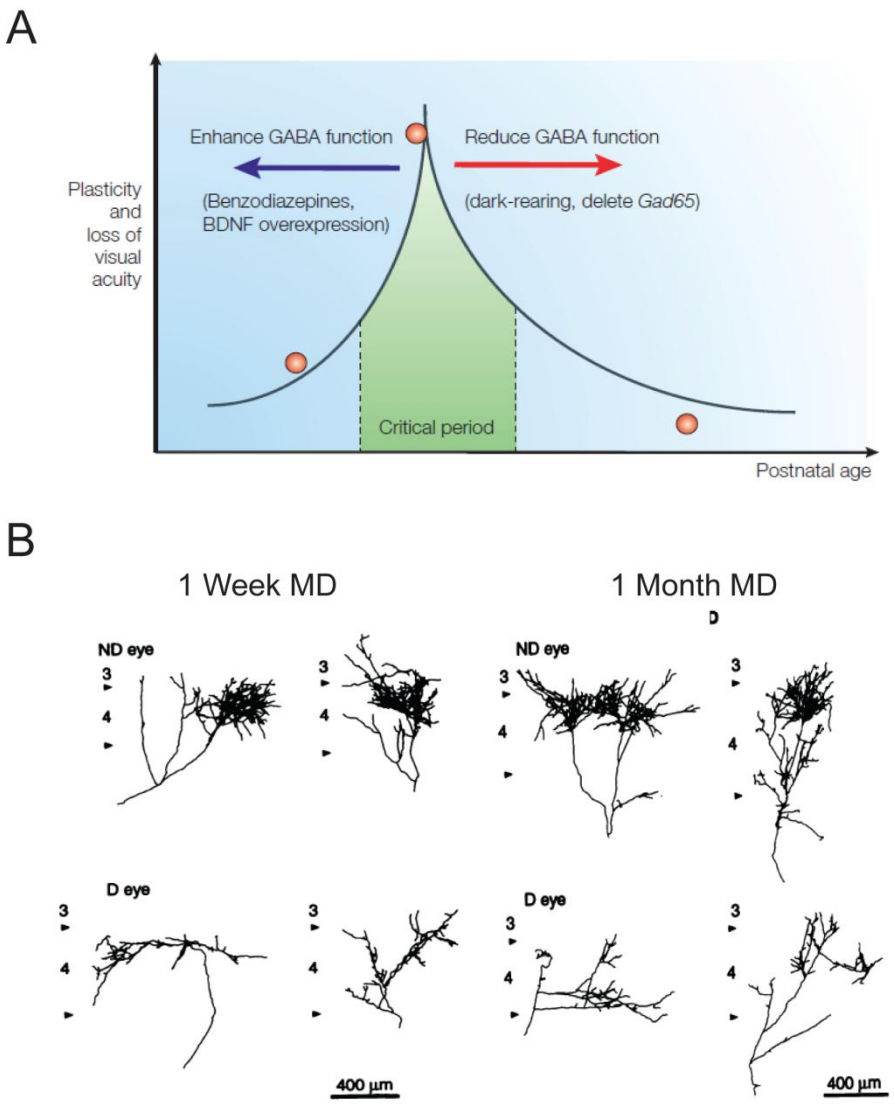

Figure 1.4: Maturation of inhibition and balanced visual drive are important for normal V1 development during the critical period. A, After eye opening, the visual cortex is highly plastic and connectivity is affected by changes in visual stimuli. The critical period for visual cortical plasticity is regulated by the maturation of GABA signaling. When GABAergic inhibition occurs earlier in development, the critical period begins earlier (blue arrow). If GABAergic inhibition is delayed, the critical period occurs later in development (red arrow). Adapted from Hensch et al., 2005. B, When visual drive is perturbed during the critical period by monocular deprivation, TC axons innervating L4 neurons withdraw from their targets in the hemisphere that receives input from the deprived eye (D). This does not occur in the nondeprived hemisphere (ND). Adapted from Antonini and Stryker, 1993.

References

Agmon A ODD (1992) NMDA receptor-mediated currents are prominent in the thalamocortical synaptic response before maturation of inhibition. The Journal of Neurophysiology 68:345-349.

Ahmed B, Anderson JC, Martin KAC (1997) Map of the Synapses Onto Layer 4 Basket Cells of the Primary Visual Cortex of the Cat. The Journal of Comparative Neurology 380:230–242.

Ahmed B, Anderson JC, Douglas RJ, Martin KAC, Nelson JC (1994) Polyneuronal Innervation of Spiny Stellate Neurons in Cat Visual Cortex. The Journal of Comparative Neurology 341:39-49.

Alonso J-M, Swadlow HA (2005) Thalamocortical Specificity and the Synthesis of Sensory Cortical Receptive Fields. The Journal of Neurophysiology 94:26-32.

Antonella Antonini MF, Michael P Stryker (1999) Anatomical Correlates of Functional Plasticity in Mouse Visual Cortex. The Journal of Neuroscience 19:4388-4406.

Antonella Antonini MPS (1993) Rapid Remodeling of Axonal Arbors in the Visual Cortex. Science 260:1819-1821.

Arianna Maffei KN, Sacha B. Nelson & Gina G. Turrigiano (2006) Potentiation of cortical inhibition by visual deprivation. Nature Letters 443:81-84.

Bortone D, Olsen SR, Scanziani M (2014) Translaminar inhibitory cells recruited by layer 6 corticothalamic neurons suppress visual cortex. Neuron 82:474-485.

Bowie D (2012) Redefining the classification of AMPA-selective ionotropic glutamate receptors. The Journal of Physiology 590:49-61.

Cabelli RJ HA, Shatz CJ (1995) Inhibition of ocular dominance column formation by infusion of NT-4/5 or BDNF. Science 267:1662-1666.

Cardin JA, Palmer LA, Contreras D (2007) Stimulus Feature Selectivity in Excitatory and Inhibitory Neurons in Primary Visual Cortex. The Journal of Neuroscience 27:10333–10344.

Catalano S (1998) Activity-dependent cortical target selection by thalamic axons. Science 281:559-562.

Chen L YC, Mower GD (2001) Developmental changes in the expression of GABA(A) receptor subunits (alpha(1), alpha(2), alpha(3)) in the cat visual cortex and the effects of dark rearing. Brain Research Molecular Brain Research 88:135-143.

Chun S IB, JA Blundon, SS Zakharenko (2013) Thalamocortical long-term potentiation becomes gated after the early critical period in the auditory cortex. The Journal of Neuroscience 33:7345-7357.

Contreras D, Palmer L (2003) Response to Contrast of Electrophysiologically Defined Cell Classes in Primary Visual Cortex. The Journal of Neuroscience 23:6936-6945.

Crair MC MR (1995) A critical period for long term potentiation at thalamocortical synapses. Nature 375:325-328.

Crair MC RE, Gillespie DC, Stryker MP (1997) Relationship between the ocular dominance and orientation maps in visual cortex of monocularly deprived cats. Neuron 19:307-318.

Cruikshank SJ, Lewis TJ, WConnors B (2007) Synaptic basis for intense thalamocortical activation of feedforward inhibitory cells in neocortex. Nature Neuroscience 10:462-468.

DaCosta NM MK (2009) The Proportion of Synapses Formed by the Axons of the Lateral Geniculate Nucleus in Layer 4 of Area 17 of the Cat. The Journal of Comparative Neurology 516:264-276.

DaCosta NM MK (2011) How Thalamus Connects to Spiny Stellate Cells in the Cat's Visual Cortex. The Journal of Neuroscience 31:2925-2937.

Douglas RJ, Martin, KAC (1991) A functional microcircuit for cat visual cortex. The Journal of Physiology 440:735-769.

Douglas RJ, Martin, KAC (2004) Neuronal circuits of the neocortex. Annual Review of Neuroscience 27:419-451.

Erisir A, Dreusicke M (2005) Quantitative Morphology and Postsynaptic Targets of Thalamocortical Axons in Critical Period and Adult Ferret Visual Cortex. The Journal of Comparative Neurology 485:11-31.

Fagiolini M PT, Berardi N, Domenici L, Maffei L (1994) Functional postnatal development of the rat primary visual cortex and the role of visual experience: dark rearing and monocular deprivation. Vision Research 34:709-720.

Ferster D LS (1983) An intracellular analysis of geniculo-cortical connectivity in area 17 of the cat. The Journal of Physiology 342:181-215.

Frenkel M BM (2004) How Monocular Deprivation Shifts Ocular Dominance in Visual Cortex of Young Mice. Neuron 44:917-923.

Freund TF, Martin KAC, Somogyi P, Whitteridge D (1985) Innervation of Cat Visual Areas 17 and 18 by Physiologically Identified X- and Y- Type Thalamic Afferents. II. Identification of Postsynaptic Targets by GABA Immunocytochemistry and Golgi Impregnation. The Journal of Comparative Neurology 242:275-291.

Gabbott PL MK, Whitteridge D (1988) Evidence for the connections between a clutch cell and a corticotectal neuron in area 17 of the cat visual cortex. Philosophical Transactions of The Royal Society B 233:385-391.

Guillery RW SS (2002) Thalamic relay functions and their role in corticocortical communication: generalizations from the visual system. Neuron 33:163-175.

Hanover JL HZ, Tonegawa S, Stryker MP. (1999) Brain-derived neurotrophic factor overexpression induces precocious critical period in mouse visual cortex. The Journal of Neuroscience 19:RC40.

Hensch TK (2004) Critical period regulation. Annual Review of Neuroscience 27:549-579.

Hensch TK (2005) Critical period plasticity in local cortical circuits. Nature Reviews Neuroscience 6:877-888.

Hensch TK FM, Mataga N, Stryker MP, Baekkeskov S, Kash SF (1998) Local GABA circuit control of experience-dependent plasticity in developing visual cortex. Science 282:1504-1508.

Hirsch JA LMM, Cinthi Pillai, Jose-Manuel Alonso, Qingbo Wang, Friedrich T Sommer (2003) Functionally distinct inhibitory neurons at the first stage of visual cortical processing. Nature Neuroscience 6:1300-1308.

Huang ZJ KA, Pizzorusso T, Porciatti V, Morales B, Bear MF, Maffei L, Tonegawa S (1999) BDNF regulates the maturation of inhibition and the critical period of plasticity in mouse visual cortex. Cell 98:739-755.

Hubel DH WT (1959) Receptive fields of single neurones in the cat's striate cortex. The Journal of Physiology 148:574-591.

Hubel DH WT (1962) Receptive fields, binocular interaction, and functional architecture in the cat's visual cortex. The Journal of Physiology 160:106-154.
Hubel DH WT (1963) Single cell responses in striate cortex of kittens deprived of vision in one eye. The Journal of Neurophysiology 26:1003-1017.
Isaac JT CM, Nicoll RA, Malenka RC (1997) Silent synapses during development of thalamocortical inputs. Neuron 18:269-280.
Iwai Y FM, Obata K, Hensch TK (2003) Rapid Critical Period Induction by Tonic Inhibition in Visual Cortex. The Journal of Neuroscience 23:6695-6702.
J Blundon IB, S Zakharenko (2011) Presynaptic gating of postsynaptically expressed plasticity at mature thalamocortical synapses. The Journal of Neuroscience 31:16012-16025.
Jason E. Coleman MN, Jeffrey P. Gavornik, Robert Haslinger, Arnold J. Heynen, Alev Erisir and Mark F. Bear (2010) Rapid Structural Remodeling of Thalamocortical Synapses Parallels Experience-Dependent Functional Plasticity in Mouse Primary Visual Cortex. The Journal of Neuroscience 30:9670-9682.
Katz LC SC (1996) Synaptic activity and the construction of cortical circuits. Science 274:1133-1138.
Kuhlman SJ TE, Trachtenberg JT (2011) Fast-spiking interneurons have an initial orientation bias that is lost with vision. Nature Neuroscience 14:1121-1123.
Lee CC, Imaizumi K (2013) Functional Convergence of Thalamic and Intrinsic Projections to Cortical Layers 4 and 6. Neurophysiology 45:396-406.
Lena A. Khibnik KKACaMFB (2010) Relative Contribution of Feedforward Excitatory Connections to Expression of Ocular Dominance Plasticity in Layer 4 of Visual Cortex. Neuron 66:493-500.
Li L-y, Li Y-t, Zhou M, Tao HW, Zhang LI (2013) Intracortical multiplication of thalamocortical signals in mouse auditory cortex. Nature Neuroscience Brief Communications 16:1179-1183.
Lopez-Bendito G MZ (2003) Thalamocortical development: how are we going to get there? Nature Reviews Neuroscience 4:276-289.
MacLean JN, Fenstermaker V, Watson BO, Yuste R (2006) A visual thalamocortical slice. Nature Methods 3:129-134.
Mainardi M SL, Laura Gianfranceschi, Sara Baldini, Roberto De Pasquale, Nicoletta Berardi, Lamberto Maffei and Matteo Caleo (2010) Environmental Enrichment Potentiates Thalamocortical Transmission and Plasticity in the Adult Rat Visual Cortex. Journal of Neuroscience Research 88:3048-3059.
Markram H, Teledo-Rodrigues, Maria, Wang, Yun, Gupta, Anirudh, Silberberg, Gilad and Wu, Caizhi (2004) Interneurons of the neocortical inhibitory system. Nature Reviews Neuroscience 5:793-807.
Monica L Linden AJH, Robert H Haslinger & Mark F Bear (2009) Thalamic activity that drives visual cortical plasticity. Nature Neuroscience Brief Communications 12:390-392.
Morales B CS, Kirkwood A (2002) Dark rearing alters the development of GABAergic transmission in visual cortex. The Journal of Neuroscience 22:8084-8090.
Mower G (1991) The effect of dark rearing on the time course of the critical period in cat visual cortex. Brain Research Developmental Brain Research 58:151-158.
Nahmani M EA (2005) VGluT2 Immunochemistry Identifies Thalamocortical Terminals in Layer 4 of Adult and Developing Visual Cortex. The Journal of Comparative Neurology 484:458-473.

Paoletti P BC, Zhou Q (2013) NMDA receptor subunit diversity: impact on receptor properties, synaptic plasticity and disease. Nature Reviews Neuroscience 14:383-400.
Prusky GT WP, Douglas RM (2000) Experience-dependent plasticity of
visual acuity in rats. European Journal of Neuroscience 116:135-140.
Rudy B FG, Lee S, Hjerling-Leffler J (2011) Three groups of interneurons account for nearly 100% or neocortical GABAergic neurons. Developmental Neurobiology 71:45-61.
Schiff ML, Reyes AD (2012) Characterization of thalamocortical responses of regular-spiking and fast-spiking neurons of the mouse auditory cortex in vitro and in silico. The Journal of Neurophysiology 107:1476-1488.
Sheng M CJ, Roldan LA, Jan YN, Jan LY (1994) Changing subunit composition of hetermeric NMDA receptors during development of rat cortex. Nature 368:144-147.
Sherman SM (2007) The thalamus is more than just a relay. Current Opinion in Neurobiology 17:417-422.
Sherman SM (2012) Thalamocortical interactions. Current Opinion in Neurobiology 22:1-5.
Sherman SM GR (2002) The role of the thalamus in the flow of information to the cortex. Proceedings of the National Academy of Sciences 357:1695-1708.
Sillito AM JH (2002) Corticothalamic interactions in the transfer of visual information. Philosophical Transactions of The Royal Society B 357:1739-1752.
Silver MA SM (1999) Synaptic density in geniculocortical afferents remains constant after monocular deprivation in the cat. The Journal of Neuroscience 19:10829-10842.
Stratford KJ, Tarczy-Hornoch K, Martin KAC, Bannister NJ, Jack JJB (1996) Excitatory synaptic inputs to spiny stellate cells in cat visual cortex. Nature Letters 382:258-261.
Stryker MP HW (1986) Binocular impulse blockade prevents the formation of ocular dominance columns in cat visual cortex. The Journal of Neuroscience 6:2117-2133.
Swadlow HA (1989) Efferent neurons and suspected interneurons in S-1 vibrissa cortex of the awake rabbit: receptive fields and axonal properties. The Journal of Neurophysiology 62:288-308.
Swadlow HA (2002) Thalamocortical control of feed-forward inhibition in awake somatosensory 'barrel' cortex. Philosophical Transactions of The Royal Society B 357:1717–1727.
Thomson AM (2010) Neocortical layer 6, a review. Frontiers in Neuroanatomy 4:1-14.
Usrey WM AJ, Reid RC (2000) Synaptic interactions between thalamic inputs to simple cells in cat visual cortex. The Journal of Neuroscience 20:5461-5467.
Vitali I JD (2014) Synaptic biology of barrel cortex circuit assembly. Seminars in cell & developmental biology 35:156-164.
White LE CD, Fitzpatrick D (2001) The contribution of sensory experience to the maturation of orientation selectivity in ferret visual cortex. Nature 411:1049-1052.

Chapter II: Layer-specific experience-dependent rewiring of thalamocortical circuits

Abstract

Thalamocortical circuits are central to sensory and cognitive processing. Recent work suggests that the thalamocortical inputs onto L4 and L6, the main input layers of neocortex, are activated differently by visual stimulation. Whether these differences depend on layer specific organization of thalamocortical circuits; or on specific properties of synapses onto receiving neurons is unknown. Here we combined optogenetic stimulation of afferents from the visual thalamus and paired recording electrophysiology in L4 and L6 of rat primary visual cortex to determine the organization and plasticity of thalamocortical synapses. We show that thalamocortical inputs onto L4 and L6 differ in synaptic dynamics and sensitivity to visual drive. We also demonstrate that the two layers differ in the organization of thalamocortical and recurrent intracortical connectivity. In L4, a significantly larger proportion of excitatory neurons responded to light activation of thalamocortical terminal fields than in L6. The local microcircuit in L4 showed a higher degree of recurrent connectivity between excitatory neurons than the microcircuit in L6. In addition, L4 recurrently connected neurons were driven by thalamocortical inputs of similar magnitude indicating the presence of local subnetworks that may be activated by the same axonal projection. Finally, brief manipulation of visual drive reduced the amplitude of light-evoked thalamocortical synaptic currents selectively onto L4. These data are the first direct indication that thalamocortical circuits onto L4 and L6 support different aspects of cortical function through layer specific synaptic organization and plasticity**.**

Authors: Lang Wang, Michelle Kloc, Yan Gu, Shaoyu Ge, Arianna Maffei

Author Contributions: L.W. and A.M. designed research; L.W. and M.K. performed research; Y.G. and S.G. contributed unpublished reagents/analytic tools; L.W., M.K., and A.M. analyzed data; L.W., M.K., and A.M. wrote the paper.

Citation: Wang L, Kloc M, Gu Y, Ge S, Maffei A (2013) Layer-Specific Experience-Dependent Rewiring of Thalamocortical Circuits. The Journal of Neuroscience 33:4181– 4191.

Introduction

Thalamocortical (TC) circuits are central to the coding of sensory information (Sherman and Guillery, 2002; Castro-Alamancos, 2004) and crucial for the synchronization of cortical activity (Llinas et al., 1999; Banitt et al., 2007; Wang et al., 2010; Bruno, 2011). Axons from the lateral geniculate nucleus of the thalamus (LGN) project largely to L4 of primary visual cortex (V1) and send a significant portion of their collateral afferents to L6 (LeVay and Gilbert, 1976; Peters and Feldman, 1977). While the inputs onto the two layers are thought to contribute to transfer of sensory information (Amitai, 2001; Lee and Sherman, 2008), experimental evidence suggests that neurons in L4 and L6 may play different functions in the processing of sensory stimuli (Gilbert, 1977; Sengpiel et al., 1998; Alonso et al., 2001). Whether the functional differences depend on layer-specific synaptic organization of the TC – intracortical (IC) circuits or on distinct responsiveness to changes in sensory input is unknown. Studies investigating the effect of long-lasting sensory deprivation suggest that reduction of driving input leads to alterations of TC projections (Tieman, 1985; Catalano and Shatz, 1998; Antonini et al., 1999) and changes in TC plasticity (Khibnik et al., 2010); however, the effects of brief sensory deprivation on these synapses have been less consistent (Coleman et al., 2010). To date, there is no direct evidence that brief changes in sensory experience affect TC inputs and that the effect is similar in L4 and L6. In V1, a major model for studying the effect of sensory drive on the synaptic organization of cortical circuits, the complex anatomy of the axons from LGN neurons has hampered the direct investigation of TC synapses. Here we devised an experimental approach that combines optogenetic stimulation of TC axons (Petreanu et al., 2007; Cruikshank et al., 2010) from the

LGN with paired recordings in V1 to investigate directly the organization, synaptic properties, and plasticity of TC synapses onto L4 and L6 excitatory neurons in acute slices. Our data demonstrate that LGN afferents in L4 and L6 excitatory neurons have layer-specific properties. More specifically, we show that there are significant differences in the proportion of neurons responding to light activation of TC terminal fields in the two layers and that the amplitude and short-term dynamics of TC synaptic responses show layer specificity. In addition, L4 and L6 have distinct organization of TC and recurrent connectivity and show different sensitivity to changes in visual drive. While brief manipulation of visual drive induced a selective decrease of TC inputs onto L4 pyramidal neurons, recurrent L4 synapses as well as TC synapses onto L6 neurons remained unaffected. These results are consistent with the idea that the two main input layers of V1 may relay different aspects of cortical function via layer-specific properties and circuit organization of TC inputs. As TC inputs onto L4 alone are exquisitely sensitive even to brief changes in visual input, the organization of the circuit in layer 4 may bias its function toward sensory processing and experience-dependent circuit refinement, while the circuit in L6 may be organized to bias its function toward gain control (Olsen et al., 2012) and corticothalamic feedback (Andolina et al., 2007; Briggs, 2010; Briggs and Usrey, 2011; Krahe and Guido, 2011).

Results

The presence of Meyer's Loops, large turns in the bundle of axons projecting from the LGN onto V1, has encumbered an acute slice preparation containing both LGN and V1 circuits. We bypassed this constraint by injecting a construct containing ChR2-GFP, expressing the light-activated conductance, ChR2 (Zhang et al., 2010), into the LGN of P14 rats. Injection of 300 nl of saline solution containing $50*10^{12}$ viral particles/nl allowed reliable injections producing consistent expression of the light-gated conductance in LGN terminal fields in V1 across

preparations (Figs. 2.1 A,C,D, 2.2 A,B). To verify the site of injection and test that the level of expression of the light-sensitive ChR2 was sufficient to activate LGN neurons above threshold, acute coronal slices containing the LGN were prepared. Patch-clamp recordings were obtained from visually identified LGN neurons and brief (1 ms/ 0.1– 0.3 mW/mm^2) pulses of blue light were delivered through a 40X water-immersion objective using a blue LED optic fiber mounted in the fluorescence light path of an upright microscope. Light intensity was adjusted to elicit action potentials in LGN neurons (Fig. 2.1 B) and different frequencies of stimulation were used to ensure that LGN neuron firing was time locked with the light pulses (data not shown). For each animal included in this study, in the beginning of the experiment a few LGN neurons were recorded to ensure reliable expression of our construct and function of ChR2.

To quantify the reproducibility of levels of expression of the construct in terminal fields in V1, we measured the fluorescence profile of the coronal slices containing V1 and included in the analysis only recordings from slices with comparable levels of expression (Fig. 2.1 D). The reliability of this experimental approach allowed us to prepare acute coronal slices containing V1 and to use blue LED light to directly stimulate LGN terminal fields while recording from visually identified pyramidal neurons in layer 4 and in layer 6.

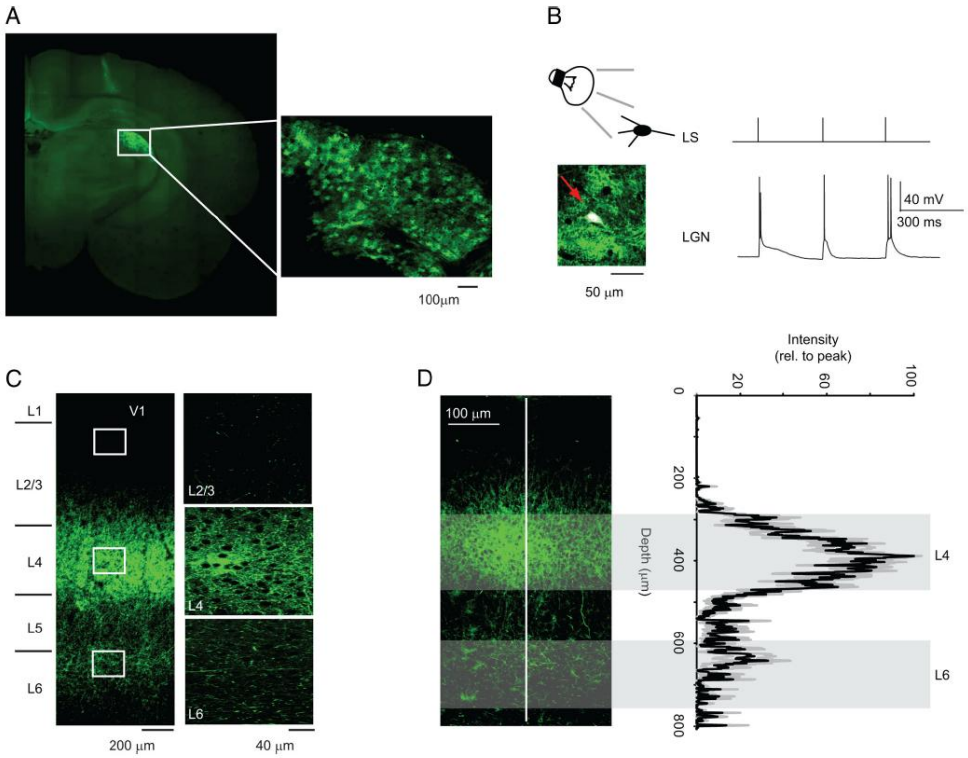

Figure 2.1. Optogenetic approach to the study of TC synapses from the LGN onto V1. A. Example of injection of ChR2-GFP in the LGN. The injection was performed on P14 rats and the image was obtained at P28. Top right: expanded image of the injection site. B. Diagram of experimental configuration and image of LGN recorded neuron (white cell stained with biocytin/Alexa647, see arrow). LS, light stimulation was delivered using 3 pulses of 1ms. LGN: sample trace of LGN neuron activity in response to light stimulation. Note that light stimulation effectively activates LGN neurons above threshold. C. Image of LGN terminal fields in acute coronal slices containing V1. The white squares indicate regions of interest that were expanded in the images on the left. D. ChR2 expression in LGN axonal fields is reliable across slices and preparations. Left: sample image of a coronal slice used for patch clamp recordings. Right. Average (black) and standard deviation (gray) of profile of the intensity of the fluorescence signal measured in the region of interest (ROI) indicated by the white line in the left image. Width of ROI: 20 □m. The average plot results from the average of measurements across all recorded slices in which neurons fit our criteria for inclusion in the data analysis. The depth axis is aligned in the plot and in the image. The shaded areas indicate the depth at which recordings in L4 and L6 were performed. Note that the low variability of the level of expression of our construct across preparations.

Baseline synaptic properties of TC inputs onto L4 and L6 neurons

Coronal slices containing V1 were prepared to visualize the extent of the LGN terminal fields. Figure 2.1 C shows confocal images indicating an intense axonal projection from the LGN onto L4 and a significant projection onto L6. The LGN and V1 images shown in Figure 2.1, A and C, were taken from the same brain. Brief pulses of light (1 ms) successfully activated TC terminal fields and evoked postsynaptic currents in L4 and L6 neurons. The identity and location of recorded neurons were confirmed by analyzing firing properties in response to depolarizing current steps and by post hoc morphological reconstruction (Fig. 2.2 A, B).

In L4 a significantly larger proportion of neurons responded to light stimulation than in L6, suggesting that TC axons contact a larger number of neurons in L4 (Fig. 2.2 E; L4: 91 of 104 tested, 88%; L6: 28 of 58 tested, 48%; χ^2 for contingency: $p < 0.03$). To verify that the evoked TC-EPSCs were indeed monosynaptic in both layers, delays from stimulus onset, rise time, and decay time constants of TC-EPSC were quantified. Latency of the responses and rise and decay time constants were normally distributed (Kolmogorov–Smirnov test, rise: $p = 0.4$; decay: $p = 0.7$; latency: $p = 0.6$). The latency of TC-EPSCs recorded from L4 pyramidal neurons was significantly shorter than that onto L6 pyramidal neurons, while rise time of TC-EPSCs was significantly longer in L4 (Fig. 2E; Latency, L4: 1.6 ± 0.03 ms, n = 54; L6: 2.0 ± 0.1 ms, n = 18; unpaired t test: $p < 0.01$; Rise, L4: 1.4 ± 0.06 ms; L6: 1.1 ± 0.09 ms; unpaired t test: $p < 0.01$). No differences in decay time constant were observed (L4: 6.4 ± 0.3 ms, n = 54; L6: 5.7 ± 0.5, n = 18; unpaired t test: $p < 0.3$). Both in L4 and L6 neurons the amplitude of the light-evoked TC-EPSC was stable for at least 20 min, the average recording time in our experiments (Fig. 2F).

TC-EPSCs onto L4 and L6 differed in a number of baseline synaptic properties. As shown in Figure 2.3, A and B, the amplitude of TC-EPSC was significantly larger onto L4 star pyramidal

neurons at every light intensity tested, resulting in layer-specific input/output curves (Fig. 2.3 A, B; L4, 0.1mW/mm^2: 19.6 ± 3.9 pA; 0.2 mW/mm^2: 58.7 ± 10.4 pA; 0.25 mW/mm^2: 167.0 ± 59.6 pA; 0.3mW/mm^2: 260.2 ± 25.9 pA; n = 34; L6, 0.1mW/mm^2: 9.6 ± 3.3 pA; 0.2 mW/mm^2: 34.8 ± 13.6 pA; 0.25 mW/mm^2: 93.4 ± 25.1 pA; 0.3mW/mm^2: 141.4 ± 34.2 pA; n = 14; unpaired Student's t tests, 0.1mW/mm^2: $p < 0.05$; 0.2mW/mm^2: $p < 0.03$; 0.25mW/mm^2: $p < 0.01$; 0.3 mW/mm^2: $p < 0.03$). The paired pulse ratio (EPSC2 / EPSC1; PPR) of TC-EPSCs recorded in L4 and L6 pyramidal neurons in response to trains of 3 stimuli was significantly different for frequencies of stimulation up to 10 Hz (Fig. 2.3 C, D; PPR, mean ± SD; 3.3 Hz, L4: 0.56 ± 0.13; L6: 0.68 ± 0.10, $p < 0.01$; 5 Hz, L4: 0.53 ± 0.13; L6: 0.63 ± 0.15, $p < 0.03$; 10 Hz, L4: 0.51 ± 0.12; L6: 0.62 ± 0.18, $p < 0.05$; 20 Hz, L4: 0.59 ± 0.17; L6: 0.66 ± 0.18, $p < 0.2$ L4: n = 21; L6: n = 14). The short-term plasticity (STP) of TC-EPSCs onto L4 and L6, expressed as ratio of the last to the first TC-EPSC in the train, was significantly different in the frequency range from 3.3 Hz to 20 Hz, further confirming that TC synaptic inputs show layer-specific dynamics (Fig. 2.3 C, D; STP, mean ± SD, 3.3 Hz, L4: 0.43 ± 0.14; L6: 0.56 ± 0.13, $p < 0.01$; 5 Hz, L4: 0.4 ± 0.1; L6: 0.53 ± 0.13, $p < 0.01$; 10 Hz, L4: 0.36 ± 0.09; L6: 0.48 ± 0.15, $p < 0.01$; 20 Hz, L4: 0.42 ± 0.13; L6: 0.52 ± 0.13, $p < 0.05$; L4: n = 21; L6: n = 14). Frequencies > 20 Hz were not tested as the ChR2 current is not reliably activated (Boyden et al., 2005). Together these data demonstrate that TC synapses onto the two main input layers in V1 are not equivalent. The differences in magnitude and dynamics suggest that L4 and L6 are likely to provide a different readout of incoming sensory stimuli.

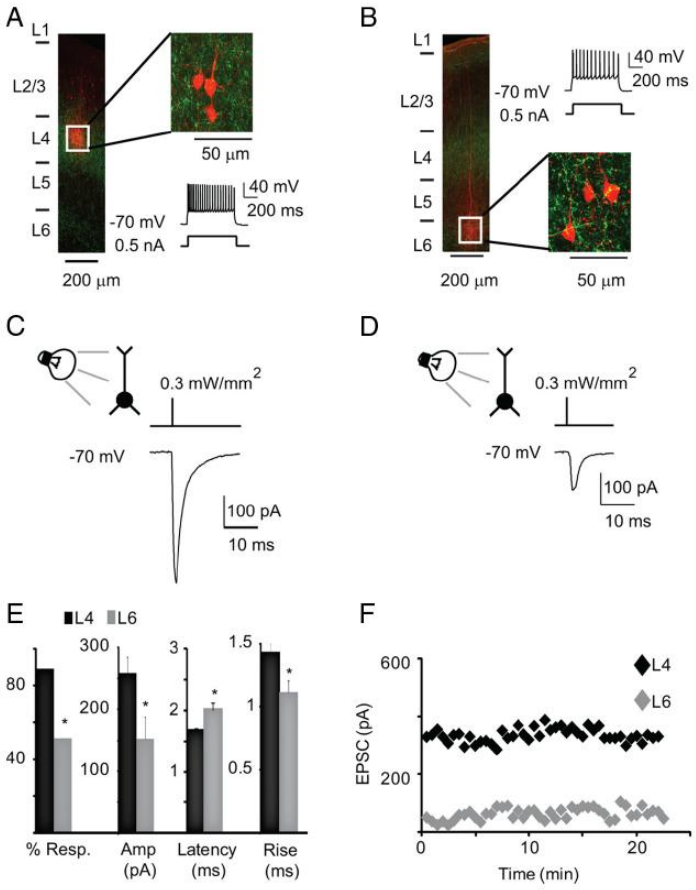

Figure 2.2. Pyramidal neurons in L4 and upper L6 respond to light activation of TC afferents. A. Post hoc reconstruction of recording configuration in L4. Left: image of a coronal slice in which a triplet of star pyramidal neurons was recorded in L4. White square: region in which neurons were recorded. Green: ChR2-GFP; red: biocytin-Alexa594. Top right: enlargement of the region indicated by the white square. Bottom right: firing pattern of recorded neurons in response to a 0.5nA current pulse. The firing pattern is typical of L4 star pyramids. B. Representative image of post hoc reconstruction of L6 recordings. Left: image of coronal slice, with neurons recorded in L6 (see white square). Green: ChR2-GFP; red: biocytin-Alexa594. Top right: firing pattern of L6 neurons in response to a 0.5nA current pulse. Firing pattern is typical of L6 pyramidal neurons. Bottom right: enlargement of region indicated by the white square. C. Brief light pulses (1ms / 6mW) evoke TC-EPSCs in L4 star pyramids. Top: recording configuration and diagram of light stimulus. Bottom: TC-EPSC evoked from one of the neurons shown in a. D. Brief light pulses (1ms / 6mW) elicits synaptic response in L6 pyramidal neurons. Top: recording configuration and diagram of light stimulus. Bottom: light evoked response evoked in one of the neurons shown in b. E. Bar plot of the % of neurons responding to light pulses (% Resp.), of average TC-EPSC amplitude at 6mW, of latency of the TC-EPSC onset from stimulus onset (Latency) and of the rise time of the light evoked TC-EPSC (Decay) in L4 (black) and L6 (gray). F. Time course of the light evoked responses for the neurons shown in c (L4; black) and d (L6; gray). Light intensity: 6mW. Data are represented as mean ± standard error; asterisks indicate significant differences.

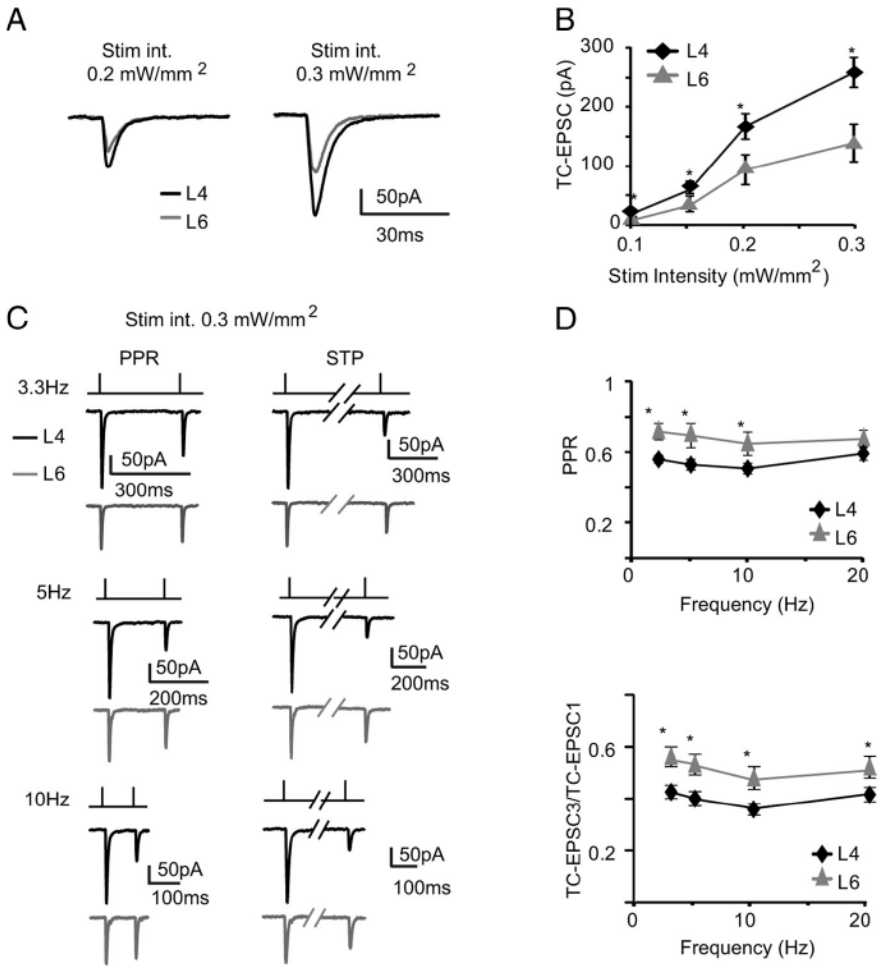

Figure 2.3. Baseline properties of TC-EPSCs in L4 and L6. A. Sample traces of light evoked TC-EPSCs in L4 and L6 neurons using different light intensities. Left: 4mW; right: 6mW. Black: L4; gray: L6. B. Input/output curves for TC-EPSCs in L4 (black) and L6 (gray). C. Representative traces of TC-EPSC dynamics in response to repetitive stimulation at different frequencies. Left column: TC-EPSC1 and 2 in a train of stimuli (at 3Hz; 5Hz; 10Hz) evoked by 1ms light pulses- 6mW light intensity in L4 (black) and L6 (gray). Right column: TC-EPSC1 and TC-EPSC3 of a train of stimuli (at 3Hz; 5Hz; 10Hz) in L4 (black) and L6 (gray). Dashes indicate that the trace was cut to show only the indicated TC-EPSCs. Light intensity: 6mW for L4 and L6. D. Top: plot of average paired pulse ratio (PPR) versus frequency of stimulation. Bottom: average TC-EPSC3/TC-EPSC1 ratio versus the frequency of stimulation. For both plots, light intensity: 6mW; black: L4; gray: L6. Data are presented as mean ± standard error, asterisks indicate significant differences.

Differences in the IC circuitry of L4 and L6

TC inputs onto L4 and L6 differ in the proportion of responsive neurons, as well as in the amplitude and dynamics of evoked TC-EPSCs. Whether this layer specificity is occurring in the incoming input alone or may be accentuated by differences in the organization of the recurrent intracortical (rIC) circuit in each layer is unknown. To address this we combined optogenetic stimulation of TC afferents with paired recording electrophysiology within each input layer (Fig. 2.4 A, F). Triple simultaneous patch clamp recordings within layer allowed the detailed analysis of rIC local circuitry. This experimental approach was instrumental to determine the synaptic organization of TC projections contacting nearby neurons in L4 and L6.

The synaptic organization of the TC and rIC circuitry in L4 differed significantly from that in L6. As shown in Figure 2.4B, only 12% of L4 pyramidal neurons did not respond to light activation of TC afferents (13 of 104). Of the 88% responsive neurons (n = 91), 34% were recurrently connected (n = 31), suggesting that, in L4, feedforward TC afferents contact a broad network of highly interconnected pyramidal neurons. The amplitude of TC-EPSCs onto L4 neurons simultaneously recorded within a 100 μm^2 region, that were not recurrently connected, was broadly distributed and peaked around 260 pA, the average amplitude of the feedforward inputs recorded in L4 (n unconnected pairs: 23).

The distribution of amplitudes of TC inputs onto simultaneously recorded and recurrently connected neurons (within a 100 μm^2 region), on the other hand, showed two clearly identifiable peaks, one centered around 162 pA and one centered around 454 pA (n connected pairs: 24). The distributions of the amplitude of TC-EPSCs onto recurrently connected and non-recurrently connected neurons were significantly different (Kolmogorov–Smirnov test, $p < 10^{-4}$). The connected neurons receiving small and large TC inputs were further analyzed to test the

possibility that they belonged to identifiable subpopulations of pyramidal neurons. No significant difference was detected in the morphology, short-term dynamics and location within L4. Rank-order correlation analysis of TC-EPSC onto the presynaptic neurons versus TC-EPSC onto the postsynaptic neurons unveiled a tight linear relationship between inputs onto recurrently connected neurons (Fig. 2.4 D, Spearman rank order coefficient: $R_s = 0.6$; $p < 10^{-5}$). In contrast, the same analysis applied to TC-EPSCs onto non-connected neurons recorded simultaneously with connected pairs within the same triplets revealed no significant correlation (Fig. 2.4 E; $R_s = 10^{-4}$; $p < 0.4$). In L4, thalamo-recipient neurons that belong to a recurrently interconnected circuit are more likely to receive feedforward inputs with similar magnitude, while neurons intermingled with recurrently connected neurons, but not belonging to a simultaneously recorded recurrently connected subnetwork, are likely to receive inputs with different magnitudes. These findings indicate that in L4, proximity does not predict similarity of the magnitude of the TC inputs, but recurrent connectivity does. In addition, weakly driven and strongly driven connected pairs of neurons were often found in the same group, indicating that the difference in TC drive is not due to differences in the levels of expression of our construct. Recurrently connected L4 pyramidal neurons thus are organized in distinct subcircuits driven either by distinct LGN axons or by the same axon contacting neurons with inputs of different power.

In Figure 2.4 F–H we show the circuit analysis for L6 pyramidal neurons. Recordings in L6 were focused in the upper portion of the layer, where the density of the LGN terminal field was more prominent. By morphological reconstruction L6 neurons included in this analysis belonged to pyramidal neurons with apical dendrites extending into the superficial layers (Bannister et al., 2002; Zarrinpar and Callaway, 2006) (Fig. 2.2 B). Of all recorded pyramidal neurons in this layer 52% responded to light stimuli (21 of 40). The remaining 48% did not respond to light

stimulation at any intensity tested (19 of 40). A total of 15% of the recorded L6 neurons were recurrently connected (10 of 66) and evenly distributed among the TC-responsive and TC-nonresponsive populations (Fig. 2.4G). This probability of connection is ≈5 times higher than previously reported for rats, and similar to the connectivity reported in cats (Mercer et al., 2005). The discrepancy with previous reports of L6 connectivity in rats may depend on differences in technical approach, multiple simultaneous patch clamp (this study) versus dual intracellular recordings (Mercer et al., 2005). The location of the recorded neurons may also account for the differences in connectivity as this study focused on neurons in the superficial portion of L6, while other studies tested the connectivity across all of L6 (Mercer et al., 2005).

Nearby, non-recurrently connected neurons within L6 received TC inputs with uncorrelated magnitudes as shown by the plot in Figure 2.4 H (Spearman rank order coefficient: - 0.1; $p = 0.6$; $n = 19$ pairs). As expected from the low response probability, non-TC-responsive neurons were often recorded simultaneously with nearby, TC-responsive ones. Our data suggest that TC afferents reaching L6 activate a recurrent IC microcircuit that is less interconnected compared with L4 (IC probability of finding connected pairs: 34% (L4) vs 15% (L6); two-tailed χ^2 for contingency: $p < 0.04$). In L6 the probability of finding recurrently connected pairs of pyramidal neurons that were also responsive to light stimuli was very low and did not allow us to obtain a sufficiently large population of connected pairs to run a rank-order correlation analysis. Only 40% of recurrently connected L6 neurons belonged to a pair in which both neurons responded to LGN stimulation (4 of 10) and only 1 of 4 received inputs of similar magnitude on presynaptic and postsynaptic neurons. In the remaining 60% of recurrently connected pairs, 2 pairs had only one neuron responding to light stimulation, without a specific preference for the presynaptic or the postsynaptic neuron; while the last 4 connected pairs were not driven by TC stimulation. In

addition, in L6, non-connected neurons that were recorded simultaneously within a 100 μm^2 area were activated by afferent TC axons with different synaptic strength, and in most groups recorded only half of the neurons responded to light pulses. These data further confirm that in L6 and L4 both TC and recurrent microcircuits have distinct synaptic organization.

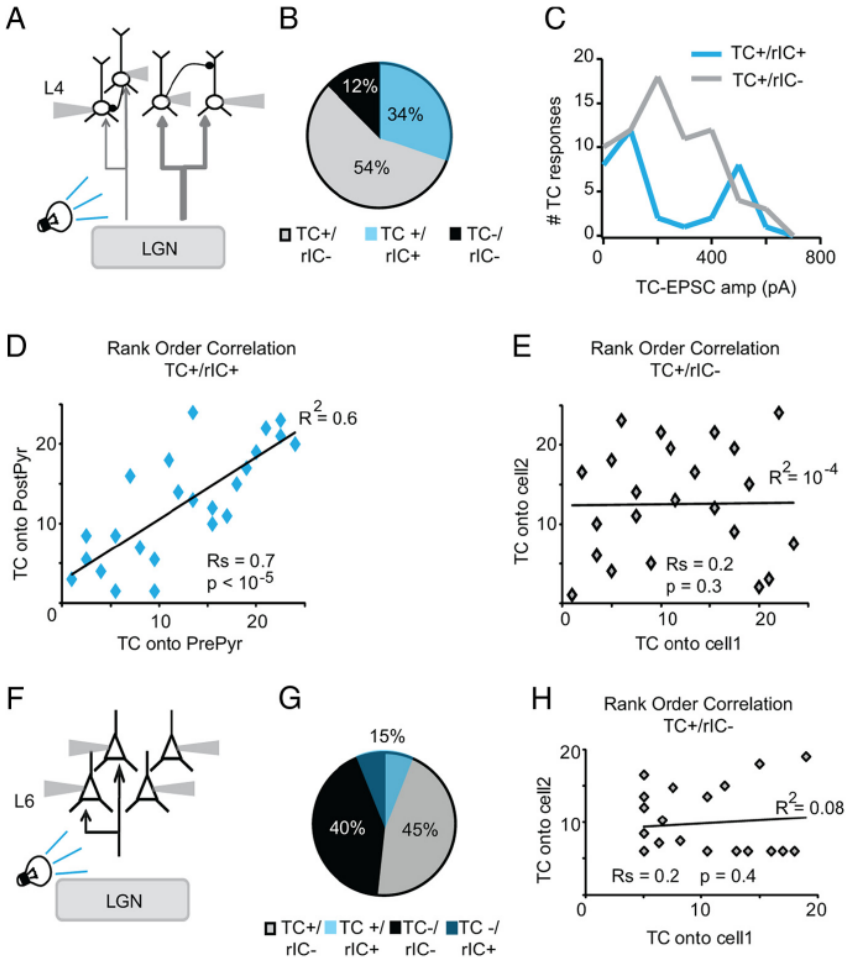

Figure 2.4. Layer specific organization of TC circuits. A. Diagram of recording configuration. Light pulses activate LGN terminal fields in V1. Simultaneous patch clamp recordings are obtained from visually identified star pyramids in L4. Stimulation and recordings are within an area of interest of 100 □m x 100 □m. Light intensity was set at 6mW. B. Pie chart indicating proportion of star pyramids not responsive to light stimulation of TC afferents and not recurrently connected in L4 (black, TC-/rIC-); of neurons responding to light stimulation of TC afferents, but not recurrently connected (gray, TC+/rIC-) and of neurons responding to light stimulation of TC afferents and also recurrently connected (blue, TC+/rIC+). C. Distribution of the amplitude of light evoked TC responses for the population of neurons that are not recurrently connected (gray) and for the population of neurons that is recurrently connected within L4 (blue). Note the bimodal distribution of the population of TC/rIC connected neurons. D. Rank order correlation of the TC-EPSC onto the presynaptic neurons versus that onto the postsynaptic

neuron on TC+/rIC+ neurons. R_s: Spearman rank-order correlation coefficient; p value of the Spearman correlation, p lower than 0.05 are considered to be significant. E. Rank order correlation of the TC-EPSC onto nearby neuron that are not recurrently connected. Note that all neurons were recorded within a 100 □m x 100 □m area of interest in L4 and often rIC- neurons were recorded in the same quadruplet with rIC+ ones. R_s: Spearman rank-order correlation coefficient; p value of the Spearman correlation. F. Diagram of recording configuration for L6. Light pulses activate the LGN terminal fields in V1, while multiple patch clamp recordings are obtained from pyramidal neurons in L6 within a 100 □m x 100 □m area of interest. Light intensity: 6mW. G. Pie chart indicating the proportion of neurons not responding to light activation of TC axons (black, TC-/rIC-), of neurons not responding to TC activation but recurrently connected (dark blue, TC-/rIC+); of neurons responsive to TC activation but not recurrently connected (gray, TC+/rIC-) and of neurons responsive to TC activation and recurrently connected in L6 (light blue, TC+/rIC+). H. Rank order correlation of TC-EPSC amplitude onto TC+/rIC- neurons. R_s: Spearman rank-order correlation coefficient; p value of the Spearman correlation.

Brief visual deprivation selectively decreases TC inputs onto L4

TC inputs onto L4 and L6 carry information about sensory stimuli (LeVay and Gilbert, 1976). However, our data show distinct magnitude, dynamics, and synaptic organization of TC inputs in the main thalamo-recipient layers in V1. We therefore asked whether L4 and L6 may differ in their responsiveness to changes in sensory drive. To address this we performed a brief (3 d) MD (Maffei et al., 2006) and compared the properties of TC inputs onto L4 and L6 neurons recorded in the monocular region of the hemispheres contralateral (MD) and ipsilateral (C) to the closed eye.

TC-EPSCs recorded in L4 of the deprived hemisphere were significantly smaller than in C at every tested intensity of light stimulation (Fig. 2.5 A, B; 0.1 mW/mm^2, C: 21.9 ± 4.3 pA; n = 33; MD 6.9 ± 2.0 pA; n = 25; $p < 0.003$; 0.2mW/mm^2, C: 54.7 ± 9.7 pA; MD: 22.4 ± 4.5 pA; $p < 0.004$; 0.25 mW/mm^2, C: 191.7 ± 26.7 pA; MD: 94.6 ± 17.3 pA; $p < 0.003$; 0.3 mW/mm^2, C: 259.7 ± 30.8 pA; MD: 132.7 ± 21.6 pA; $p < 0.001$). The reduction in TC-EPSC amplitude was not accompanied by changes in paired pulse ratio at any frequency of stimulation tested (Fig. 2.5 C; 0.3mW/mm^2, C: n = 33; MD: n = 25; one-way ANOVA: $p = 0.6$; post hoc unpaired t test: 3.3 Hz: $p = 0.6$; 5 Hz: $p = 0.9$; 10 Hz: $p = 0.64$; 20 Hz: $p = 0.69$). In addition, the latency of TC-EPSC from the time of stimulation was increased, and the decay time constant of TC-EPSCs decreased significantly (Fig. 2.5 D; Latency, C: 1.6 ± 0.04 ms; n = 33; MD: 1.9 ± 0.09 ms; n = 25; $p < 0.004$; Decay, C: 6.4 ± 0.3 ms; MD: 5.2 ± 0.2 ms; $p < 0.01$).

In L6 MD did not affect TC-EPSC amplitude onto pyramidal neurons at any intensity of light stimulation (Fig. 2.5 E, F; 0.1 mW/mm^2, C: 10.2 ± 3.5 pA; n = 14; MD 8.1 ± 4.3 pA; n = 19; $p < 0.82$; 0.2 mW/mm^2, C: 35.9 ± 14.5 pA; MD: 28.2 ± 16.9 pA; $p = 0.84$; 0.25mW/mm^2,C: 96.9 ± 26.5 pA; MD: 78.8 ± 34.7 pA; $p < 0.88$; 0.3 mW/mm^2, C: 152.6 ± 35.1 pA; MD: 140.6 ± 46.9

pA; p = 0.85). No significant differences in paired pulse ratio were observed at any frequency of stimulation (Fig. 2.5 G; C: n = 14; MD: n = 19; ANOVA: p = 0.5; post hoc unpaired t test: 3.3 Hz: p = 0.3; 5 Hz: p = 0.8; 10 Hz: p = 0.5; 20 Hz: p = 0.8). The latency of TC-EPSC onset from light stimulation and decay time constant were also unchanged (Fig. 2.5 H; Latency, C: 2.0 ± 0.11 ms, n = 14; MD: 2.4 ± 0.2 ms, n = 19; p < 0.1; Decay, C: 5.1 ± 0.4 ms; MD: 5.4 ± 0.6 ms; p < 0.7). Thus, TC-EPSCs onto L6 pyramidal neurons are not affected by MD. Based on these results we conclude that LGN inputs onto V1 pyramidal neurons have distinct sensitivity to changes in visual drive depending on the location of the postsynaptic neuron. LGN synapses onto L4 are significantly weakened even by MD too short to induce anatomical reorganization of axonal arbors (Antonini et al., 1999); in contrast, TC inputs onto L6 pyramidal neuron are stable in the face of brief changes in sensory drive.

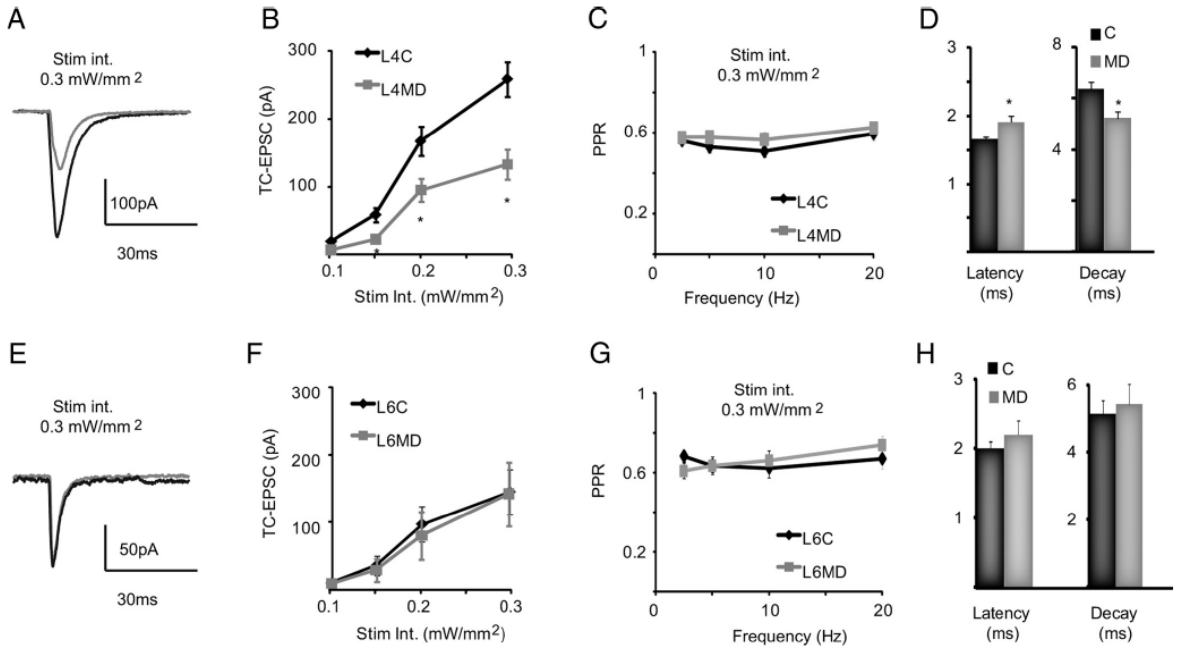

Figure 2.5. Layer specific experience-dependent depression of TC-EPSCs. A. Example traces of TC-EPSCs evoked in L4 star pyramids by light activation of TC afferents in control (black) and deprived (gray) slices. Light intensity: 6mW. B. Input/output curve of TC-EPSCs in L4. Control: black; deprived: gray. C. Plot of paired pulse ratio (PPR) in response to stimulation at 6mW and different frequencies. Control: black; deprived: gray. D. Bar plot of average latency of L4 TC-EPSC onset from onset of light pulse and decay time constant of L4 TC-EPSCs. Light intensity: 6mW. Control: black; deprived: gray. E. Example traces of TC-EPSCs evoked in L6 pyramidal neurons by light activation of TC afferents in control (black) and deprived (gray) slices. Light intensity: 6mW. F. Input/output curve of TC-EPSCs from L6 pyramidal neurons. Control: black; deprived: gray. G. Plot of PPR in response to stimulation at different frequencies. Light intensity: 6mW. Control: black; deprived: gray. H. Bar plot of average latency of L6 TC-EPSC onset from the onset of the light pulse and decay time constant of L6 TC-EPSCs. Light intensity: 6mW. Control: black; deprived: gray. Data are presented as mean ± standard error, asterisks indicate significant differences.

Layer-specific experience-dependent reorganization of TC–IC circuits

The layer specificity of the effects of MD on LGN inputs onto L4 and L6 prompted us to investigate whether rIC circuits within these layers might be affected by 3d MD differently. In a subset of experiments paired recordings within L4 or in L6 were combined with light stimulation of TC afferents. In L6 we observed no changes in the overall patterns of rIC connectivity and responsiveness to activation of LGN afferents (Fig. 2.6 A). The overall proportion of nonresponsive neurons was 40%, while the remaining 60% produced reliable TC-EPSCs in response to light activation of LGN terminal fields (χ^2 for contingency, % TC responsive neurons in C vs % TC-responsive neurons after MD: $p = 0.5$). A total of 8% of pyramidal neurons in L6 were recurrently connected. This group was evenly distributed across the population of neurons that responded to activation of TC afferents and the ones that were not responsive (total connected pairs, C: 6 of 58; MD: 4 of 49; χ^2 for contingency: $p = 0.4$). The distribution of TC-EPSC amplitudes was not significantly different in slices from the Control and Deprived hemispheres, confirming the stability of TC as well as rIC connectivity in L6 after brief MD (Fig. 2.6 B).

When a similar analysis was performed in L4 we found that the proportions of TC and rIC connected neurons were not affected by MD (Fig. 2.7 A; χ^2 for contingency, % TC-responsive neurons in C versus % TC-responsive neurons after MD: $p = 0.6$). The amplitude of TC-EPSCs onto all L4 star pyramids was reduced significantly (Fig. 2.7 B–D; TC-EPSC onto TC+ /rIC+, C: 270 ± 35 pA; MD: 172 ± 25 pA; $p < 0.03$; TC+/rIC-, C: 280 ± 22 pA; MD: 160 ± 23 pA; $p < 0.001$). Differently, the amplitude of recurrent IC EPSPs was not affected by MD, as shown in previous reports (Maffei et al., 2006; Wang et al., 2012) (Fig. 2.7 B; rIC EPSP, C: 0.8 ± 0.1 mV; MD: 0.6 ± 0.1 mV; $p < 0.2$). These results indicate that MD specifically weakened TC inputs

onto L4 star pyramids, while leaving recurrent rIC excitatory synapses unaffected. A closer analysis of the distribution of TC-EPSC amplitudes on the population of nearby-not recurrently connected neurons revealed a uniform shift toward smaller amplitudes after MD (Fig. 2.7 C; Kolmogorov–Smirnov test: $p < 0.003$). The distribution of TC-EPSC amplitudes onto recurrently connected neurons, instead, showed that MD affected predominantly the proportion of large-amplitude TC-EPSCs (Fig. 2.7 D, arrow), which was reduced from 33% to 8% (χ^2 for contingency: $p < 0.01$). Thus, the MD-dependent decrease in TC-EPSC amplitude is driven by a reduction in the proportion of the more powerful TC inputs onto L4 star pyramidal neurons. In addition, there was a loss of correlation of TC-EPSC amplitude onto recurrently connected neurons (Fig. 2.7 D, inset; $R_s = 0.04$; $p = 0.1$). Although MD did not affect the probability of finding recurrent connections and the proportion of L4 neurons responding to TC afferents, it induced a reorganization of the relationship between TC and recurrent IC connectivity through a nonuniform decrease of TC-EPSC amplitude onto L4 neurons.

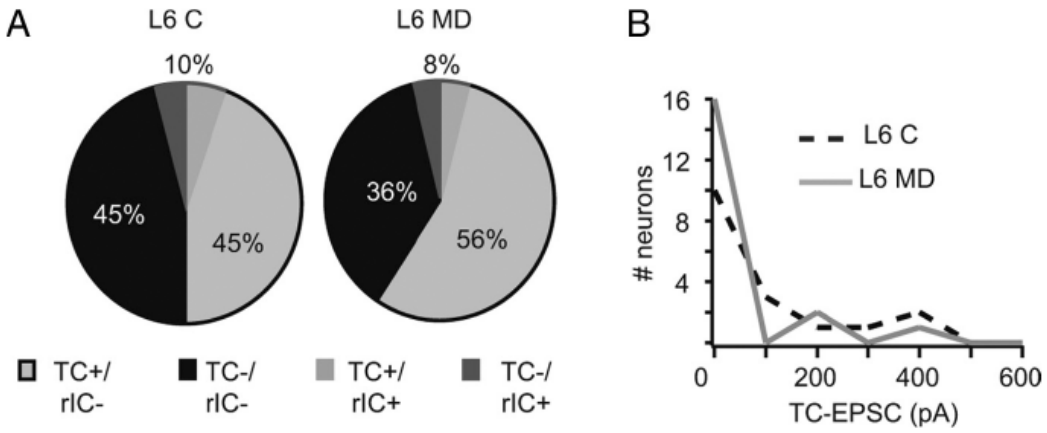

Figure 2.6. MD does not affect the organization of TC/rIC inputs onto L6 pyramidal neurons. A. Pie charts of the proportion of L6 pyramidal neurons not responding to light activation of TC afferents and not recurrently connected (black, TC-/rIC-), of L6 pyramidal neurons not responding to light activation of TC afferents but recurrently connected (dark blue, TC-/rIC+), of L6 pyramidal neurons responding to light activation of TC afferents and not recurrently connected (gray, TC+/rIC-) and of L6 pyramidal neurons responding to light activation of TC afferents and recurrently connected (light blue, TC+/rIC+). Left chart: control hemisphere (C); right chart: deprived hemisphere (MD). B. Distribution of TC-EPSC amplitudes for L6 TC+/rIC- pyramidal neurons. Light intensity: 6 mW. Control: black dotted line; deprived: gray solid line.

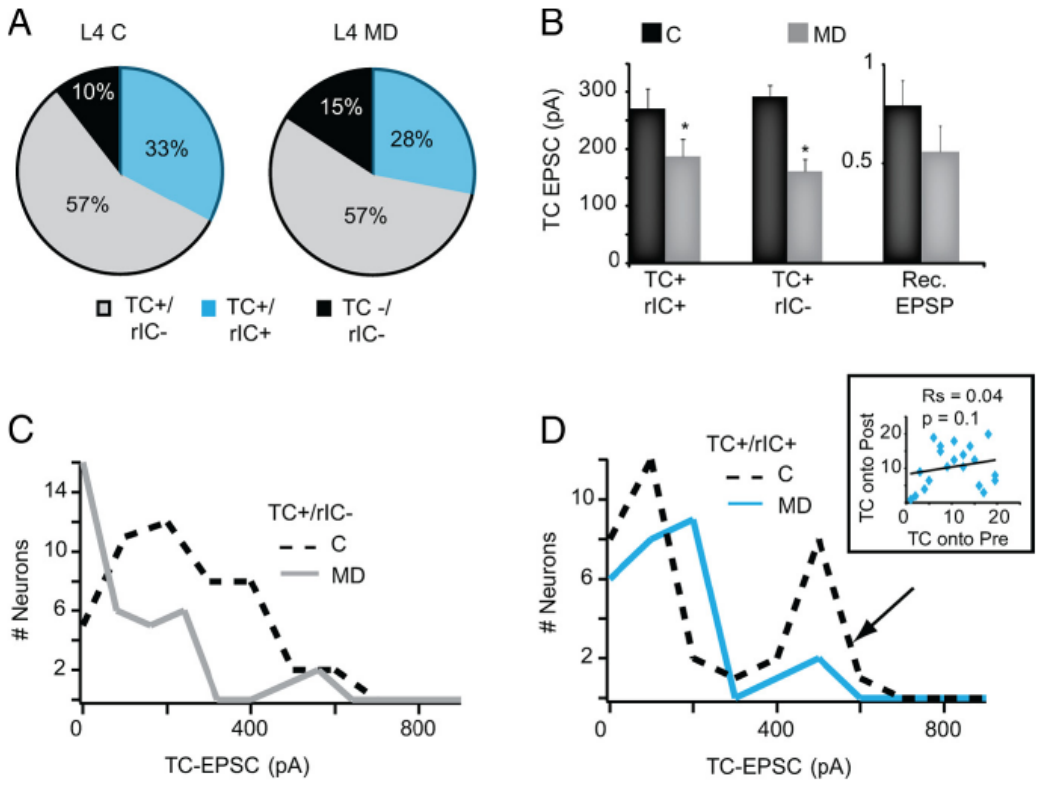

Figure 2.7. Experience-dependent reorganization of TC/IC inputs onto L4 star pyramids. A. Pie charts of the proportion of L4 star pyramids not responsive to activation of TC afferents and not recurrently connected (black, TC-/rIC-), of L4 star pyramids responsive to activation of TC afferents and not recurrently connected (gray, TC+/rIC-) and of recurrently connected L4 star pyramids that responded to light activation of TC afferents (light blue, TC+/rIC+). Left chart: control hemisphere (C); right chart: deprived hemisphere (MD). B. Bar plot of average amplitude of TC-EPSC onto TC+/rIC+ L4 star pyramids, of TC-EPSCs onto TC+/rIC- star pyramids and of rIC-EPSP between L4 star pyramids. Light intensity: 6mW. Control: black; deprived: gray. Data are represented as average ± standard error; asterisks indicate significant differences. C. Distribution of TC-EPSC amplitudes onto TC+/rIC- L4 star pyramids. Control: dashed black line; deprived: gray line. Note that the entire distribution is shifted toward smaller amplitudes. D. Distribution of TC-EPSC amplitudes onto TC+/rIC+ star pyramids in L4. Control: dashed black line; deprived: light blue line. Arrow: peak of the distribution strongly affected by MD. Inset: Spearman rank order correlation of TC-EPSP amplitudes onto presynaptic (Pre) and postsynaptic (Post) neurons of TC+/rIC+ L4 star pyramids. Note the MD-induced loss of correlation compared to control conditions (see Figure 4d). R_s: Spearman rank-order correlation coefficient; p value of the Spearman correlation.

Discussion

L4 and L6 excitatory neurons receive direct input from the LGN (Gilbert, 1977; Hendrickson et al., 1978; Kageyama and Robertson, 1993) and are characterized by fairly large TC-EPSC amplitude and short-term depression in response to trains of stimuli (Sherman, 2012). Studies of thalamocortical (TC) inputs focused primarily on the basic properties of these inputs (Bannister et al., 2002; Binzegger et al., 2004; da Costa and Martin, 2009; Medini, 2011), but did not address possible differences in capacity for plasticity in thalamo-recipient circuits (LeVay and Gilbert, 1976; Landry and Deschenes, 1981; Rose and Metherate, 2001; Bruno and Sakmann, 2006; Cruikshank et al., 2007, 2010 Lee and Sherman, 2008). Differently, studies of experience-dependent plasticity addressed layer specificity, but focused on the comparison of TC and IC circuits (Feldman et al., 1998; Desai et al., 2002; McLaughlin and Juliano, 2003; Maffei et al., 2004; Fox and Wong, 2005; Hensch, 2005; Maffei et al., 2006; Jiang et al., 2007; Maffei and Turrigiano, 2008; Feldman, 2009; Nataraj et al., 2010; Medini, 2011; Oberlaender et al., 2012). In this article we compared synaptic organization and plasticity of LGN inputs onto excitatory neurons in the two main thalamo-recipient layers in V1. Our data demonstrate for the first time that TC inputs onto excitatory neurons in L4 and L6 of V1 have layer-specific magnitude, connectivity, short-term dynamics, and sensitivity to changes in visual experience.

Our data indicate that fewer L6 excitatory neurons responded to stimulation of TC afferents than did those in L4 (88% in L4 vs 48% in L6; χ^2 for contingency: $p < 0.01$). This effect was not due to spatial sampling: in both layers recordings were within a 100 μm^2 region and our L6 study was limited to the upper portion of the layer, where the density of TC afferents was highest. Our data suggest that in L6 LGN afferents contact fewer neurons as previously reported (Hubel and Wiesel, 1972; Hendrickson et al., 1978; da Costa and Martin, 2009). The proportion of TC

responsive neurons accounts for a macroscopic organization of LGN inputs in L4 and L6, but does not explain differences in TC-EPSC amplitude. Minimal TC-EPSCs onto V1 pyramidal neurons, similar in size to those expected for putative single axons (Cruikshank et al., 2010), was significantly smaller in L6 than in L4. Input/output curves for L4 and L6 neurons showed similar trends: increasing stimulation intensity successfully recruited inputs in both layers, but activated smaller TC-EPSCs onto L6. Anatomical studies showed that pyramidal neurons in L6 have fewer synapses than those onto L4 neuron (Bannister et al., 2002; Binzegger et al., 2004; da Costa and Martin, 2009). Fewer synaptic contacts could justify the difference in TC-EPSC amplitude. In L4 and L6 the TC-EPSC we recorded could be classified as type I responses: fast, fairly large, and characterized by short-term depression, indicating that the differences in TC-EPSCs did not depend on activation of different populations of inputs (Viaene et al., 2011a, b). Short-term synaptic dynamics of TC-EPSC were layer-specific, with less short-term depression onto L6 neurons, suggesting distinct release properties or saturation of postsynaptic receptors (Zucker and Regher, 2002). Thus, the differences in TC-EPSCs amplitude and dynamics onto L4 and L6 neurons are likely to depend on differences in the number of inputs and on distinct synaptic properties. Short-term dynamics may have a prominent role in information processing at synapses (Klug et al., 2012); thus, L4 and L6 may process incoming information differently because of the different dynamics of TC-EPSCs.

The onset of TC-EPSCs onto L6 showed longer delays from stimulus than those onto L4. Understanding this difference will require direct investigation; however, a number of possibilities can be excluded. Both synaptic delays are below 2 ms; thus, both inputs were monosynaptic. TC-EPSC rise times were shorter in L6; therefore, dendritic filtering does not explain longer delays. As TC afferents send collaterals to L4 and L6 neurons (Freund et al.,

1989; Wiser and Callaway, 1996), differences in axonal conduction velocity are not expected to occur. As many L4 and L6 neurons were recorded simultaneously within the same slice, intrinsic properties of ChR2 do not account for the layer specificity of TC synapses. One may speculate that the distinct delay from stimulus may be due, in part, to different dynamics of release or properties of postsynaptic receptors (Hull et al., 2009).

Organization of TC circuits in L4 and L6

TC afferents contact profoundly different IC circuits within L4 and L6. While in L4 approximately one third of TC-responsive pyramidal neurons were recurrently connected, in L6 only a small proportion of thalamo-recipient neurons were interconnected (≈34% in L4 vs 5% in L6;χ^2 for contingency: $p < 0.01$). In L4, recurrently connected neurons received TC-ESPCs with similar magnitude and bimodal amplitude distribution, suggesting that L4 is composed of strongly driven and weakly driven subcircuits. The functional significance of a bimodal distribution of TC-EPSC amplitudes at the moment is unclear. No differences in synaptic and intrinsic properties, or morphology, were identified between neurons receiving strong or weak TC inputs, suggesting that the distribution may represent contacts from different LGN axons. Weakly and strongly driven subcircuits were found in the same slice, thus variability in the level of expression of the ChR2 does not account for the results. Recordings were performed in the monocular region of V1, which is thought to be driven by the contralateral eye. A contribution of weaker ipsilateral inputs is unlikely, but cannot be fully excluded. The relationship between amplitude and distribution of TC inputs does not depend on the distance between neurons. Connected and non-connected neurons were often part of the same triplet and in close proximity. A possible interpretation of these data is that non-connected neurons are part of different subcircuits, possibly driven either by inputs with different synaptic properties or by distinct TC

afferents. Together, these data suggest that geometrical proximity is not sufficient to predict patterns of connectivity of neurons in L4 (Stepanyants et al., 2008), but that connectivity depends on coordination of TC and IC inputs. This finding is consistent with data about the synaptic organization of inputs from L4 onto L2/3 in V1 (Yoshimura et al., 2005).

Recent findings indicate that IC recurrently connected neurons are more likely to share similar orientation preference (Ko et al., 2011). In addition, recurrently connected neurons may belong to groups of sister-neurons originating from the same progenitor (Yu et al., 2009) and sister neurons are more likely to share similar visual responsiveness (Li et al., 2012). When interpreting our results in the context of these findings, one may speculate that local subgroups of connected neurons, possibly sister-cells, might be driven by similar LGN inputs. The potential implication of these results would be that IC microcircuits may be composed of recurrently connected neurons with predetermined properties because they belong to a group of neurons generated from the same progenitor and are contacted by LGN afferents carrying the same information. Alternatively, the connectivity of subpopulations of neurons may be determined by experience-dependent refinement of TC and IC connectivity and Hebbian processes (Katz and Shatz, 1996).

We did not observe a significant projection from the LGN into L1 (Antonini et al., 1999). Only few sparse axonal fibers expressed the ChR2-GFP construct right below the pial surface. The age of the animals used in this study may explain these differences: our recordings were limited to P28 instead of adult rodents (Antonini et al., 1999).

Layer specificity and implication for cortical function

The differences in synaptic organization may represent circuit correlates of layer-specific functions. TC inputs to L4 and L6 are carriers of information (Sherman, 2012); however, several

findings, including those in this article, suggest that sensory inputs are relayed through very powerful and numerous TC inputs to L4, but weaker and fewer TC inputs to L6 (Hubel and Wiesel, 1972; Binzegger et al., 2004; da Costa and Martin, 2009). The number and amplitude of LGN inputs onto L4 excitatory neurons may explain the similarity between the receptive fields of LGN neurons and L4 simple cells (Alonso et al., 2001). The propagation of similar functional properties from the LGN to L4 may also be favored by high recurrent IC connectivity and by recurrent IC subcircuit driven by similar TC inputs.

Differences in the proportion of TC-responsive neurons, layer-specific synaptic dynamics, and distinct sensitivity to visual experience suggest that L4 and L6 are activated differently by the sensory input, and may convey different sensory information to V1 (Klug et al., 2012). Brief MD reduces TC-EPSC amplitude onto L4 neurons only. This effect was specific to TC synapses as the amplitude of IC inputs between L4 pyramidal neurons was unchanged. Thus, L4 detects changes in visual activity rapidly and possibly relays them to the other layers in V1. On the other hand, TC inputs onto L6 pyramidal neurons are not affected by brief MD, but can adjust in response to longer periods of visual deprivation (Krahe and Guido, 2011; Petrus et al., 2011). L4 and L6 neurons are interconnected (Binzegger et al., 2004), thus the layer-specific changes in TC-EPSCs may unbalance TC and IC activity, initiating a cascade of events that will lead to loss of visual responsiveness (Frenkel and Bear, 2004). Recent findings indicate that L6 plays a major role in gain modulation and actively suppresses the activity of all other layers (Olsen et al., 2012). Delayed response of L6 to altered visual drive (Petrus et al., 2011) may allow L4 to sense differential activation from the LGN and rewire accordingly, while L6-dependent gain modulation is adjusted only later. This process may lead to desynchronized activation of TC and IC circuits, a phenomenon occurring in several brain areas (Butler et al., 2001; Llina´s and

Ribary, 2001; Butler and Javitt, 2005; Normann et al., 2007; Oberlaender et al., 2012) and thought to be implicated in neurological disorders of sensory (Sehatpour et al., 2010) and cognitive functions (Yeap et al., 2006, 2009; Leitman et al., 2010).

References

Alonso J, Usrey W, Reid R (2001) Rules of connectivity between geniculate cells and simple cells in cat primary visual cortex. J Neuroscience 21:4002-4015.

Amitai Y (2001) Thalamocortical synaptic connections: efficacy, modulation, inhibition and plasticity. Rev Neurosci 12:159-173.

Antonini A, Fagiolini M, Stryker M (1999) Anatomical correlates of functional plasticity in mouse visual cortex. J Neuroscience 19:4388-4406.

Binzegger T, Douglas R, Martin K (2004) A quantitative map of the circuit of cat primary visual cortex. J Neuroscience 24:8441-8453.

Boyden E, Zhang F, Bamberg E, Nagel G, Deisseroth K (2005) Millisecond-timescale, genetically targeted optical control of neural activity. Nature Neuroscience 8:1263-1268.

Bruno R (2011) Synchrony in sensation. Current Opinion in Neurobiology 21:701-708.

Butler P, Javitt D (2005) Early-stage visual processing deficits in schizophrenia. Current Opinion in Psychiatry 18:151-157.

Butler P, Schechter I, Zemon V, Schwartz S, Greenstein V, Gordon J, Schroeder C, Javitt D (2005) Dysfunction of early-stage visual processing in schizophrenia. American Journal of Psychiatry 158:1126-1133.

Castro-Alamancos M (2004) Dynamics of sensory thalamocortical synaptic networks during information processing states. Progress in Neurobiology 74.

Catalano S, Shatz C (1998) Activity-dependent cortical target selection by thalamic axons. Science 281:559-562.

Coleman J, Nahmani M, Gavornik J, Haslinger R, Heynen A, Erisir A, Bear M (2010) Rapid structural remodeling of thalamocortical synapses parallels experience-dependent functional plasticity in mouse primary visual cortex. J Neuroscience 30:9670-9682.

Cruikshank S, Urabe H, Nurmikko A, Connors B (2010) Pathway-specific feedforward circuits between thalamus and neocortex revealed by selective optical stimulation of axons. Neuron 65:230-245.

da Costa N, Martin K (2009) Selective targeting of the dendrites of corticothalamic cells by thalamic afferents in area 17 of the cat. J Neuroscience 29:13919-13928.

Frenkel M, Bear M (2004) How monocular deprivation shifts ocular dominance in visual cortex of young mice. Neuron 44:917-923.

Freund T, Martin K, Soltesz I, Somogyi P, Whitteridge D (1989) Arborisation pattern and postsynaptic targets of physiologically identified thalamocortical afferents in striate cortex of the macaque monkey. J Comp Neurology 289:315-336.

Gilbert C (1977a) Laminar differences in receptive field properties of cells in cat primary visual cortex. Journal of Physiology 266:391-421.

Gilbert C (1977b) Laminar differences in receptive field properties of cells in cat primary visual cortex. Journal of Physiology 268:391-421.

Hendrickson A, Wilson J, Ogren M (1978) The neuroanatomical organization of pathways between the dorsal lateral geniculate nucleus and visual cortex in Old World and New World primates. J Comp Neurology 182:123-136.
Hubel D, Wiesel T (1972) Laminar and columnar distribution of geniculo-cortical fibers in the macaque monkey. J Comp Neurology 146:421-450.
Hull C, Isaacson J, Scanziani M (2009) Postsynaptic mechanisms govern the differential excitation of cortical neurons by thalamic inputs. J Neuroscience 29:9127-9136.
Kageyama G, Robertson R (1993) Development of geniculocortical projections to visual cortex in rat: evidence early ingrowth and synaptogenesis. J Comp Neurology 335:123-148.
Khibnik L, Cho K, Bear M (2010) Relative contribution of feedforward excitatory connections to expression of ocular dominance plasticity in layer 4 of visual cortex. Neuron 66:493-500.
Ko H, Hofer S, Pichler B, Buchanan K, Sjöström P, Mrsic-Flogel T (2011) Functional specificity of local synaptic connections in neocortical networks. Nature 473:87-91.
Lee C, Sherman S (2008) Synaptic properties of thalamic and intracortical inputs to layer 4 of the first- and higher-order cortical areas in the auditory and somatosensory systems. Journal of Neurophysiology 100:317-326.
Leitman D, Sehatpour P, Higgins B, Foxe J, Silipo G, Javitt D (2010) Sensory deficits and distributed hierarchical dysfunction in schizophrenia. American Journal of Psychiatry 167:818-827.
LeVay S, Gilbert C (1976) Laminar patterns of geniculocortical projection in the cat. Brain Research 113:1-19.
Li Y, Lu H, Cheng P, Ge S, Xu H, Shi S, Dan Y (2012) Clonally related visual cortical neurons show similar stimulus feature selectivity. Nature 486:118-121.
Llinas R, Ribary U (2001) Consciousness and the brain. The thalamocortical dialogue in health and disease. Annals of the New York Academy of Science 929:166-175.
Llinás R, Ribary U, Jeanmonod D, Kronberg E, Mitra P (1999) Thalamocortical dysrhythmia: A neurological and neuropsychiatric syndrome characterized by magnetoencephalography. Proc Natl Acad Sci U S A 96:15222-15227.
Maffei A, Turrigiano G (2008) Multiple modes of network homeostasis in visual cortical layer 2/3. J Neuroscience 28:4377-4384.
Maffei A, Nelson S, Turrigiano G (2004) Selective reconfiguration of layer 4 visual cortical circuitry by visual deprivation. Nature Neuroscience 7:1353-1359.
Maffei A, Nataraj K, Nelson S, Turrigiano G (2006) Potentiation of cortical inhibition by visual deprivation. Nature 443:81-84.
Normann C, Schmitz D, Furmaier A, Doing C, Bach M (2007) Long term plasticity of visually evoked potentials in humans is altered in major depression. Biological Psychiatry 62.
Olsen S, Bortone D, Adesnik H, Scanziani M (2012) Gain control by layer six in cortical circuits of vision. Nature 483:47-52.
Peters A, Feldman M (1977) The projection of the lateral geniculate nucleus to area 17 of the rat cerebral cortex. IV. Terminations upon spiny dendrites. Journal of Neurocytology 6:669-689.
Petreanu L, Huber D, Sobczyk A, Svoboda K (2007) Channelrhodopsin-2-assisted circuit mapping of long-range callosal projections. Nature Neuroscience 10:663-668.
Petrus E, Anguh T, Pho H, Lee A, Gammon N, Lee H (2011) Developmental switch in the polarity of experience-dependent synaptic changes in layer 6 of mouse visual cortex. J Neurophysiology 106:2499-2505.

Puntel M, Kroeger K, Sanderson N, Thomas C, Castro M, Lowenstein P (2010) Gene transfer into rat brain using adenoviral vectors. Current Protocols in Neuroscience chapter 4:Unit 4.24.
Sehatpour P, Dias E, Butler P, Revheim N, Guilfoyle D, Foxe J, Javitt D (2010) Impaired visual object processing across an occipital-frontal-hippocampal brain network in schizophrenia: an integrated neuroimaging study. Arch Gen Psychiatry 67:772-782.
Sengpiel F, Baddeley R, Freeman T, Harrad R, Blakemore C (1996) Different mechanisms underlie three inhibitory phenomena in cat area 17. Vision Research 38:2067-2080.
Sherman S (2012) Thalamocortical interactions. Current Opinion in Neurobiology 22:1-5.
Sherman S, Guillery R (2002) The role of the thalamus in the flow of information to the cortex. Philos Trans R Soc Lond B Biol Sci 347:1695-1708.
Tieman S (1985) The anatomy of geniculocortical connections in monocularly deprived cats. Cell Mol Neurobiol 5:35-45.
Wang L, Fontanini A, Maffei A (2012) Experience-dependent switch in sign and mechanisms for plasticity in layer 4 of primary visual cortex. J Neuroscience:in press.
Wiser A, Callaway E (1996) Contributions of individual layer 6 pyramidal neurons to local circuitry in macaque primary visual cortex. J Neuroscience 16:2724-2739.
Yeap S, Kelly S, Reilly R, Thakore J, Foxe J (2009) Visual sensory processing deficits in patients with bipolar disorder revealed through high-density electrical mapping. J Psychiatry Neurosci 34:549-564.
Yeap S, Kelly S, Sehatpour P, Magno E, Javitt D, Garavan H, Thakore J, Foxe J (2006) Early visual sensory deficits as endophenotypes for schizophrenia: high-density electrical mapping in clinically unaffected first-degree relatives. Arch Gen Psychiatry 63:1180-1188.
Yu Y, Bultje R, Wang X, Shi S (2009) Specific synapses develop preferentially among sister excitatory neurons in the neocortex. Nature 458:501-504.
Zhang F, Gradinaru V, Adamantidis A, Durand R, Airan R, de Lecea L, Deisseroth K (2010) Optogenetic interrogation of neural circuits: technology for probing mammalian brain structures. Nature protocols 5:439-456.

Chapter III: Target-specific properties of thalamocortical synapses onto layer 4 of mouse primary visual cortex

Abstract

In primary sensory cortices, thalamocortical (TC) inputs can directly activate excitatory and inhibitory neurons in the main input layer (L4). In vivo experiments in the L4 of primary visual cortex (V1) have shown that excitatory and inhibitory neurons have different tuning properties. The different functional properties may arise from distinct intrinsic properties of L4 neurons, but could also depend on cell type-specific properties of the synaptic inputs from the lateral geniculate nucleus of the thalamus (LGN) onto L4 neurons. While anatomical studies identified LGN inputs onto both excitatory and inhibitory neurons in L4 of V1, their synaptic properties are poorly understood.

Here we used an optogenetic approach to selectively activate LGN terminal fields in acute coronal slices containing V1, and recorded monosynaptic currents from excitatory and inhibitory neurons in L4. LGN afferents made monosynaptic connections with pyramidal (Pyr) and fast spiking (FS) neurons. TC-EPSCs onto FS neurons were larger and showed steeper short term depression to repetitive stimulation than those onto Pyr neurons. LGN inputs onto Pyr and FS neurons also differed in postsynaptic receptor composition and organization of presynaptic release sites. Together, our results demonstrate that LGN input onto L4 neurons in mouse V1 have target-specific presynaptic and postsynaptic properties. Distinct mechanisms of activation of feedforward excitatory and inhibitory neurons in the main input layer of V1 are likely to endow neurons with different response properties to incoming visual stimuli.

Authors: Michelle Kloc and Arianna Maffei

Author Contributions: M.K. and A.M. designed research; M.K. performed research; M.K. and A.M. analyzed data; M.K. and A.M. wrote the manuscript.

Introduction

The responsiveness of cortical circuits to sensory stimuli depends on the dynamics of activation of different neuron types. Excitatory and inhibitory neurons differ in their tuning to stimulus features and interocular bias. These differences are particularly marked in layer 4 (L4), the layer that receives the strongest thalamocortical projection (Cardin et al., 2007; daCosta and Martin, 2011). When compared with pyramidal neurons, inhibitory neurons are generally more broadly tuned to stimulus orientation (Niell and Stryker, 2008; Kuhlman et al., 2011; Zariwala et al., 2011; Atallah et al., 2012; Li et al., 2012b; Cottam et al., 2013; Runyan and Sur, 2013), fire at higher frequencies in response to moving grating stimuli (Zhuang et al, 2013), and show less interocular bias (Yazaki-Sugiyama et al, 2009; Kameyama et al, 2010). The mechanisms regulating these differences are incompletely understood. Biophysical properties and firing patterns of excitatory and inhibitory neurons may partly explain their distinct responsiveness (Agmon and Connors, 1992; Contreras and Palmer, 2003). In addition, some of these differences could be shaped by TC inputs, if they showed target-specific properties as in other sensory cortical circuits.

Recordings *in vivo* strongly suggest that excitatory and FS neurons are directly activated by incoming visual inputs (Contreras and Palmer, 2003; Cardin et al., 2007) from retinotopically aligned neurons in the dorso-lateral geniculate nucleus of the thalamus (dLGN) (Zhuang et al, 2013). Inputs from the dLGN are thought to activate a small number of powerful inputs onto L4 neurons (Freund et al., 1985; Stratford et al., 1996). The presynaptic and postsynaptic properties of dLGN inputs onto excitatory and inhibitory neurons in L4 of V1 have not been investigated. Thus it is currently unknown whether the distinct response properties of these neuronal populations could be due at least in part to target-specific dynamics of activation.

Here we confirm that LGN afferents make direct synaptic contacts with excitatory pyramidal (Pyr) and FS neurons in L4 of mouse V1. Consistent with previous studies in S1 (Viaene et al., 2010) and in the primary auditory cortex (A1; Viaene et al., 2010; Schiff and Reyes, 2012), LGN inputs onto both Pyr and FS neurons can be classified as type I (or drivers; Sherman, 2007, 2012), as their activation evokes large currents showing short term depression to repetitive stimulation. LGN inputs onto distinct neuron types differ significantly in the number of presynaptic release sites, postsynaptic receptor composition, conductance, and number of postsynaptic channels contributing to the evoked response. Our data suggest that target-specific mechanisms of activation of LGN inputs contribute to the distinct dynamics of activation of excitatory and inhibitory neurons evoked by visual stimuli.

Results

Selective activation of thalamocortical afferents in acute V1 slices.

Obtaining a reliable preparation for the detailed study of the synaptic properties of LGN inputs to V1 has proven difficult due to the complex anatomy of the LGN projection (MacLean et al, 2006), which is why the synaptic properties of TC inputs onto L4 neurons is poorly understood. To selectively activate LGN inputs we used an optogenetic approach that allowed for stimulation of LGN terminal fields in V1 (see Chapter II). After a 10 day incubation period, LGN slices were prepared to assess the effectiveness of the expression of the ChR2-GFP construct. Whole cell current clamp recordings confirmed that LGN neurons expressed the construct and could be driven above action potential threshold using brief light stimuli (LS: 2 ms, 0.3 mW/mm^2) even in the presence of AMPA and NMDA receptor blockers (Fig. 3.1 B). The ability of LGN neurons to fire action potentials following the frequency of stimulation was assessed experimentally. In the presence of AMPA and NMDA receptor blockers LGN neuron fired action potentials reliably in

response to trains of light pulses up to 20Hz (Fig. 3.1 B). This is consistent with the reported kinetics of activation and deactivation of ChR2 (Zhang et al, 2006). Acute coronal slices containing V1 were also prepared to visualize and activate LGN terminal fields. To assess consistency of expression across preparations a fluorescence intensity profile was measured across laminae and a calibration curve for the intensity of GFP fluorescence was obtained by averaging 15 slices from 6 animals that received the AAV9-ChR2-GFP injection in the LGN (Fig. 3.1 C; see also Chapters II and VII). GFP expression for all preparations were then compared against a calibration curve and only data recorded from slices whose fluorescence profile fell within one standard deviation of the mean calibration curve were included in the analysis. The possible presence of backfilled somata in every layer of V1was assessed for each preparation. No backfilled somata were observed in any layer, confirming that LGN afferents were the only light sensitive component of V1 in our preparation.

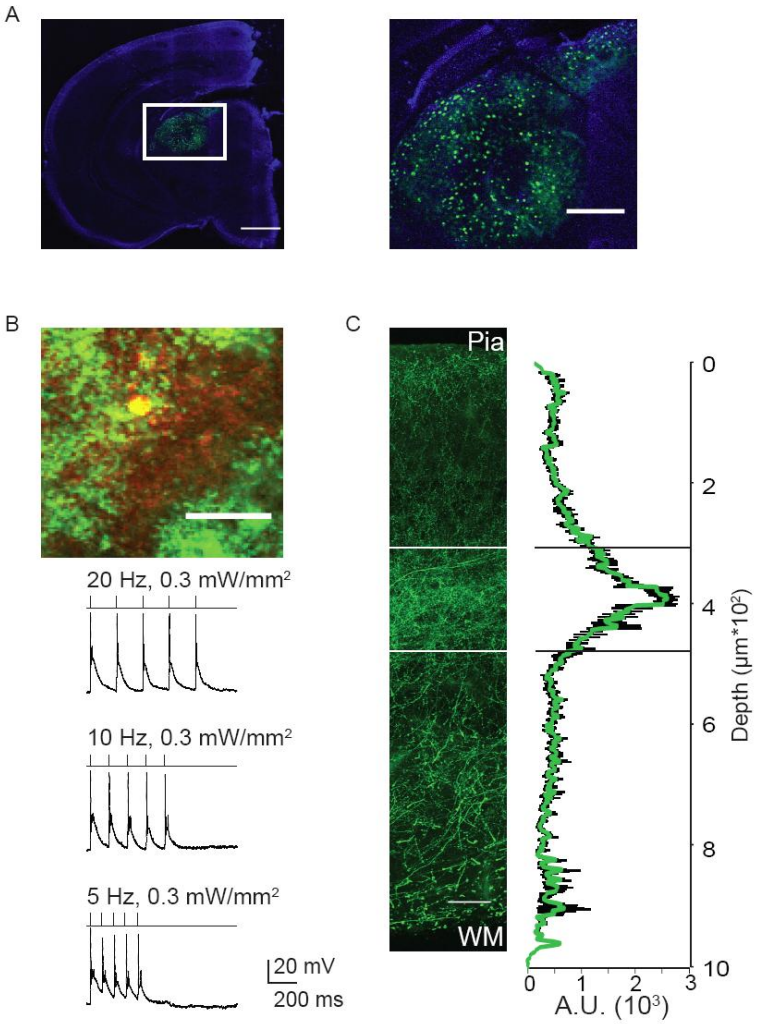

Figure 3.1. Expression of ChR2-GFP in LGN and V1. **A.** Left. Representative histology of a section showing expression of ChR2-GFP at P27 (injection at P15). Green: ChR2-GFP; blue: DAPI. Scale bar = 1mm. Right. Enlarged image of the region indicated by the white square in the image on the left. Scale bar = 40 µm. **B.** Top. Slice of LGN expressing ChR2-GFP and containing a recorded neuron (indicated by the arrowhead). The somatic expression of the injected construct (green) is colocalized with the biocytin staining (red), thus the recorded neuron appears yellow. Scale bar = 40 µm. Bottom. Light evoked action potentials in the LGN neuron shown in the top image. Light stimulus intensity: 0.3 mW/mm^2. Trains of light pulses at 5 Hz, 10 Hz and 20 Hz were delivered while the neuron was recorded in the presence of AMPA and NMDA receptor blockers to ensure that the action potentials depended on the activation of the light gated protein. **C.** Left. Expression of ChR2-GFP in the LGN terminal fields in V1. Right. Calibration curve of GFP intensity across the cortical mantle (see Methods). Green: average GFP intensity across 15 slices from 6 animals; black traces: ± 1 standard deviation from the average fluorescence calculated across the 15 slices. Scale bar = 100 µm.

LGN inputs have cell type specific properties in layer 4 of V1.

Anatomical evidence suggests that the LGN directly innervates both pyramidal and inhibitory neurons in L4 (Freund et al., 1985; Ahmed et al., 1994, 1997; Erisir and Dreusicke, 2005), but whether LGN inputs onto distinct neuron types differ in their synaptic properties has not been investigated. To address this, we recorded from pyramidal (Pyr) and two distinct populations of inhibitory neurons and compared their synaptic responses to activation of LGN terminal fields. Light activation of LGN axons elicited reliable thalamocortical postsynaptic currents (TC-EPSCs) in every pyramidal (Pyr; Fig. 3.2 A, D) and fast spiking (FS; Fig. 3.2 B, D) neuron recorded. In a subset (3 out of 6) of regular spiking non pyramidal neurons (RSNP), a small but reliable current was also detected (Fig 3.2 C, D). When the latency from stimulus onset of postsynaptic responses was quantified and compared across cell types, only responses from Pyr and FS neurons were consistent with monosynaptic inputs, while responses in the RSNP were not (Fig 3.2 E; Pyr: 1.62 ± 0.05 ms; n = 29; FS: 1.34 ± 0.1 ms; 242 n = 15; RSNP: 7.34 ± 0.2 ms; n = 6). The three distinct neuron types were often recorded simultaneously using quadruple patch clamp, thus the differences observed are not due to artifacts of light stimulation or inconsistencies across preparations. Together, these results support the interpretation that Pyr and FS neurons receive strong and reliable LGN inputs with delay from stimulus compatible with monosynaptic connections, while RSNP neurons do not.

Because they receive reliable LGN inputs compatible with the presence of monosynaptic connections, we focused our analysis on the comparison of synaptic properties and dynamics of TC responses evoked onto Pyr and FS neurons. TC-EPSCs recorded from Pyr neurons had significantly slower rise and decay time constants than those recorded from FS neurons (Rise Time, Pyr: 1.76 ± 0.08 ms; n = 29; FS: 0.9 ± 0.09 ms; n = 15; unpaired t-test: $p < 0.001$; Decay

Time Constant, Pyr: 12.1 ± 0.9 ms; FS: 6.4 ± 0.4 ms; $p < 0.001$). Stimuli with increasing light intensity (0.1 - 0.3 mW/mm^2) were used to examine the input/output relationship of LGN inputs onto Pyr and FS neurons. The amplitude of TC-EPSCs onto FS neurons was significantly larger than those onto Pyr neurons for all stimulus intensities except for the lowest (Fig 3.3 A, B, C; 0.1 mW/mm^2, Pyr: 160 ± 39.3 pA; FS: 236.4 ± 132.7; $p = 0.07$; 0.15 mW/mm^2, Pyr: 217.04 ± 42.9 pA; FS: 541.9 ± 134.8 pA; $p < 0.02$; 0.2 mW/mm^2, Pyr: 269.1 ± 37.8 pA; FS: 680.1 ± 154.5 pA, $p < 0.03$; 0.3 mW/mm^2, Pyr: 328.3 ± 41.9 pA, FS: 1009.56 ± 169.2; $p < 0.05$; Pyr: $n = 29$; FS: $n = 15$). Furthermore, the slope of the input/output curve was steeper for FS than Pyr neurons (Pyr: 0.83 nA/mW; FS: 2.91 nA/mW; $p < 0.05$). These results suggest that a single incoming stimulus would likely activate the feedforward inhibitory circuit more effectively than the excitatory circuit.

We next examined the short term dynamics of TC-EPSCs to assess how trains of stimuli may engage feedforward excitatory and inhibitory circuits. We chose to use a 10 Hz frequency of repetitive stimulation, because this frequency is reliably followed by the kinetics of activation and inactivation of ChR2 (Zhang et al, 2006; Gu et al., 2012; Wang et al., 2013), and is reliably followed by LGN neurons (see Fig. 3.1 B). In response to trains of 5 light pulses we observed short term depression of TC-EPSCs of different magnitude depending on the postsynaptic target. TC- EPSCs onto FS neurons showed a larger initial TC-EPSC followed by much smaller subsequent events. Pyramidal neurons showed a less dramatic decrease in amplitude of successive TC- EPSCs (Fig. 3.3 D). These distinct short term dynamics resulted in significantly different paired pulse ratios (EPSC2 / EPSC1; PPR) and steady state ratios (EPSC5 / EPSC1; SSR) between neuron types (PPR, Pyr: 0.66 ± 0.04; FS: 0.56 ± 0.05; $p < 0.01$; SSR, Pyr: 0.38 ± 0.03; FS: 0.25 ± 0.03; $p < 0.006$; Pyr: $n = 29$; FS: $n = 15$). Thus, LGN inputs onto Pyr and FS

neurons differ in both synaptic strength and short term dynamics.

Before analyzing the specific synaptic mechanisms determining TC-EPSCs cell type-specific properties, we assessed how repetitive activation of TC terminal fields may affect the ability to fire action potentials in Pyr and FS neurons. To do that, Pyr and FS neurons were recorded in current clamp. Pyr and FS neurons showed detectable TC-EPSPs at all stimulus intensities (Fig 3.4 A, B). However, every recorded FS neuron fired at least one action potential at both the minimum and maximum light intensity (Fig 3.4 C, 14 out of 14). Conversely, 23.8% (Fig 3.4 C, 15 out of 63; Pearson χ^2: $p < 0.02$) of Pyr neurons fired an action potential at the lowest light intensity, and only 44 % (Fig 3.4 C, 28 out of 63; Pearson χ^2: $p < 0.05$) fired at least one action potential at the highest light intensity. The ratio of action potentials per light stimulus was used to calculate a spike reliability ratio (SRR). At all stimulus intensities, FS neurons fired significantly more action potentials per light stimulus than pyramidal neurons (Fig 3.4 D; SRR, 0.1mW/mm^2, Pyr: 0.09 ± 0.03; FS: 0.62 ± 0.16; unpaired t-test: $p < 0.03$; 0.15 mW/mm^2, Pyr: 0.1 ± 0.03; FS: 1 ± 0.001; $p < 0.001$; 0.2 mW/mm^2, Pyr: 0.16 ± 0.04; FS: 1.56 ± 0.2; $p < 0.001$; 0.3 mW/mm^2, Pyr: 0.3 ± 0.05; FS: 1.7 ± 0.2; $p < 0.001$; Pyr: $n = 63$; FS: $n = 14$). The difference in the ability of LGN inputs to drive Pyr and FS neurons above threshold did not depend on differences in resting input resistance as FS input resistance was lower than that of Pyr neurons (Ri, Pyr: 192 ± 10 MΩ; FS: 138 ± 8 MΩ; unpaired t-test: $p < 0.02$). We hypothesized that the ability of Pyr neurons to fire action potentials in response to LGN terminal field activation may be shunted by feedforward inhibition. Consistent with this, partial blockade of GABAA receptors with bath application of picrotoxin (10 μM) allowed all recorded Pyr neurons to fire action potential in response to a single light pulse at 0.1 mW/mm^2 (Fig 3.4 A, gray overlay; 10 out of 10 Pyr). These data indicate that TC afferents drive feedforward

inhibition in V1 more effectively than feedforward excitation, and that feedforward inhibition acts as a brake on LGN activation of V1 pyramidal neurons.

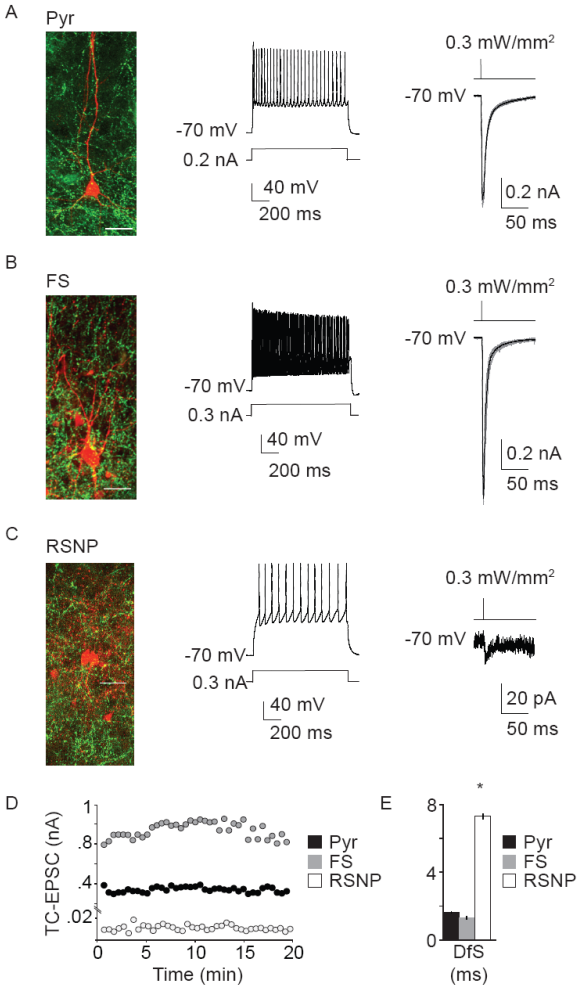

Figure 3.2. Monosynaptic inputs from the LGN onto pyramidal and FS neurons. **A.** Left. Post hoc reconstruction of a L4 pyramidal neuron (green: ChR2-GFP; red: biocytin - Alexa Fluor 594 as in B and C left panels). Middle. Firing pattern of the Pyr neuron on the left in response to a 0.2 nA – 1 s square current step. Right. Light evoked TC-EPSCs recorded from the neuron shown on the left panel (light pulse: 2 ms, 0.3 mW/mm^2, same for right panels in B and C and for panel D). Gray: single traces; black: average of 30 traces. **B.** Left. FS neuron recorded in L4 of V1. Middle. Firing pattern of the FS neuron on the left in response to 0.3 nA – 1 s square current step. Right. Light evoked TC-EPSC recorded from the FS neuron on the left. Gray: single traces; black: average of 30 traces. **C.** A. Left: post hoc reconstruction of a RSNP neuron recorded in L4. Middle. Firing pattern of the L4 RSNP shown on the left in response to a 0.2 nA current pulse. Right. TC-EPSC evoked by a brief light pulse and recorded from the RSNP neuron on the left. Gray: single traces; black: average of 30 traces. **D.** Time course of light evoked TC-EPSCs for neurons shown in A (black), B (gray), and C (white) indicating that responses were stable over time. **E.** Average TC-EPSC latency from stimulus onset for Pyr, FS, and RSNP neurons. Data are presented as mean ± SE. Asterisks indicate significant differences.

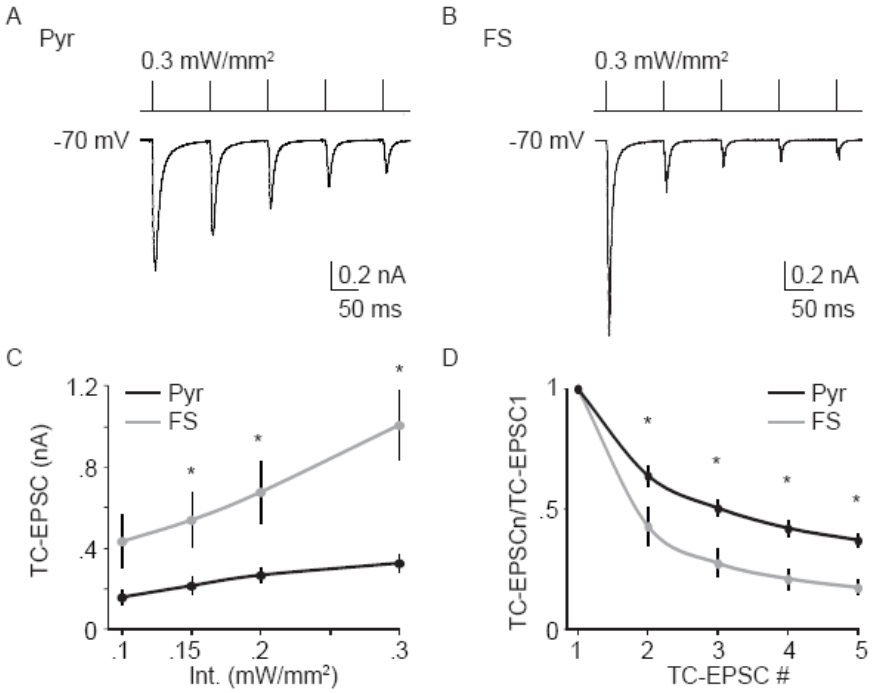

Figure 3.3. Distinct input/output curves and short term dynamics of TC-EPSCs onto FS and Pyr neurons. **A.** Sample TC-EPSCs recorded from L4 Pyr neurons, in response to a train of 5 light pulses at 10 Hz. Light pulses, intensity: 0.3 mW/mm^2. **B.** Sample TC-EPSCs recorded from L4 FS neurons in response to a train of 5 light pulses at 10 Hz. Light pulses intensity: 0.3 mW/mm^2. **C.** Input/ output curves for L4 Pyr (black) and FS (gray). **D.** Normalized amplitude of TC-EPSC in the train for Pyr (black) and FS (gray) neurons. Data are presented as mean ± SE. Asterisks indicate significant differences.

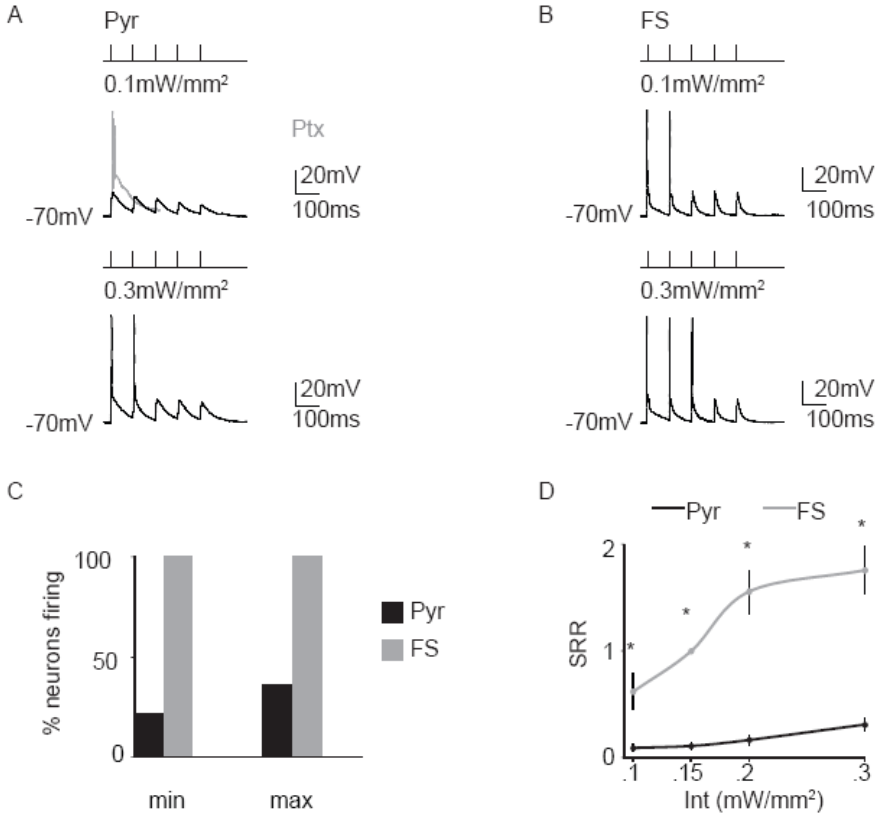

Figure 3.4. Feedforward inhibition prevents Pyr neurons from firing action potentials. A. Top. TC-EPSPs recorded from a Pyr neuron in current clamp (light pulses intensity: 0.1 mW/mm^2) in the absence (black) and in the presence of picrotoxin (10 μM; gray). Bottom. TC-EPSPs recorded from a Pyr neuron in response to light pulses with the highest stimulus intensity (0.3 mW/mm^2). **B.** Top. TC-EPSPs recorded from a FS neuron in current clamp at the lowest stimulus intensity (0.1 mW/mm^2). Bottom. TC-EPSPs from a FS neuron evoked using the highest stimulus intensity (0.3 mW/mm^2). **C.** Percentage of Pyr (black) and FS (gray) neurons that fired at least one action potential in response to light stimuli at the minimum (0.1 mW/mm^2) and maximum (0.3 mW/mm^2) light intensity. **D.** Spike reliability ratio, defined as the number of action potentials / light pulse, quantified for Pyr (black) and FS (gray) neurons as a function of the stimulus intensity. Data are presented as mean ± SE. Asterisks indicate significance.

Cell type specific postsynaptic differences of TC-EPSCs in V1.

Our findings so far suggest that LGN inputs onto Pyr and FS neurons in L4 of V1 show differences in kinetics, strength and short term dynamics. The differences in decay kinetics and average amplitude suggest that these inputs may be driving different receptor types on Pyr and FS neurons. To assess the contribution of different glutamatergic receptors to the TC-EPSC recorded from Pyr and FS neurons, we sequentially and additively applied blockers for AMPA and NMDA receptors (20 μM DNQX and 50 μM APV). For these experiments the TC terminal fields were stimulated using minimal light intensity to limit the contribution of the recurrent circuit to the evoked response. Neurons were recorded at -70 mV to isolate the component of the TC-EPSC driven by AMPA receptors (AMPAR) and at +40 mV to isolate the NMDA receptor (NMDAR) component. After acquisition of a 10 minute baseline in regular ACSF, 20 μM DNQX was bath applied for 10 - 15 minutes. After that, a mix of 20 μM DNQX and 50 μM APV was perfused. The AMPAR and NMDAR mediated currents were then isolated and analyzed following offline subtraction (Fig 3.5 A, B). TC-EPSCs onto Pyr neurons comprised both an NMDAR and an AMPAR mediated component (Fig 3.5 C; NMDAR-mediated: 54.9 ± 10.3 pA; AMPAR-mediated: 244.2 ± 45.7 pA; n = 10). The NMDAR component accounted for about one third of the TC-EPSC (Fig. 3.5 D; NMDA / AMPA: 0.27 ± 0.06, n = 10). The AMPAR – mediated current showed no rectification at +40 mV suggesting that TC-EPSCs onto L4 Pyr neurons contain the AMPAR subunit GluA2 (Boulter et al., 1990; Verdoorn et al., 1991; Jonas and Burnashev, 1995). Differently, bath application of 20 μM DNQX completely blocked the TC-EPSC onto FS neurons, indicating that NMDAR did not contribute to the TC-EPSCs onto FS (Fig 3.5 C, AMPAR: 554.6 ± 90.7 pA, n = 5). No AMPAR and NMDAR-dependent components were detected at +40 mV, indicating that TC-EPSCs onto FS are mediated by Ca^{2+}-permeable

GluA2-lacking AMPAR (Bowie and Mayer, 1995; Geiger et al., 1995), and lack NMDAR (Fig. 3.5 D; the NMDA / AMPA ratio for FS neurons was equal to 0). All FS neurons were recorded simultaneously with Pyr neurons, thus the differences observed cannot be ascribed to possible inconsistencies in the experimental preparation.

We further analyzed TC-EPSCs to identify possible additional mechanisms contributing to the differences in the AMPAR – mediated component of TC-EPSCs onto Pyr and FS neurons. We used peak-scaled non-stationary noise analysis of TC-EPSCs recorded at -70 mV in the presence of 50 μM APV and evoked by minimal light intensity (0.1 mW/mm^2) to assess possible differences in single channel current and number of open channels contributing to the AMPA current of the TC-EPSC (Sigworth, 1980; Traynelis and Jaramillo, 1998; Hartveit and Veruki, 2007). The peaks of 10 evoked TC-EPSCs were scaled to the average peak amplitude (Fig 3.6 A, B), and the variance (σ^2) during the decay phase was measured and plotted against the average amplitude (Fig. 3.6 C, D). The plots were fitted with a parabolic curve (Fig. 3.6 C, D; equation inset), and values for unitary current (i_u) and number of open channels (N_o) were estimated from the equation. This analysis showed that TC-EPSCs onto Pyr neurons were mediated by a large number of open channels passing a small unitary current (Fig 3.6 E; Pyr, N_o: 101.9 ± 21.9; i_u: 4.01 ± 1.48 pA; n = 11); differently, TC-EPSCs onto FS neurons were mediated by a small number of open channels with large unitary current (Fig 3.6 E; FS, N_o: 22.7 ± 3.6; i_u: 26.2 ± 6.1 pA; n = 6). Statistical comparisons of number of open channels and unitary currents between cell types indicated significant differences (unpaired t-test, N_o: $p < 0.02$; i_u: $p < 0.02$). Taken together these data demonstrate that differences in receptor composition, number of open channels and single channel conductance explain part of the cell type-specific properties of TC- EPSCs in L4 of V1.

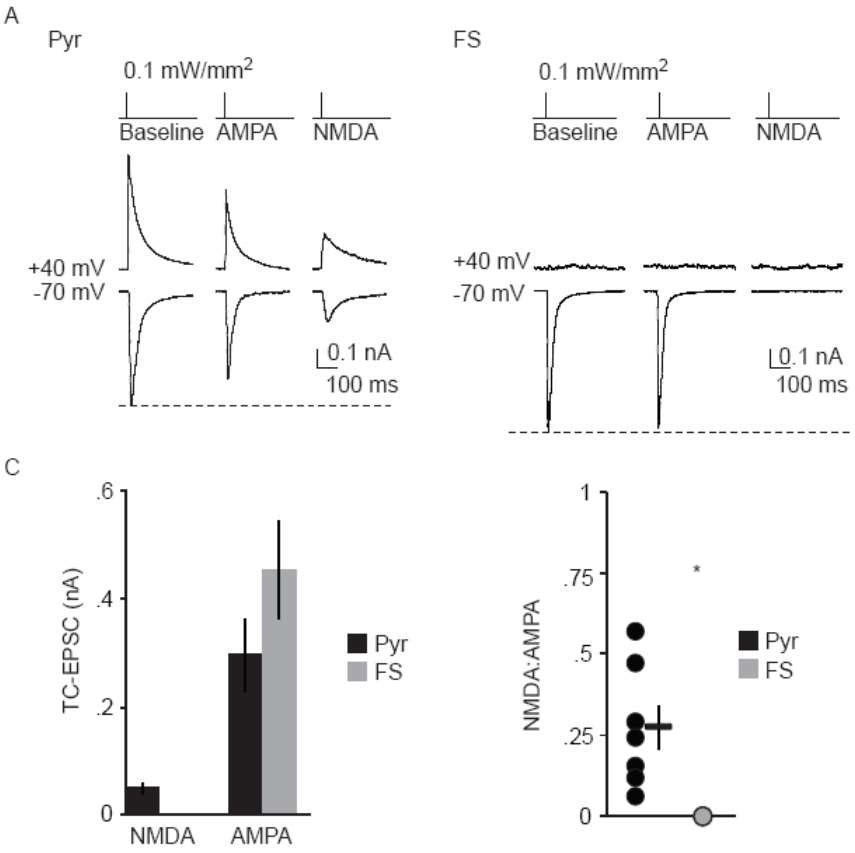

Figure 3.5. Different postsynaptic receptor contributions to TC-EPSCs onto Pyr and FS neurons. **A.** TC-EPSCs (light intensity: 0.1 mW/mm^2) recorded at -70 mV and +40 mV to isolate baseline (left), AMPAR - mediated (middle), and NMDAR-mediated (right) currents onto a Pyr neuron. **B.** TC-EPSCs (light intensity: 0.1 mW/mm^2) recorded at -70 mV and +40 mV to isolate baseline (left), AMPAR - mediated (middle), and NMDAR - mediated (right) currents onto a FS neuron. **C.** Average amplitude of NMDAR - and AMPAR - mediated currents from Pyr (black) and FS (gray) neurons. Data are presented as mean ± SE. **D.** NMDA / AMPA current ratio for Pyr (black) and FS (gray) neurons. Circles show individual ratios; the black bar shows mean ± SE. Asterisks indicate significant differences.

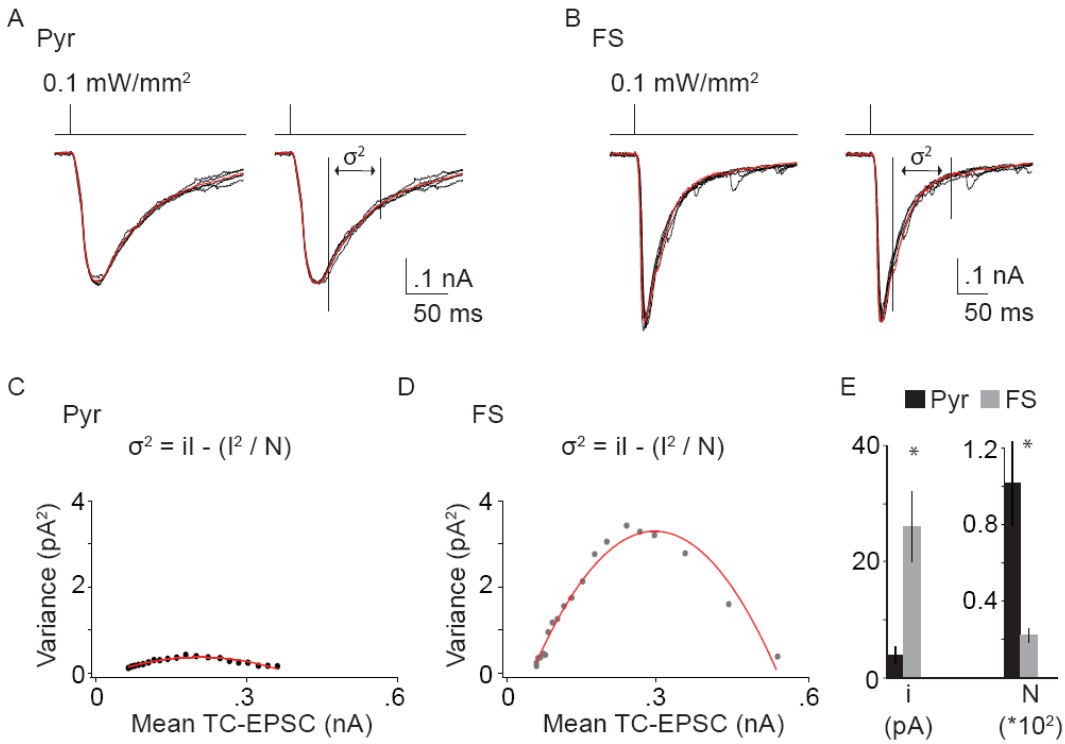

Figure 3.6. Cell type-specific single channel conductance and number of open channels at LGN synapses onto Pyr and FS neurons. **A.** Raw traces of TC-EPSCs recorded from one Pyr neuron (black) overlayed by their average TC-EPSC (red). The left panel shows an example of variation around the mean amplitude; while the right panel shows the peak-scaled variation around the mean (right). Vertical lines in the right panel indicate the region of the decay phase where the variance was measured. Light intensity: 0.1 mW/mm^2. **B.** Raw traces of TC-EPSCs recorded from one FS neuron (black) overlayed by their average TC-EPSC (red). The left panel shows an example of variation around the mean amplitude; while the right panel shows the peak scaled variation around the mean (right). Vertical lines in the right panel indicate the region of the decay phase where the variance was measured. Light intensity: 0.1 mW/mm^2. **C.** Peak-scaled decay phase variance (bin size: 2 ms) plotted against the mean Pyr (left panel, black dots) and FS neurons (right panel, gray dots), and fitted with a parabolic curve (red). The curve equation is shown above the graphs. The fit was used to estimate values for unitary current (i_u) and number of open channels (N_o). **E.** Bar graph comparing iu and No for Pyr (black) and FS (gray) neurons. Data are presented as mean ± SE. Asterisks indicate significant differences.

Cell type-specific presynaptic properties of LGN inputs in L4 of V1.

TC-EPSCs in L4 of V1 show cell type-specific short term depression. This suggests that presynaptic mechanisms may also contribute to differentiate these inputs (O'Donovan and Rinzel, 1997; Stevens and Wesseling, 1998). To compare presynaptic properties we recorded TC-EPSCs onto Pyr and FS neurons in the presence of strontium chloride ($SrCl_2$, 10 mM). $SrCl_2$ desynchronizes release sites (Goda and Stevens, 1994; Bartley et al., 2008) and can be used to assess the number of release sites of a specific synapse (Gil et al., 1999; Daw et al., 2009; Hull et al., 2009). Following bath application of $SrCl_2$ there was a significant reduction of TC-EPSCs amplitude onto both Pyr and FS neurons (Fig 3.7 A, B, C; Pyr, baseline: 408.5 ± 62.2 pA; $SrCl_2$: 332.2 ± 47.7 pA; FS, baseline: 675.8 ± 102.9 pA, $SrCl_2$: 505.03 ± 89.05 pA; unpaired t-test: $p < 0.04$; Pyr: $n = 17$; FS: $n = 6$). The magnitude of the decrease was significantly larger for TC-EPSCs onto FS than Pyr neurons (One way ANOVA: $p < 0.03$). $SrCl_2$ application did not affect response latency (Pyr, baseline: 2.54 ± 0.09 ms; $SrCl_2$: 2.65 ± 0.09 ms; unpaired t-test: $p = 0.5$; FS, baseline: 1.93 ± 0.17 ms; $SrCl_2$: 2.16 ± 0.07 ms; $p = 0.12$), or rise time (Pyr, baseline: 1.9 ± 0.12 ms; $SrCl_2$: 2.1 ± 0.15 ms; $p = 0.2$; FS, baseline: 0.96 ± 0.16 ms; $SrCl_2$: 1.03 ± 0.17; unpaired t-test: $p = 0.23$). Application of $SrCl_2$ also led to prolonged TC-EPSCs with multiple events becoming detectable during the decay phase. When the distribution of the number of events on the tail of TC-EPSCs was quantified and compared between Pyr and FS neurons we observed that a significantly larger number of events was detectable in FS (Fig 3.7 D). The larger amplitude decrease and number of events following $SrCl_2$ strongly suggest that TC-EPSCs onto FS neurons depend on the activation of a larger number of release sites compared to those activated onto Pyr neurons.

In order to further understand the presynaptic mechanisms that differentiate LGN inputs onto L4

Pyr and FS neurons we compared the coefficient of variation (CV) of TC-EPSCs before and after bath application of $SrCl_2$. The baseline CV of TC-EPSCs onto both Pyr and FS neurons was already quite low suggesting that LGN inputs on both neuron types have a high release probability. However, the CV of TC-EPSCs onto FS neurons was significantly lower than that onto Pyr neurons (Fig 3.7 E; baseline CV, Pyr: 0.12 ± 0.01; FS: 0.07 ± 0.01; unpaired t-test: $p < 0.006$; Pyr: $n = 17$; FS: $n = 6$). This indicates that LGN inputs onto FS neurons likely have a higher release probability than those onto Pyr neurons in response to a single stimulus. After $SrCl_2$ application, the CV of TC-EPSCs onto Pyr neurons decreased significantly (Fig 3.7 E; $SrCl_2$, Pyr: 0.07 ± 0.01; paired t-test against baseline CV: $p < 0.01$), suggesting that TC-EPSCs onto Pyr neurons are mediated by the activation of a small number of inputs composed of few, highly reliable release sites (Freund et al., 1985; Stratford et al., 1996). Although the amplitude of TC-ESPCs onto FS neurons was significantly reduced by $SrCl_2$, their CV remained unaltered (Fig 3.7 E; $SrCl_2$, FS: 0.067 ± 0.005), suggesting that this input is mediated by clusters of highly reliable release sites (Bagnall et al., 2011).

Quantal analysis of TC-EPSCs before and after $SrCl_2$ application was performed to further determine what mechanisms could account for the decrease in amplitude observed in TC-EPSCs onto FS neurons: release probability (p), quantal size (q), or number of release sites (n; Sola, et al 2004). As shown in figure 3.7 F, all of the data points for TC-EPSCs onto FS neurons fell on or close to the unity line, suggesting that $SrCl_2$ affected mostly the number of release sites at the LGN-FS synapse. As for Pyr neurons the single data points were more scattered, although their average value was also positioned on the unity line. This suggests that $SrCl_2$ at the LGN-Pyr neuron synapse affects the number of release sites simultaneously activated by the light stimulus, but that additional effects of $SrCl_2$ on release probability may also be involved.

Spearman rank order correlation analysis was used to determine whether the magnitude of the effect of $SrCl_2$ was correlated with the baseline amplitude of TC-EPSCs. Pyr neurons showed no significant correlation (Rs: 0.39, $p = 0.11$), consistent with the small or no effect of $SrCl_2$ on the amplitude of TC-EPSC on most (14 out of 17) Pyr neurons recorded (Fig 3.7 G, Rs: 0.15; $n = 17$). Differently, FS neurons showed a significant correlation between the initial TC-EPSC amplitude and the magnitude of the effect of $SrCl_2$ (Fig 3.7 H; Rs: 0.83; $p < 0.05$; $n = 6$). These results support the interpretation that the amplitude of the TC-EPSC onto FS depends on the number of release sites located at the LGN terminals onto FS synapse. All FS neurons were recorded simultaneously with pyramidal neurons and only the lowest stimulus intensity was used for these experiments (0.1 mW/mm^2) to minimize the contribution of recurrent intracortical circuits. Our results indicate that LGN inputs onto pyramidal and FS neurons rely on target-specific presynaptic and postsynaptic mechanisms. Thus, differences in LGN activation of Pyr and FS neurons may account at least in part for their distinct functional properties.

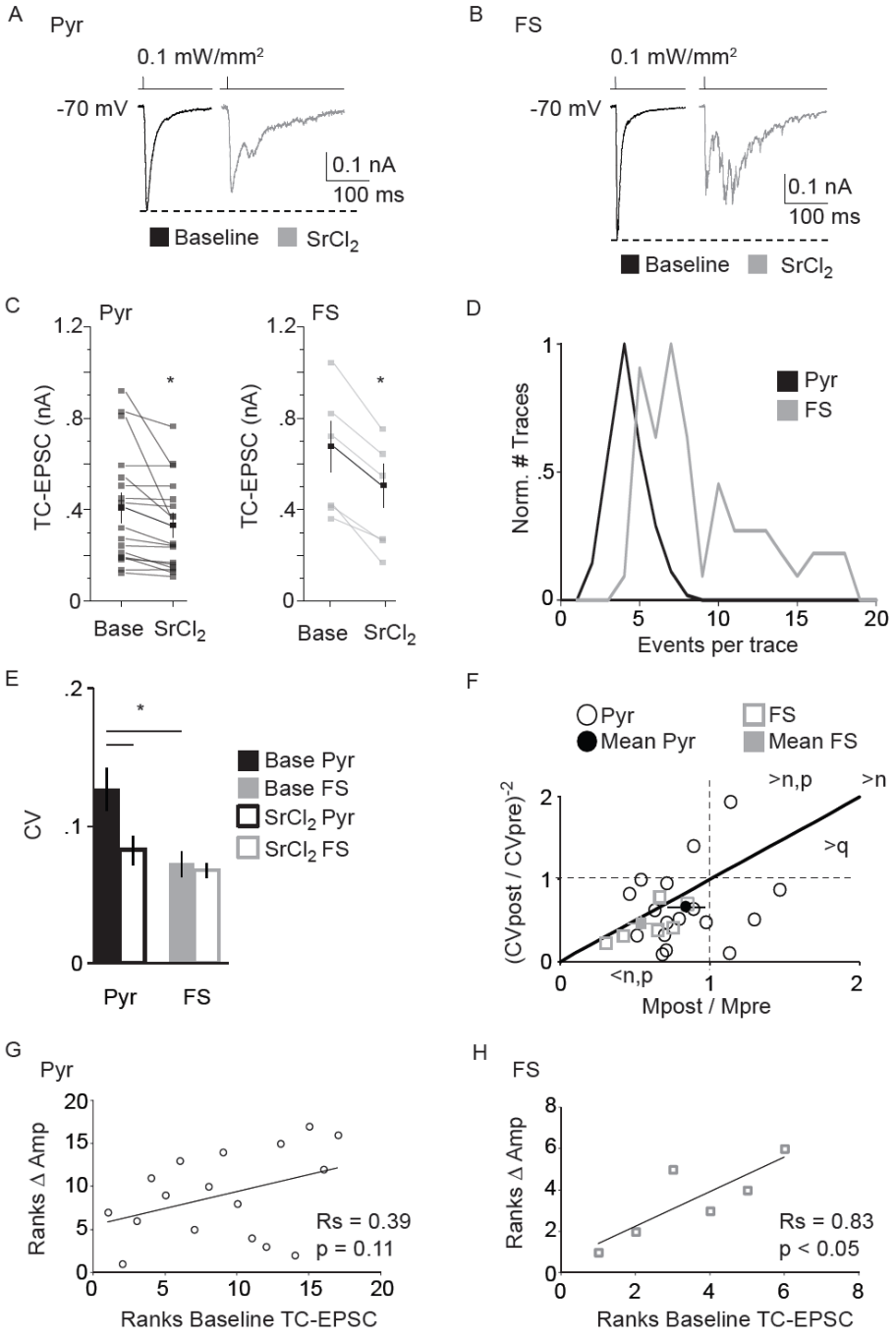

Figure 3.7. Physiological evidence for target-specific presynaptic properties at LGN-V1 inputs. **A.** Left. Average TC-EPSC recorded from one Pyr neuron before (baseline; black) application of $SrCl_2$. Right. Single evoked TC-EPSC recorded from the same Pyr neuron in the presence of 10 mM $SrCl_2$/ 0 mM $CaCl_2$ (gray). Light stimulus, 0.1 mW/mm^2. **B.** Left. Average TC-EPSC (black) recorded from one FS neuron before perfusion of SrCl2. Right. Single evoked TC-EPSC recorded from the same FS neuron in the presence of 10 mM $SrCl_2$/ 0 mM $CaCl_2$ (gray). Light stimulus, 0.1 mW/mm^2. **C.** Effect of strontium on the amplitude of TC-EPSCs for Pyr (left; dark gray) and FS (right; light gray) neurons, the average effect for both neuron types is shown in black in both plots. The dark gray and light gray markers indicate single recordings for

Pyr and FS neurons respectively. **D.** Distribution of the number of events in the 200 ms time window following the onset of the stimulus (the first evoked TC-EPSC is excluded from the count). Black: Pyr; gray: FS. Bin size, 1 event. **E.** Coefficient of variation (CV) of the amplitude of the first evoked TC-EPSC before (Filled bars) and after (open bars) application of $SrCl_2$/ 0 mM $CaCl_2$ for Pyr (black) and FS (gray) neurons. Data are presented as mean ± SE. Asterisks indicate significant difference. **F.** Graphic representation of quantal analysis of TC-EPSC amplitudes. Black open circles: data from each Pyr neuron, black filled circle: Pyr average. Gray open squares: data from each FS neuron; filled gray square: FS average. CV pre: baseline CV; CV post: CV after $SrCl_2$/ 0 mM $CaCl_2$; M pre: mean baseline TC-EPSC amplitude; M post: mean TC-EPSC after $SrCl_2$/ 0 mM $CaCl_2$; n: number of release sites; p: release probability; q: quantal size; solid line: unity line. Average data are presented as mean ± SE. **G.** Spearman rank order correlation of baseline TC-EPSC amplitude onto Pyr neuron versus the change in TC-EPSC amplitude in $SrCl_2$/ 0 mM $CaCl_2$. **H.** Spearman rank order correlation of the baseline TC-EPSC amplitude onto FS neurons versus the change in TC-EPSC amplitude in $SrCl_2$/ 0 mM $CaCl_2$. For G and H, Rs: Spearman coefficients; p values < 0.05 indicate significant correlations.

Discussion

We have analyzed the properties of LGN synapses onto Pyr and FS neurons in L4 in V1. LGN inputs onto Pyr and FS neurons presented some similarities – they were powerful, reliable, and showed short term depression in response to repetitive stimulation – but relied on distinct presynaptic and postsynaptic mechanisms. A larger proportion of FS neurons reliably fired action potentials at all stimulation intensities, indicating that single incoming stimuli likely activate feedforward inhibitory circuitry more effectively than excitatory circuits. This is consistent with previous findings showing that in vivo putative inhibitory neurons show higher activity evoked by visual stimuli than excitatory neurons (Zhuang et al, 2013). TC-EPSCs onto FS neurons were larger and depressed more in response to repetitive stimulation than TC-EPSC onto Pyr neurons suggesting that stimuli containing trains of spikes could successfully overcome feedforward inhibition and drive excitatory neurons.

TC-EPSC onto Pyr and FS neurons showed target-specific pre- and postsynaptic properties. LGN synapses onto Pyr neurons activated both NMDAR and AMPAR. The AMPAR – mediated current had similar amplitude at positive and negative potentials, indicating a contribution of calcium impermeable AMPAR (Boulter et al., 1990; Verdoon et al., 1991; Jonas and Burnashev, 1995). The NMDAR – mediated current was large at -70 mV, suggesting that these receptors contain Mg^{2+} insensitive subunits and contribute to evoked responses at resting membrane potential (Fleidervish et al., 1998; Binshtok et al., 2006). LGN synapses onto FS lacked a NMDAR - mediated currents and contained inwardly rectifying AMPAR - mediated currents, indicating that these receptors lack the GluA2 subunit, and are likely calcium permeable (Bowie and Mayer, 1995; Geiger et al., 1995). Peak-scaled non-stationary noise analysis of the AMPAR mediated current showed that TC-EPSCs onto Pyr neurons resulted from the activation of many

open channels with small unitary current, consistent with the presence of GluA2 containing AMPA receptors (Swanson et al., 1997). Differently, TC-EPSCs onto FS neurons depend on a small number of open channels with large unitary current, consistent with the presence of GluA2-lacking AMPARs (Hestrin et al., 1993).

The differences in short term dynamics and the effects of strontium chloride on TC-EPSCs indicate that LGN inputs have target specific presynaptic properties, too. Strontium chloride induced small, although significant, changes in the amplitude of TC-EPSCs onto Pyr neurons. Few quantal events were detected after the first evoked response, suggesting that LGN synapses onto Pyr neurons contain a small number of powerful release sites. This is consistent with the shallow slope of the input/output curve for TC-EPSCs onto Pyr neurons, their low coefficient of variation, and with previous reports that single LGN axons make a small number of synaptic contacts with L4 excitatory neurons in V1 (Freund et al., 1985; Peters and Payne, 1993; Da Costa and Martin, 2009). The amplitude of TC-EPSCs onto FS neurons was reduced by one third to one half by strontium chloride. Up to 20 quantal events could be detected in the window following the onset of the light stimulus. The magnitude of the effect of strontium strongly correlated with baseline TC-EPSC amplitude, suggesting that at LGN-FS synapses the larger the TC-EPSC, the higher the number of release sites activated by a stimulus. Combined with lack of changes in CV following strontium chloride, these results suggest that LGN-FS synapses contain clusters of release sites that account for one third to one half of the amplitude of a TC-EPSC (Bagnall et al., 2011). This interpretation fits well with the observation that the input/output curve of TC-EPSCs onto FS neurons has a steeper slope than that for Pyr neurons.

Our results demonstrate that LGN afferents engage target-specific pre- and postsynaptic mechanisms to activate feedforward excitatory and inhibitory circuits in L4 of V1. LGN inputs

in principle carry the same information. Target specific synaptic properties may contribute at least in part to explain why Pyr and FS neurons present distinct responsiveness to incoming stimuli (Bruno and Simons, 2002; Contreras and Palmer, 2003; Swadlow, 2003; Alonso and Swadlow, 2005; Cardin et al., 2007). FS neurons have lower input resistance and higher spike threshold than Pyr neurons, but the large amplitude of TC-EPSCs they receive is quite effective at driving them above threshold. This is likely due to the organization of LGN inputs on FS neurons, which, according to our analysis, is consistent with the presence of clusters of release sites (Bagnall et al., 2011) with high release probability that activate few postsynaptic channels with large conductance. It is also consistent with the finding that FS neurons receive powerful direct inputs from retinotopically aligned LGN neurons (Zhuang et al, 2013). The powerful short term depression, fast rise and decay kinetics and lack of NMDAR at LGN-FS synapses is likely contributing to evoking fast and precisely timed responses to visual stimuli. These properties likely narrow the temporal window of activation of these neurons (Jonas et al., 2004). In our experiments FS neurons were driven above threshold even by relatively weak light pulses. The large evoked TC-EPSCs are consistent with previous reports that inhibitory neurons directly driven by the LGN respond more strongly than excitatory neurons to visual stimuli (Zhuang et al, 2013). Differently, LGN-Pyr neuron synapses rely on few powerful release sites which activate a large number of channels with small conductance. The moderate short term depression of these inputs, the presence of NMDAR on postsynaptic terminals, and the control of feedforward inhibition on their ability to fire action potentials may explain favoring Pyr neurons narrower tuning to visual stimuli. The target specific properties of TC inputs onto FS and Pyr neurons may provide a synaptic mechanism to explain the broader tuning of FS neurons for stimulus orientation, direction, and spatial and temporal frequency of visual stimuli observed *in vivo*

(Zhuang et al, 2013).

Co-activation of feedforward excitatory and inhibitory neurons by TC afferents is thought to be critical for regulating precision of cortical neurons activation and cortical excitability. The properties of LGN-FS neuron inputs suggest that this feedforward inhibitory circuit provide a "window of excitability" (Swadlow, 2003) that ensures temporal precision of the transformation of synaptic inputs into neuronal firing rates (Wehr and Zador, 2003; Gabernet et al., 2005; Priebe and Ferster, 2005). The high spike reliability ratio of FS neurons in response to LGN terminal field activation supports the interpretation that LGN inputs successfully drive pyramidal neurons above threshold in a narrow window preceding the arrival of the inhibitory signal from FS neurons.

LGN-FS neuron synapses may also regulate circuit excitability by preventing runaway excitation (Swadlow, 2003; Sun et al., 2006). Indeed, blockade of inhibition increased the ability of L4 Pyr neurons to fire action potentials. Finally, the activation of synapses containing NMDAR versus Ca^{2+} permeable AMPAR provide a differential mode of regulation of intracellular calcium dynamics (Geiger et al., 1995; Dingledine et al., 1999), which can drive distinct signaling mechanisms for synaptic plasticity (Isaac et al., 2007; Gainey et al., 2009). As a consequence, the different mechanisms of activation of LGN inputs onto Pyr and FS neurons may provide a substrate for connection-specific plasticity in L4 of V1.

When our results are compared with findings from other sensory areas, it becomes evident that LGN inputs onto L4 of V1 present some similarities, but also significant differences. In S1 and A1, TC inputs onto excitatory neurons activate AMPAR and NMDAR on postsynaptic terminals (Rose and Metherate, 2005; Hull et al., 2009; Schiff and Reyes, 2012). The AMPAR mediated components onto excitatory neurons has similar properties to those we report in V1. In S1 and

V1 the NMDAR - mediated component of the TC-EPSC can be detected at negative potentials, that these TC inputs activate NMDAR with low sensitivity to Mg^{2+} block (Fleidervish et al., 1998; Binshtok et al., 2006; Hull et al., 2009).

Similar to S1 and A1, stimulation of LGN inputs onto FS neurons evokes TC-EPSCs that have larger amplitudes than those onto excitatory neurons (Hull et al., 2009; Cruikshank et al., 2010; Schiff and Reyes, 2012). TC inputs onto FS neurons are mediated by GluRA2-lacking AMPA receptors in both S1 and V1. No NMDAR-mediated current contributed to TC-EPSCs onto FS neurons in V1; whereas in S1 and A1 TC-EPSCs onto FS neurons contain NMDAR-mediated currents albeit smaller than those recorded from excitatory neurons (Hull et al., 2009). The data from V1 are consistent with observations in the prefrontal cortex, where TC-EPSCs onto 78% of FS neurons were mediated by GluA2-lacking AMPAR, and lacked NMDAR-mediated currents (Wang and Gao, 2010). Differences in short term depression were observed at TC inputs onto excitatory neurons and FS neurons in S1 (Beierlein et al., 2003; Cruikshank et al., 2010; Viaene et al., 2011; but see Hull et al., 2009), A1 (Lee and Sherman, 2008; Shiff and Reyes, 2012), and V1 (present study), suggesting that distinct short term dynamics are a general property of TC circuits, although the mechanisms engaged may differ across areas (Hull et al., 2009).

The organization of TC inputs also shows similarities and significant differences across sensory cortices. Our results suggest that LGN inputs onto L4 of V1 are mediated by few powerful release sites, or clusters of release sites in the case of FS neurons, consistent with anatomical studies (Stratford et al, 1996; Ahmed et al., 1997; Erisir and Dreusicke, 2005; Freund et al., 1985). TC inputs are outnumbered by intracortical inputs (Peters and Payne, 1993; Ahmed et al, 1994, 1997; Da Costa and Martin, 2009); however feedforward stimuli are effectively propagated in cortical circuits. It was proposed that amplification of signals by intracortical

synapses may be necessary to propagate incoming activity in V1 and A1 (Da Costa and Martin, 2011; Shiff and Reyes, 2012; Li et al, 2013; Lee, 2013). This presents significant differences with models of S1 activation. In S1, TC inputs onto excitatory neurons have similar quantal size to intracortical inputs (Gil et al, 1999; Schoonover et al, 2014). S1 activation by TC afferents is thought to depend on synchronous activation of numerous weak synapses (Bruno and Sakmann, 2006) with 3 times the number of release sites of intracortical synapses and a higher release probability (Schoonover et al., 2014; Hull et al., 2009). The similarities reported across sensory cortices likely underlie a set of general principles of TC circuit organization. The differences suggest that region specific properties of TC inputs may depend on the specific demands of distinct sensory modalities.

References

Agmon A, Connors BW (1992) Correlation between Intrinsic Firing Patterns and Thalamocortical Synaptic Responses of Neurons in Mouse Barrel Cortex. The Journal of Neuroscience 12:319-329.

Ahmed B, Anderson JC, Martin KAC (1997) Map of the Synapses Onto Layer 4 Basket Cells of the Primary Visual Cortex of the Cat. The Journal of Comparative Neurology 380:230–242.

Ahmed B, Anderson JC, Douglas RJ, Martin KAC, Nelson JC (1994) Polyneuronal Innervation of Spiny Stellate Neurons in Cat Visual Cortex. The Journal of Comparative Neurology 341:39-49.

Alonso J-M, Swadlow HA (2005) Thalamocortical Specificity and the Synthesis of Sensory Cortical Receptive Fields. The Journal of Neurophysiology 94:26-32.

Atallah, B.V., Bruns, W., Carandini, M., and Scanziani, M. (2012). Parvalbumin-expressing interneurons linearly transform cortical responses to visual stimuli. *Neuron* 73**,** 159-170.

Bagnall MW, Hull C, Bushong EA, Ellisman MH, Scanziani M (2011) Multiple Clusters of Release Sites Formed by Individual Thalamic Afferents onto Cortical Interneurons Ensure Reliable Transmission. Neuron 71:180–194.

Bartley AF, Huang ZJ, Huber KM, Gibson JR (2008) Differential Activity-Dependent, Homeostatic Plasticity of Two Neocortical Inhibitory Circuits. The Journal of Neurophysiology 100:1983–1994.

Beierlein M, Gibson JR, Connors BW (2003) Two Dynamically Distinct Inhibitory Networks in Layer 4 of the Neocortex. The Journal of Neurophysiology 90:2987–3000.

Binshtok AM, Fleidervish IA, Sprengel R, Gutnick MJ (2006) NMDA Receptors in Layer

4 Spiny Stellate Cells of the Mouse Barrel Cortex Contain the NR2C Subunit. The Journal of Neuroscience 26:708 –715.
Boulter J, Hollmann M, O'Shea-Greenfield A, Hartley M, Deneris E, Maron C, Heinemann S (1990) Molecular cloning and functional expression of glutamate receptor subunit genes. Science 249:1033-1037.
Bowie D, Mayer ML (1995) Inward rectification of both AMPA and kainate subtype glutamate receptors generated by polyamine-mediated ion channel block. Neuron 15:453-462.
Bruno RM, Simons DJ (2002) Feedforward Mechanisms of Excitatory and Inhibitory Cortical Receptive Fields. The Journal of Neuroscience 22:10966–10975.
Bruno RM, Sakmann B (2006) Cortex Is Driven by Weak but Synchronously Active Thalamocortical Synapses. Science 312:1622-1627.
Cardin JA, Palmer LA, Contreras D (2007) Stimulus Feature Selectivity in Excitatory and Inhibitory Neurons in Primary Visual Cortex. The Journal of Neuroscience 27:10333–10344.
Cardin JA, Kumbhani RD, Contreras D, Palmer LA (2010) Cellular Mechanisms of Temporal Sensitivity in Visual Cortex Neurons. The Journal of Neuroscience 30:3652–3662.
Contreras D, Palmer L (2003) Response to Contrast of Electrophysiologically Defined Cell Classes in Primary Visual Cortex. The Journal of Neuroscience 23:6936-6945.
Cottam, J.C., Smith, S.L., and Häusser, M. (2013). Target-specific effects of somatostatin expressing interneurons on neocortical visual processing. *J Neurosci* 33**,** 19567-19578.
Da Costa NM, Martin KAC (2009) The Proportion of Synapses Formed by the Axons of the Lateral Geniculate Nucleus in Layer 4 of Area 17 of the Cat. The Journal of Comparative Neurology 516:264–276.
Da Costa NM, Martin KAC (2011) How Thalamus Connects to Spiny Stellate Cells in the Cat's Visual Cortex. The Journal of Neuroscience 31:2925-2937.
Cruikshank SJ, Rose HJ, 583 Metherate R (2002) Auditory Thalamocortical Synaptic Transmission In Vitro. The Journal of Neurophysiology 87:361–384.
Cruikshank SJ, Lewis TJ, WConnors B (2007) Synaptic basis for intense thalamocortical activation of feedforward inhibitory cells in neocortex. Nature Neuroscience 10:462-468.
Cruikshank SJ, Urabe H, Nurmikko AV, Connors BW (2010) Pathway-Specific Feedforward Circuits between Thalamus and Neocortex Revealed by Selective Optical Stimulation of Axons. Neuron 65:230–245.
Daw MI, Tricoire L, Erdelyi F, Szabo G, McBain CJ (2009) Asynchronous Transmitter Release from Cholecystokinin-Containing Inhibitory Interneurons Is Widespread and Target-Cell Independent. The Journal of Neuroscience 29:11112–11122.
Dingledine R, Borges K, Bowie D, Traynelis SF (1999) The Glutamate Receptor Ion Channels. Pharmacological Reviews 51:7-62.
Erisir A, Dreusicke M (2005) Quantitative Morphology and Postsynaptic Targets of Thalamocortical Axons in Critical Period and Adult Ferret Visual Cortex. The Journal of Comparative Neurology 485:11-31.
Fleidervish IA, Binshtok AM, Gutnick MJ (1998) Functionally Distinct NMDA Receptors Mediate Horizontal Connectivity within Layer 4 of Mouse Barrel Cortex. Neuron

21:1055-1065.
Freund TF, Martin KAC, Somogyi P, Whitteridge D (1985) Innervation of Cat Visual Areas 17 and 18 by Physiologically Identified X- and Y- Type Thalamic Afferents. II. Identification of Postsynaptic Targets by GABA Immunocytochemistry and Golgi Impregnation. The Journal of Comparative Neurology 242:275-291.
Gabernet L, Jadhav SP, Feldman DE, Carandini M, Scanziani M (2005) Somatosensory Integration Controlled by Dynamic Thalamocortical Feed-Forward Inhibition. Neuron 48:315-327.
Geiger JRP, Melcher T, Koh DS, Sakmann B, Seeburg PH, Jonas P, Monyer H (1995) Relative abundance of subunit mRNAs determines gating and Ca2+ permeability of AMPA receptors in principal neurons and interneurons in rat CNS. Neuron 15:193-204.
Gil Z, Connors BW, Amitai Y (1999) Efficacy of Thalamocortical and Intracortical Synaptic Connections: Quanta, Innervation, and Reliability. Neuron 23:385–397.
Goda Y, Stevens CF (1994) Two components of transmitter release at a central synapse. Proceedings of the National Academy of Sciences 91:12942-12946.
Gu Y, Arruda-Carvalho M, Wang J, Janoschka SR, Josselyn SA, Frankland PW, Ge S (2012) Optical controlling reveals time-dependent roles for adult-born dentate granule cells. Nature Neuroscience 15:1700-1708.
Hartveit E, Veruki ML (2007) Studying properties of neurotransmitter receptors by non stationary noise analysis of spontaneous postsynaptic currents and agonist-evoked responses in outside-out patches. Nature Protocols 2:434-448.
Hestrin S (1993) Different glutamate receptor channels mediate fast excitatory synaptic currents in inhibitory and excitatory cortical neurons. Neuron 11:1083-1091.
Hull C, Isaacson JS, Scanziani M (2009) Postsynaptic Mechanisms Govern the Differential Excitation of Cortical Neurons by Thalamic Inputs. The Journal of Neuroscience 29:9127–9136.
Isaac JTR, Ashby MC, McBain CJ (2007) The Role of the GluR2 Subunit in AMPA Receptor Function and Synaptic Plasticity. Neuron 54:859-871.
Jonas P, Burnashev N (1995) Molecular mechanisms controlling calcium entry through AMPA type glutamate receptor channels. Neuron 15:987-990.
Jonas P, Bischofberger J, Fricker D, Miles R (2004) Interneuron Diversity series: Fast in, fast out – temporal and spatial signal processing in hippocampal interneurons. Trends in Neuroscience 27:30-40.
Kameyama, K., Sohya, K., Ebina, T., Fukuda, A., Yanagawa, Y., and Tsumoto, T. (2010). Difference in binocularity and ocular dominance plasticity between GABAergic and excitatory cortical neurons. *J Neurosci* 30**,** 1551-1559.
Kuhlman, S.J., Tring, E., and Trachtenberg, J.T. (2011). Fast-spiking interneurons have an initial orientation bias that is lost with vision. *Nat Neurosci* 14**,** 1121-1123.
Lee CC (2013) Thalamic and cortical pathways supporting auditory processing. Brain & Language 126:22-28.
Lee CC, Sherman SM (2008) Synaptic Properties of Thalamic and Intracortical Inputs to Layer 4 of the First- and Higher-Order Cortical Areas in the Auditory and Somatosensory Systems. The Journal of Neurophysiology 100:317–326.
Lee CC, Imaizumi K (2013) Functional Convergence of Thalamic and Intrinsic Projections to Cortical Layers 4 and 6. Neurophysiology 45:396-406.
Li, Y.T., Ma, W.P., Pan, C.J., Zhang, L.I., and Tao, H.W. (2012b). Broadening of cortical

inhibition mediates developmental sharpening of orientation selectivity. *J Neurosci* 32**,** 3981-3991.
Li L-y, Li Y-t, Zhou M, Tao HW, Zhang LI (2013) Intracortical multiplication of thalamocortical signals in mouse auditory cortex. Nature Neuroscience Brief Communications 16:1179-1183.
MacLean JN, Fenstermaker V, Watson BO, Yuste R (2006) A visual thalamocortical slice. Nature Methods 3:129-134.
Moore AK, Wehr M (2013) Parvalbumin-Expressing Inhibitory Interneurons in Auditory Cortex Are Well-Tuned for Frequency. The Journal of Neuroscience 33:13713–13723.
Morishita W, Alger BE (1997) Sr2+ supports depolarization-induced suppression of inhibition and provides new evidence for a presynaptic expression mechanism in rat hippocampal slices. The Journal of Physiology 505:307-317.
Niell, C.M., and Stryker, M.P. (2008). Highly selective receptive fields in mouse visual cortex. *J Neurosci* 28**,** 7520-7536.
O'Donovan MJ, Rinzel J (1997) Synaptic depression: a dynamic regulator of synaptic communication with varied functional roles. Trends in Neuroscience 20:431-433.
Peters A, Payne BR (1993) Numerical Relationships between Geniculocortical Afferents and Pyramidal Cell Modules in Cat Primary Visual Cortex. Cerebral Cortex 3:69-78.
Priebe NJ, Ferster D (2005) Direction Selectivity of Excitation and Inhibition in Simple Cells of the Cat Primary Visual Cortex. Neuron 45:133-145.
Rose HJ, Metherate R (2005) Auditory Thalamocortical Transmission Is Reliable and Temporally Precise. The Journal of Neurophysiology 94:2019–2030.
Runyan, C.A., and Sur, M. (2013). Response selectivity is correlated to dendritic structure in parvalbumin-expressing inhibitory neurons in visual cortex. *J Neurosci* 33**,** 11724-11733.
Schiff ML, Reyes AD (2012) Characterization of thalamocortical responses of regular-spiking and fast-spiking neurons of the mouse auditory cortex in vitro and in silico. The Journal of Neurophysiology 107:1476-1488.
Schoonover CE, Tapia J-C, Schilling VC, 673 Wimmer V, Blazeski R, Zhang W, Bruno R (2014) Comparative Strength and Dendritic Organization of Thalamocortical and Corticocortical Synapses onto Excitatory Layer 4 Neurons. The Journal of Neuroscience 34:6746–6758.
Sherman SM (2007) The thalamus is more than just a relay. Current Opinion in Neurobiology 17:417-422.
Sherman SM (2012) Thalamocortical interactions. Current Opinion in Neurobiology 22:1-5.
Sigworth FJ (1980) The variance of sodium current fluctuations at the node of Ranvier. The Journal of Physiology 307:97-129.
Sola E, Prestori F, Rossi P, Taglietti V, D'Angelo E (2004) Increased neurotransmitter release during long-term potentiation at mossy fiber-granule cell synapses in rat cerebellum. The Journal of Physiology 557:843-861.
Stevens C, Wesseling J (1998) Activity-dependent modulation of the rate at which synaptic vesicles become available to undergo exocytosis. Neuron 21:415-424.
Stratford KJ, Tarczy-Hornoch K, Martin KAC, Bannister NJ, Jack JJB (1996) Excitatory synaptic inputs to spiny stellate cells in cat visual cortex. Nature Letters 382:258-261.
Sun Q-Q, Huguenard JR, Prince DA (2006) Barrel Cortex Microcircuits: Thalamocortical

Feedforward Inhibition in Spiny Stellate Cells Is Mediated by a Small Number of Fast-Spiking Interneurons. The Journal of Neuroscience 26:1219-1230.
Swadlow HA (2002) Thalamocortical control of feed-forward inhibition in awake somatosensory 'barrel' cortex. Philosophical Transactions of The Royal Society B 357:1717–1727.
Swadlow HA (2003) Fast-spike Interneurons and Feedforward Inhibition in Awake Sensory Neocortex. Cerebral Cortex 13:25-32.
Swanson GT, Kamboj SK, Cull-Candy SG (1997) Single-Channel Properties of RecombinantAMPA Receptors Depend on RNA Editing, Splice Variation, and Subunit Composition. The Journal of Neuroscience 17:58-69.
Traynelis S, Jaramillo F (1998) Getting the most out of noise in the central nervous system. Trends in Neuroscience 21:137-145.
Verdoorn TA, Burnashev N, Monyer H, Seeburg PH, Sakmann B (1991) Structural determinants of ion flow through recombinant glutamate receptor channels. Science 252:1715-1718.
Viaene AN, Petrof I, 703 Sherman SM (2011) Synaptic Properties of Thalamic Input to the Subgranular Layers of Primary Somatosensory and Auditory Cortices in the Mouse. The Journal of Neuroscience 31:12738-12747.
Wang H-X, Gao W-J (2010) Development of calcium-permeable AMPA receptors and their correlation with NMDA receptors in fast-spiking interneurons of rat prefrontal cortex. The Journal of Physiology 588:2823–2838.
Wang L, Fontanini A, Maffei A (2012) Experience-Dependent Switch in Sign and Mechanisms for Plasticity in Layer 4 of Primary Visual Cortex. The Journal of Neuroscience 32:10562-10573.
Wang L, Kloc M, Gu Y, Ge S, Maffei A (2013) Layer-Specific Experience-Dependent Rewiring of Thalamocortical Circuits. The Journal of Neuroscience 33:4181– 4191.
Wehr M, Zador AM (2003) Balanced inhibition underlies tuning and sharpens spike timing in auditory cortex. Nature Letters 426:442-446.
Wernig A (1975) Estimates of statistical release parameters from crayfish and frog neuromuscular junction. The Journal of Physiology 244:207-221.
Wilent WB, Contreras D (2004) Synaptic Responses to Whisker Deflections in Rat Barrel Cortex as a Function of Cortical Layer and Stimulus Intensity. The Journal of Neuroscience 24:3985–3998.
Xu-Friedman MA, Regehr WG (2000) Probing Fundamental Aspects of Synaptic Transmission with Strontium. The Journal of Neuroscience 20:4414–4422.
Yazaki-Sugiyama, Y., Kang, S., Câteau, H., Fukai, T., and Hensch, T.K. (2009). Bidirectional plasticity in fast-spiking GABA circuits by visual experience. *Nature* 462**,** 218-221.
Zariwala, H.A., Madisen, L., Ahrens, K.F., Bernard, A., Lein, E.S., Jones, A.R., and Zeng, H. (2011). Visual tuning properties of genetically identified layer 2/3 neuronal types in the primary visual cortex of cre-transgenic mice. *Front Syst Neurosci* 4**,** 162.
Zhang F, Wang LP, Boyden ES and Deisseroth K (2006) Channelrhodopsin – 2 and optical control of excitable cells. Nature Methods 3: 785-792
Zhuang J, Stoelzel CR, Bereshpolova Y, Huff JM, Xiaojuan H, Alonso JM and Swadlow

HA (2013) Layer 4 in prmary visual cortex of the awake rabbit: contrasting properties of simple cells and putative feedforward inhibitory interneurons. The Journal of Neuroscience 33: 11372-11389.

Chapter IV: Local corticothalamic feedback via presynaptic $GABA_A$ receptors on thalamocortical terminals in rat V1

Abstract

Thalamocortical inputs directly activate both excitatory and inhibitory neurons in L4 of V1, and fast inhibitory GABAergic transmission plays a fundamental role in neural circuit function. GABAergic inhibition is complex, and acts at a variety of loci in neocortical circuits. Current thinking is that phasic or tonic fast GABAergic inhibition modulates neocortical activity via $GABA_A$ receptors exclusively located on postsynaptic neurons. While evidence for presynaptic $GABA_A$ receptors modulation of the efficacy of glutamatergic transmission has been shown in the hippocampus, it is currently unknown whether similar mechanisms may be operating in other circuits. Here we demonstrate that in rat primary visual cortex, α4-containing $GABA_A$ receptors are located at thalamocortical terminals and selectively modulate thalamocortical inputs. Our data provide a novel mechanism for local corticothalamic feedback, and suggest a possible new target through which inhibition may shape cortical excitability, processing, and development.

Authors: Lang Wang, Michelle Kloc, Alev Erisir, Arianna Maffei.

Author Contributions: L.W., M.K., A.M. and A.E. designed experiments; L.W., M.K., and A.E. performed experiments, L.W., M.K., A.M. and A.E. analyzed data; L.W., M.K., and A.M. wrote the manuscript.

Introduction

GABA is the major inhibitory neurotransmitter in the central nervous system. Its inhibitory action can be exerted slowly via activation of metabotropic $GABA_B$ receptors (Kerr and Ong, 1995), or via tonic activation of extrasynaptic $GABA_A$ receptors (Cope et al., 2005; Kullman et al., 2005); or rapidly via activation of $GABA_A$ receptors. In neocortical circuits the general assumption is that phasic and tonic GABA regulates circuit excitability by acting on $GABA_A$ receptors located on postsynaptic neurons. However, $GABA_A$ receptors may also be located presynaptically. In the hippocampus, cerebellum, brainstem and spinal cord $GABA_A$ receptors can be found at presynaptic glutamatergic terminals (Eccles, 1963; Pouzat and Marty, 1999; Kullman et al., 2005; Ruiz et al., 2010). They are involved in modulating both presynaptic release, and capacity for plasticity of excitatory inputs (Ruiz et al., 2010; Kim et al., 2011; Ruiz and Kullman, 2013). Differently, in neocortex GABA modulation of presynaptic release has been ascribed solely to the activation of $GABA_B$ receptors (Porter and Nieves, 2004). Whether or not $GABA_A$ receptors may also be present presynaptically at glutamatergic synapses in neocortex has not been studied. The presence of presynaptic $GABA_A$ receptors would have important implications not only for GABA regulation of excitability of glutamatergic synapses, but also synaptic plasticity and development. Here we tested the possibility that presynaptic $GABA_A$ receptors may be present in neocortical circuits, and may play an important role in regulating how cortical circuits are activated by incoming inputs. For this study, we focus on both thalamocortical (TC) and recurrent intracortical synapses (rIC) in layer 4 (L4) of rat primary visual cortex (V1).

Layer 4 (L4) of V1 receives the largest TC projection from the lateral geniculate nucleus (LGN) of the thalamus. TC input to V1 drives the activity of L4 through a powerful input (Sherman

2012; Stratford et al., 1996; Wang et al., 2013), which is then amplified throughout rIC circuits in L4 (Li et al, 2013; Lee, 2013). Both TC and rIC synapses are critically important for information processing in V1, and $GABA_A$ modulation of presynaptic terminals could have profound effects on how either or both circuits are activated. Presynaptic $GABA_A$ modulation of TC excitability could be important for receptive field formation, experience dependent plasticity, and the relay of visual information. Furthermore, presynaptic $GABA_A$ receptors on TC terminals could provide a mechanism of cortical feedback on TC input.

We used optogenetic, physiological, immunohistochemical and electron microscopy approaches to determine the site and effect of $GABA_A$ receptor activation in L4 in an acute slice preparation of V1. We found that $GABA_A$ receptors are located presynaptically on a subset of glutamatergic synapses in V1, the TC synapses innervating L4 neurons. We found that these GABAA receptors are diazepam insensitive, suggesting that they contain the α4 and/ or α6 subunits. We also provide evidence to show that presynaptic $GABA_A$ receptors cluster on TC terminals with the scaffolding protein gephyrin, and that they contain the α4 subunit. We found no evidence for presynaptic $GABA_A$ receptors at glutamatergic rIC synapses in L4, suggesting that this phenomenon is limited to the TC terminals. This could have important implications not only for circuit function, but also for the field of study. Many conclusions of neocortical development, plasticity, and function have been derived from studies that pharmacologically alter inhibition. The presence of presynaptic, diazepam insensitive, $GABA_A$ receptors would require a reevaluation of current models of inhibition in neocortical circuit function.

Results

To selectively activate TC inputs onto layer 4 (L4) neurons in V1 we used an optogenetic approach (Wang et al, 2013). Whole cell patch clamp recordings were obtained from visually

identified pyramidal (Pyr) and fast spiking inhibitory (FS) neurons in L4, and monosynaptic TC excitatory postsynaptic currents (TC-EPSC) were evoked using trains of 5 light pulses (1 ms) at 10Hz. After acquiring a 10 min stable baseline, the $GABA_A$ receptor agonist muscimol (Mus; 1 mM) was bath applied and its effect on the holding potential of the recorded neurons as well as on amplitude and short term dynamics of TC-EPSCs onto Pyr and FS was assessed. Muscimol acts by binding to the GABA binding site, thus mimicking the presence of GABA. Consistent with previous findings on tonic activation of $GABA_A$ receptors in cortical neurons, bath application of muscimol significantly increased the holding current (IHold) of both Pyr and FS neurons (Fig. 4.1 C-H; IHold Pyr: baseline: 2.2 ± 3.7 pA; Mus: -87.0 ± 9.7 pA; n = 52; $p < 0.0001$; FS: n = 12; $p < 0.0001$; IHold FS baseline: -31.5 ± 9.0 pA; Mus: -143.0 ± 16.0 pA; n = 12; paired t-test: $p < 0.0001$). The increase in holding currents is evidence in favor of the tonic activation of extrasynaptic $GABA_A$ receptors on the postsynaptic neuron. Activation of extrasynaptic receptors has been shown to alter IHold, but leave evoked EPSCs unaffected.

In L4 of V1, however, bath application of muscimol significantly decreased the amplitude of evoked TC-EPSCs onto both pyramidal and FS neurons (Fig 4.1 B, G; Pyr baseline: 191.7 ± 18.7 pA; Mus: 86.0 ± 10.0 pA; n = 52; paired t-test: $p < 0.0001$; FS baseline: 335.4 ± 68.6 pA; muscimol: 196.1 ± 54.6 pA; n = 12; paired t-test: $p < 0.001$). In a subset of recorded neurons we tested the effect of muscimol on paired pulse ratio (PPR) using 2 - 1ms pulses delivered at 10 Hz, and observed a significant increase in this parameter for TC-EPSCs onto both Pyr and FS (PPR Pyr, baseline: 0.52 ± 0.03; Mus: 0.59 ± 0.03; n = 49; $p < 0.001$; FS baseline: 0.42 ± 0.03; Mus: 0.49 ± 0.04; n = 12; paired t-test: $p < 0.01$). These results support a presynaptic locus for TC-EPSC modulation by muscimol. In a different subset of recordings we also assessed the effect of muscimol on short term depression using 5 - 1 ms long light pulses delivered at 10 Hz,

and detected significant changes in TC-EPSC short term depression onto both neuron types (Steady state ratio (SSR), Pyr, baseline: 0.2 ± 0.02; Mus: 0.27 ± 0.02; $p < 0.0001$; FS; FS baseline: 0.15 ± 0.02; Mus: 0.21 ± 0.03; n = 12; paired t-test: $p < 0.01$). These two sets of data strongly suggest that muscimol was interfering with synaptic transmission at TC afferents.

Bath application of 20 μM picrotoxin (Ptx), which acts by occluding the pore of the $GABA_A$ receptor chloride channel, prior to muscimol application blocked the effect of muscimol on IHold (Pyr IHold baseline: 13.0 ± 10.4 pA; picrotoxin: 23.5 ± 10.7 pA; picrotoxin and muscimol: 10.0 ± 11.9 pA; n = 15; One Way ANOVA: p = 0.8; FS IHold baseline: 5.3 ± 10.1 pA; picrotoxin: 2.4 ± 11.0 pA; picrotoxin and muscimol: -0.3 ± 12 pA; n = 7; One Way ANOVA: p = 0.9) and on TC-EPSC amplitude (Pyr baseline: 178.2 ± 30.4 pA; picrotoxin: 164.9 ± 26.5 pA; picrotoxin and muscimol: 156.4 ± 25.6; n = 15; One Way ANOVA: p = 0.8; FS TC-EPSC baseline: 155.42 ± 42.0 pA; picrotoxin: 152.4 ± 43.3 pA; picrotoxin and muscimol: 135.3 ± 38.8 pA; n = 7; One Way ANOVA: p = 0.9) and dynamics for both Pyr and FS neurons. These data support the interpretation that muscimol activation of $GABA_A$ receptors mediates both changes in TC-EPSC amplitude and IHold.

Diazepam is a benzodiazepine that enhances $GABA_A$ receptor signaling by binding to regulatory sites on specific subunits, namely α1, α3, and α5. Bath application of diazepam (DZ, 10 μM), which acts on $GABA_A$ receptors predominantly located on postsynaptic terminals, did not alter IHold (Pyr IHold baseline: -1.6 ± 4.2 pA; diazepam: -4.1 ± 4.5 pA; n = 45; paired t-test: p = 0.1; FS IHold baseline: -31.9 ± 12.3 pA; diazepam: -32.8 ± 16.1 pA; n = 12; paired t-test: p = 0.9). Diazepam also did not alter TC-EPSC amplitude (Pyr TC-EPSC baseline: 191.2 ± 20.7 pA; diazepam: 190.6 ± 24.8 pA; n = 45; paired t-test: p = 0.9; FS TC-EPSC baseline: 356.3 ± 66.8 pA; diazepam: 364.7 ± 79.0 pA; n = 12; paired t-test: p = 0.7) and short term dynamics of TC-

EPSC onto Pyr and FS (Fig. 4.1 F; Pyr PPR, paired t-test: p = 0.3; SSR, paired t-test: p = 0.8, n = 46; FS PPR, paired t-test: p = 0.9; SSR, paired t-test: p = 0.6, n = 12). The lack of effect of diazepam suggests that the effect of muscimol is mainly mediated by the activation of extrasynaptic $GABA_A$ receptors (Derry et al., 2004). These results also support the interpretation that presynaptic $GABA_A$ receptors that lack the benzodiazepine sensitive subunits α4 and α6 may mediate the effect of muscimol on TC-EPSCs. Thus, the muscimol-induced decrease in TC-EPSC depended on $GABA_A$ receptors activation. Taken together these data indicate that activation of extrasynaptic $GABA_A$ receptors mediate the effect of muscimol on TC-EPSCs and holding current onto both pyramidal and FS neurons. The significant changes in TC-EPSC short term depression also suggest that the effect of muscimol on TC-EPSCs may be mediated by $GABA_A$ receptors located on presynaptic terminals.

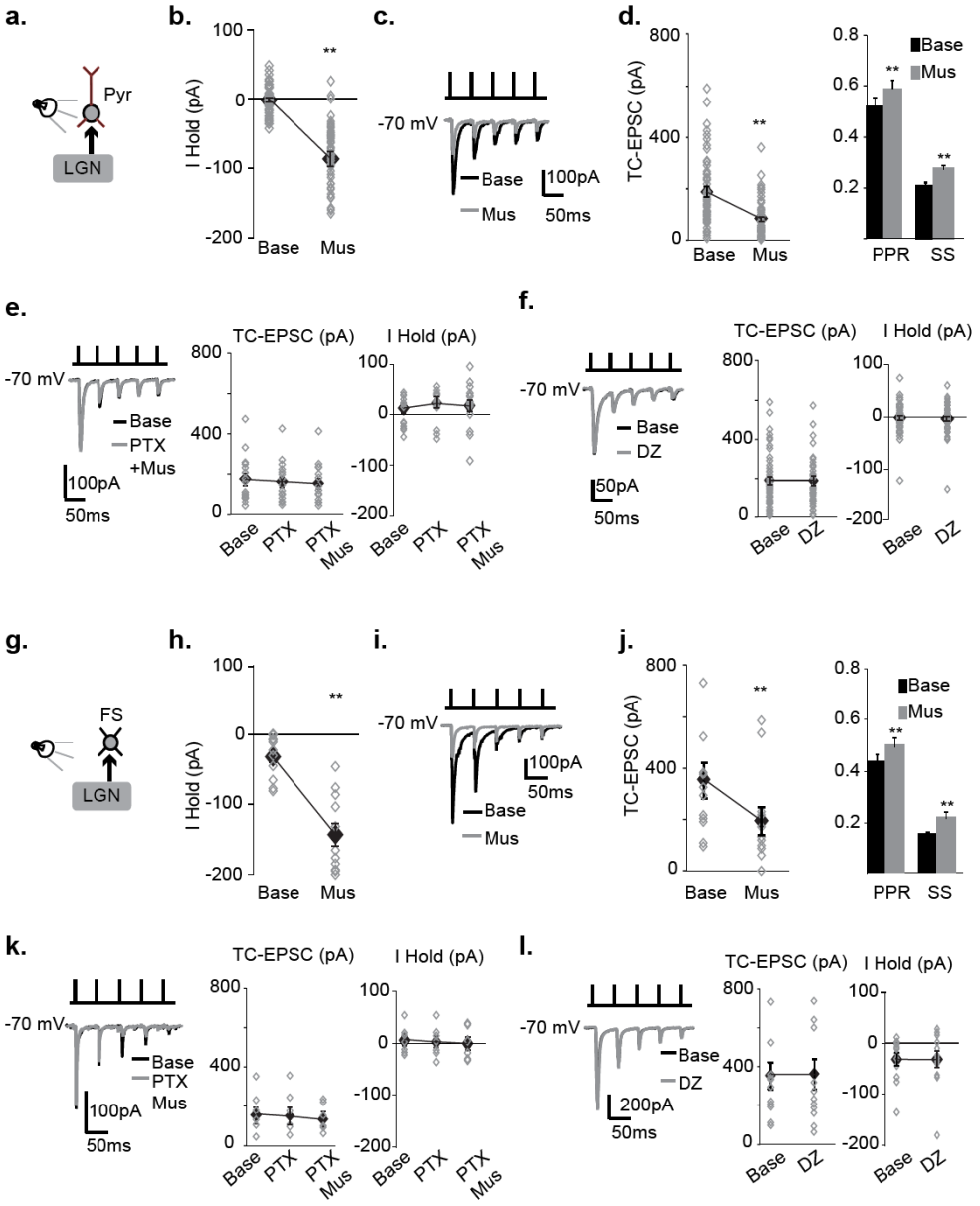

Figure 4.1. Muscimol, but not diazepam, effects the TC-EPSC amplitude, PPR, and IHold of Pyr and FS. a. Diagram of recording configuration. Patch clamp recordings, in voltage clamp mode, were obtained from visually identified L4 pyramidal neurons (Pyr). Photoactivation of terminal fields from the lateral geniculate nucleus (LGN) was used to evoke TC-EPSCs. Neurons were maintained at -70 mV throughout the recording. **b**. Bath application of muscimol (1 mM) significantly increased the holding current of the recorded pyramidal neuron. The plot shows the average effect of muscimol on IHold (black diamonds) as well as the data obtained from each recording (gray diamonds). The lines connecting each pair of data points have been omitted to facilitate readability. **c.** Sample traces of TC-EPSCs evoked by 5, 1ms long light pulses delivered at 10 Hz. **d**. Left: plot of average changes in TC-EPSC amplitude (black diamonds) and of data from each recorded Pyr before and after muscimol application. Connecting lines are shown only for average values to favor readability. Right: muscimol also affected TC-EPSC short term

dynamics, shown as PPR and SS. Baseline is shown in black, Mus is shown in gray. **e**. Left: sample traces of TC-EPSC recorded in the presence of picrotoxin (PTX; black) and a cocktail of picrotoxin and muscimol (PTX + Mus: gray). Middle: Cumulative effect of picrotoxin on TC-EPSC amplitude onto pyramidal neurons. **f.** Bath application of diazepam did not affect TC-EPSC amplitude and I Hold. Left: sample traces of TC-EPSCs recorded before (black) and after (gray) bath application of 10 μM diazepam. Middle: effect of bath application of diazepam on the amplitude of TC-EPSCs. Right: diazepam did not affect the holding current of pyramidal neurons. **g.** The effect of muscimol was not specific to TC-EPSCs onto L4 pyramidal neurons, but extended to TC-EPSCs onto FS inhibitory neurons. The diagram indicates that the recordings shown in the following panels were obtained from FS neurons while photoactivating the LGN terminal fields. **h.** Bath application of muscimol (1 mM) significantly increased the holding current of FS neurons. The black diamonds indicate average values; while the gray diamonds indicate each recorded neuron. The lines connecting each pair of data points have been omitted to facilitate readability. **i.** Similarly to what observed for pyramidal neurons, bath application of muscimol significantly decreased the amplitude of TC-EPSCs. Panel I shows sample traces of TC-EPSCs onto FS neurons before (black) and after (gray) application of muscimol. **j.** Left: effect of muscimol on TC-EPSCs onto FS neurons. Right: cumulative plot of changes in PPR and SSR. Baseline is shown in black, Mus in gray. **k.** Left: sample traces recorded in the presence of picrotoxin (PTX; black) and picrotoxin with muscimol (PTX Mus; gray). Middle: bath application of picrotoxin occluded the effect of muscimol on TC-EPSC recorded from FS neurons. Right: picrotoxin also occluded the effect of muscimol on FS neurons holding current. Bath application of diazepam did not affect the amplitude and holding current of TC-EPSCs recorded from FS neurons. Left: sample traces of TC-EPSCs recorded from FS neurons. Black diamonds indicate average effects; while gray diamonds indicate single recordings. (FS baseline (Base): black; diazepam (DZ): gray). Middle: effect of diazepam on TC-EPSC amplitude onto FS. Right: effect of diazepam on the holding current of recorded FS neurons.

We assessed whether the effect of muscimol was specific for TC-EPSCs, or was observed also at recurrent glutamatergic inputs between Pyr and from Pyr onto FS. Quadruple simultaneous patch clamp recordings were obtained from visually identified L4 neurons to isolate monosynaptically connected pairs as previously described (Wang and Maffei, 2014). Unitary excitatory currents (uEPSCs) were recorded at monosynaptic connections between L4 Pyr, and from Pyr onto FS.

There were no significant changes in uEPSC amplitude and short term dynamics induced by muscimol (uEPSC amplitude: baseline: 16.5 ± 1.8 pA; Mus: 14.1 ± 2.3 pA; n = 10; p = 0.2; uEPSC PPR, baseline: 0.72 ± 0.04; muscimol: 0.76 ± 0.05; p = 0.43; uEPSC SSR, baseline: 0.47 ± 0.06; muscimol: 0.49 ± 0.04; p = 0.69) or diazepam (uEPSC amplitude: baseline: 15.5 ± 1.7 pA; diazepam: 16.9 ± 1.9 pA; n = 9; p = 0.06; uEPSC PPR, baseline: 0.69 ± 0.03; diazepam: 0.7 ± 0.06; p = 0.64; uEPSC SSR, baseline: 0.42 ± 0.04; diazepam: 0.48 ± 0.07; p = 0.2) at recurrent inputs between Pyr neurons. In addition, no significant changes on amplitude (Muscimol uEPSC, baseline: 82.2 ± 17.7 pA; muscimol: 73.6 ± 10.0 pA; n = 6; paired t-test: p = 0.4; Diazepam uEPSC, baseline: 99.0 ± 30.4 pA; diazepam: 102.6 ± 19.8 pA; n = 7; paired t-test: p = 0.8) and short term dynamics (Muscimol PPR, baseline: 0.69 ± 0.07; muscimol: 0.70 ± 0.05; n = 6; paired t-test: p = 0.9; Muscimol SSR, baseline: 0.52 ± 0.03; muscimol: 0.45 ± 0.04; n = 7; paired t-test: p = 0.3; Diazepam PPR, baseline: 0.72 ± 0.04; diazepam: 0.76 ± 0.05; n = 7; paired t-test: p = 0.5; Diazepam SSR, baseline: 0.51 ± 0.04; diazepam: 0.51 ± 0.05; n = 7; paired t-test: p = 0.6) of Pyr to FS inputs were induced by either $GABA_A$ agonist.

Muscimol, but not diazepam, induced changes in the holding current of both pyramidal neurons (Muscimol uEPSC IHold, baseline: 8.4 ± 5.3 pA; muscimol: -56.1 ± 16.3 pA; n = 10; paired t-test: p < 0.001; Diazepam uEPSC IHold, baseline: 12.4 ± 3.7; diazepam: 8.9 ± 4.6 pA; n = 9; paired t-test: p = 0.3) and FS neurons (Muscimol IHold, baseline: -24.1 ± 8.1 pA; muscimol:

-103.0 ± 19.9 pA; n = 6; paired t-test: $p < 0.01$; Diazepam IHold, baseline: -27.0 ± 9.3 pA; diazepam: -37.6 ± 20.0 pA; n = 7; paired t-test: $p = 0.5$).

These results further confirm the presence of tonically activated extrasynaptic receptors onto both Pyr and FS. Consistent with previous findings showing that postsynaptic tonic inhibition does not affect the amplitude of evoked glutamatergic responses, no changes in uEPSCs are observed. Together, our results for TC-EPSCs and uEPSCs support the interpretation that tonic activation of $GABA_A$ receptors may modulate the excitability of the circuit in L4 via two distinct mechanisms. Tonic GABA can alter the excitability of excitatory and inhibitory neurons through the shunting action of GABAergic extrasynaptic receptors (Brickley et al., 1996; Kullman et al., 2005). In addition, tonic inhibition can provide selective modulation of TC neurotransmission onto both Pyr and FS, through a yet unidentified mechanism.

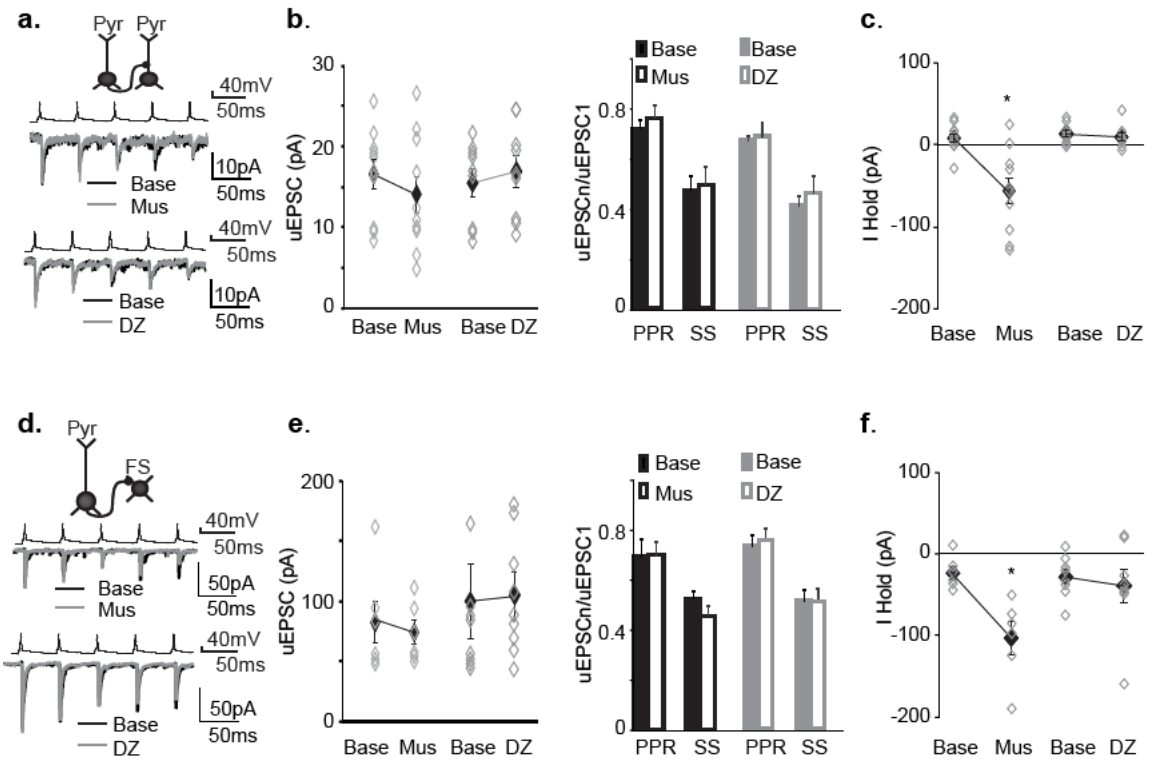

Figure 4.2. Tonic activation of $GABA_A$ receptors does not affect recurrent excitatory synapses in L4. a. Top: diagram of recording configuration. Paired recordings were obtained to selectively record monosynaptic glutamatergic inputs between pyramidal neurons (Pyr). Middle: sample traces of recurrent unitary excitatory postsynaptic currents (uEPSCs) recorded before (Baseline; Base; black) and after (Mus; gray) bath application of muscimol. Bottom: sample traces of uEPSCs recorded before (Base; black) and after (DZ; gray) bath application of diazepam. **b.** Bath application of muscimol or diazepam did not affect the amplitude of uEPSCs (left), or short term dynamics (right). Left panel: the black diamonds indicate average uEPSC amplitude; gray diamonds indicate single recordings for the data sets recorded in the presence of muscimol and diazepam. Right panel, short term dynamics: Baseline for muscimol is shown as a black bar, muscimol as a white bar with a black border, baseline for diazepam is shown as a gray bar, diazepam as a white bar with a gray border. **c.** Bath application of muscimol increased the holding current of L4 pyramidal neurons (left), while diazepam did not (right). **d.** The uEPSC onto FS neurons were not affected by tonic inhibition. Top: diagram of recording configuration. Paired recordings were obtained to selectively isolate uEPSC onto FS neurons. Middle: sample of uEPSCs recorded from FS neurons before (Base; black) and after (Mus; gray) bath application of muscimol (1 mM). Bottom: sample uEPSCs recorded before (Base; black) and after (DZ; gray) bath application of diazepam (10 μM). **e.** Left: cumulative plots of the effect of muscimol and diazepam on uEPSC amplitude. Left panel: black diamonds indicate average data; while gray diamonds indicate data obtained for each pair. Right: effect of muscimol and diazepam on uEPSC short term dynamics in response to spikes evoked in the presynaptic pyramidal neuron with 5 – 5 ms long suprathreshold depolarizing steps at 20 Hz. Short term dynamics: Baseline for muscimol is shown as a black bar, muscimol as a white bar with a black border, baseline for diazepam is shown as a gray bar, diazepam as a white bar with a gray border. **f.** Muscimol increased the holding current of FS neurons; while diazepam did not.

Bath application of muscimol induced changes in TC-EPSC amplitude and short term dynamics suggesting a presynaptic site of action for the $GABA_A$ receptor agonist. While presynaptic $GABA_A$ receptors have been reported in a number of brain regions (Eccles, 1963; Pouzat and Marty, 1999; Ruiz et al., 2010), it is currently believed that they are not present in neocortical circuits, where silencing of cortical circuits with muscimol is often used to investigate the properties and connectivity of thalamocortical inputs *in vivo*. However, no direct study excludes the presence of presynaptic $GABA_A$ receptors in neocortex, because not every $GABA_A$ subunit has been studied in detail. To better understand the mechanism through which muscimol modulates TC-EPSCs we tested the possibility that TC terminals may contain $GABA_A$ receptors. We used two separate anatomical approaches: 1- In one set of experiments we determined the possible colocalization of markers for the scaffold protein for $GABA_A$ receptors, gephyrin; for the glutamate transporter selectively expressed at TC terminals, VGluT2 (Nahmani and Erisir, 2005), and the reporter tag for the ChR2 construct we used in our physiology experiments, GFP. Slices obtained from injected animals were co-immunostained for VGluT2 and gephyrin. A region of interest (ROI) of 100 μm x 100 μm was generated on each image to define and normalize the region of analysis. A colocalization function was used to assess possible overlap of the three markers in putative synaptic terminals (puncta) located in L4 of V1. The fluorescence intensity profile was measured across the center of each colocalized punctum. The three markers were considered colocalized if their peak fluorescence was within ± 0.1 μm (Fig. 4.3 A - C; n = 24 slices from 3 rats). For each ROI, the number of colocalized puncta (5 ± 2.1 puncta) and total number of cell bodies (15 ± 2.8 cells) was quantified. Cell bodies were defined as black spaces with elliptic shape with a diameter of 10 - 15 μm. While this is an underestimate of the total number of putative synapses received by a L4 neuron, it was a first step toward quantifying the

relative proportion of colocalized puncta. As shown in Fig 4.3 C, puncta stained for all three markers accounted for 33.0 ± 16.0 % of the total puncta/cell in L4. These results indicate that about one third of putative TC terminals in L4 of V1 contain clusters of gephyrin, suggesting the presence of clustered presynaptic $GABA_A$ receptors at TC synapses.

To further assess the possible presence of presynaptic $GABA_A$ receptors, a subset of ChR2-GFP injected animals was prepared for electron microscopy (EM) and co-stained with antibodies against the α4 subunit of $GABA_A$ receptors (Fig 4.3 D). In Fig 4.3 D, a black arrow points to immunogold labeling of $GABA_A$ α4 subunits in L4 of V1. The choice of the $GABA_A$ receptor subunit was based on findings indicating significant levels of α4 expression in thalamic neurons (Chandra et al, 2006), and preferential binding of muscimol to α4 containing $GABA_A$ receptors (Chandra et al, 2010). It was also supported by our physiological results indicating that TC-EPSCs are sensitive to muscimol; but not to diazepam, which acts at $GABA_A$ receptors primarily located at synapses and containing the α1, α3 and α5. Qualitative analysis of EM images indicates the presence of $GABA_A$ receptors containing the α4 subunit at TC terminals in L4 of V1 (Fig 4.3 D, left). These have been shown to belong to thalamocortical afferents due to their large size, large number of vesicles, and presence of cytoplasmic inclusions (Nahmani and Erisir, 2005). $GABA_A$ α4 subunits were also identified near intracortical synapses on V1 neurons, however were not located at the terminal as they were at TC synapses (Fig. 4.3D, right). This is consistent with previous findings and our conclusions that extrasynaptic $GABA_A$ receptors are present on V1 neurons and responsible for the changes in IHold that followed $GABA_A$ receptor agonist application. Together our data provide electrophysiological, immunohistochemical and EM evidence for the presence of clusters of α4 containing $GABA_A$ receptors at thalamocortical terminals in the main input layer of V1.

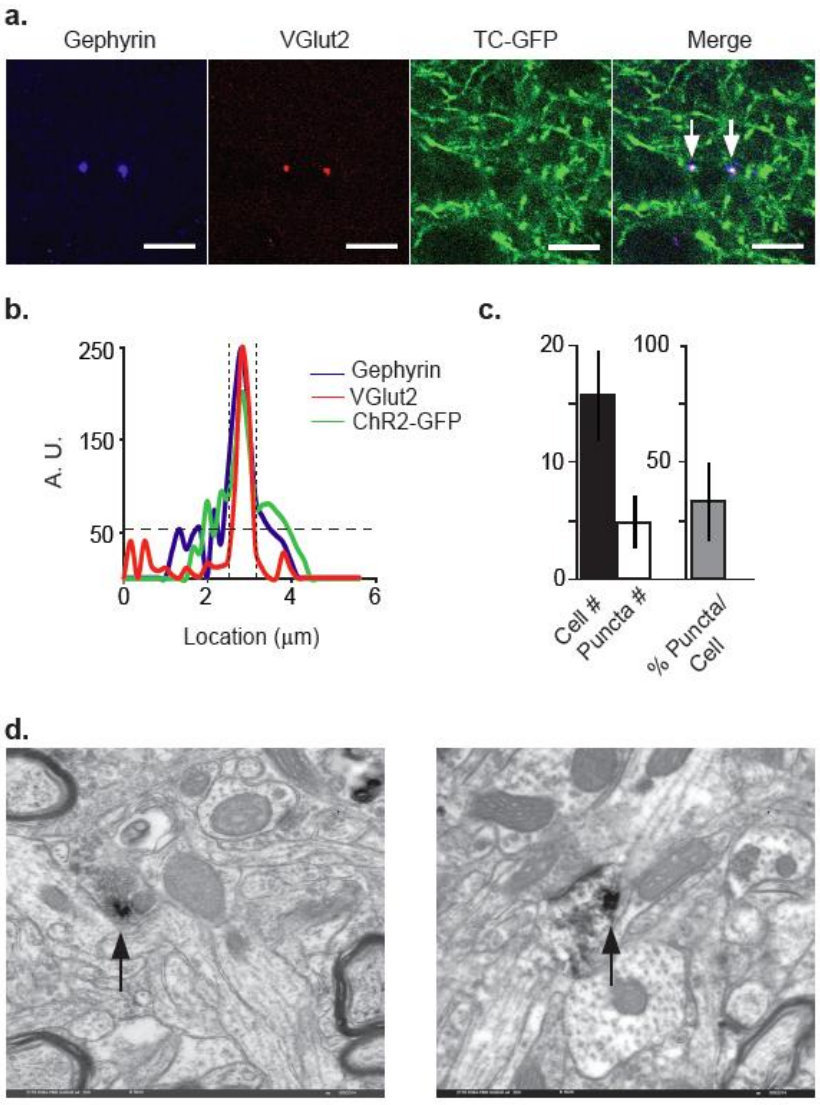

Figure 4.3. Colocalization of TC-GFP, Gephyrin, and VGlut2. a. In this set of experiments we assessed possible colocalization of markers for the scaffold protein for GABAA receptors (gephyrin; blue), TC terminals (the glutamate transporter VGluT2; red) and the reporter construct used for our virus injections (GFP; green). The example shows two colocalized puncta in L4 of V1. The first three images display individual channels, and the fourth shows merge of the three channels. The white arrows point to areas of colocalization. Scale bar: 10 µm. **b.** The plot shows the fluorescence intensity profiles of gephyrine, VGluT2 and GFP signals across the left punctum shown in **a.** The horizontal dashed line indicates the baseline signal intensity, while the vertical dotted lines outline the peak of the signal corresponding with the punctum. N = 24 slices from 3 rats. The fluorescence signal was quantified in a region of interest (ROI) extending across the center of each punctum and the three markers were considered colocalized if their peak fluorescence was within ± 0.1 µm. **c.** Bar graph showing the total number of cells per ROI (black), the total number of colocalized puncta per ROI (white with black border), and the ratio of colocalized puncta per cell (gray). **d.** Two example electron micrographs of TC terminals located in L4 of mV1, with gold particle staining against the α4 subunit of $GABA_A$ receptors. Black arrows point to areas of gold staining, located on the TC terminal.

Discussion

Selective $GABA_A$ modulation of TC terminals

Here, we have provided physiological, immunhistochemical, and electron microscopy evidence to show that $GABA_A$ receptors containing the diazepam-insensitive α4 subunit cluster on TC terminals that form synapses with neurons in L4 of V1. To study the location and action of $GABA_A$ receptors at TC and rIC synapses in L4, we selectively activated TC terminal fields using optogenetics, and recorded TC-EPSCs from postsynaptic neurons (Wang et al., 2013). To study rICs, paired recordings of L4 neurons were used to measure uEPSC and uIPSC amplitude and short term dynamics (Wang and Maffei, 2014). When muscimol was bath applied to the recording preparation, TC-EPSC amplitude onto Pyr and FS neurons were significantly reduced, and the short term dynamics were significantly increased, suggesting a presynaptic site of action. Muscimol application led to a significant change in the holding current of both Pyr and FS neurons, which is consistent with previous studies that confirm the role of tonic activation of $GABA_A$ receptors and also suggests that muscimol is acting on extrasynaptic $GABA_A$ receptors (Brickley et al., 1996; Stell and Mody, 2002). These effects could be blocked by the prior application of picrotoxin, which non-competitively blocks $GABA_A$ receptors chloride channels. Diazepam did not induce changes to TC-EPSC amplitude and dynamics, which suggests that these $GABA_A$ receptors lack benzodiazepine insensitive subunits (α4 and/or α6; Yang et al., 1995). Muscimol had no effect on uEPSCs recorded at rIC synapses. As expected, muscimol application significantly decreased the uIPSC amplitude of the FS-Pyr synapse, but this was not accompanied by a change in short term dynamics, indicated a postsynaptic effect. These data suggest that extrasynaptic, diazepam-insensitive $GABA_A$ receptors may be located on TC terminals.

Clustered α4 subunit containing $GABA_A$ receptors mediate the effect of muscimol at TC terminals

The functional evidence described above strongly suggests that $GABA_A$ are present on TC terminals that innervate L4 of V1, and may modulate TC terminal excitability. To confirm this, we showed that the $GABA_A$ receptor scaffolding protein gephyrin colocalized with ChR2-GFP labeled TC terminals, and VGluT2, a known marker of TC terminals (Nahmani and Erisir, 2005). We further confirmed the presence of extrasynaptic $GABA_A$ receptors by labeling the α4 subunit, and showing their location on putative TC terminals in L4 of V1. Together, these results demonstrate the presence of clusters of presynaptic $GABA_A$ receptors TC terminals, and support the interpretation that these receptors mediate the effect of muscimol on TC-EPSCs. Activation of presynaptic $GABA_A$ receptors is likely to shunt the depolarization of the glutamatergic terminal and decrease glutamate release as reported in the hippocampus.

Feedback Inhibition

Both feedforward and feedback inhibition in primary sensory neocortical circuits are critical for sensory processing and receptive field formation. Furthermore, inhibition has an important role in maintaining cortical excitability. TC activation of inhibitory circuits is more powerful than that of excitatory circuits (Cruikshank et al., 2007; Shiff and Reyes 2012; and see Chapter III). When the thalamus activates L4, FS neurons fire action potentials. The repetitive activation of FS neuron terminals onto other local neurons leads to an increase in the ambient level of GABA in L4, also known as the GABAergic tone. The specificity of the effect of muscimol, which affects TC, but not recurrent intracortical excitatory inputs, indicates that presynaptic $GABA_A$ receptors activation may provide an effective mechanism for local corticothalamic feedback mediated by increased GABAergic tone.

There is also anatomical evidence to suggest this role for ambient GABA at TC terminals. In V1 and the prefrontal cortex (PFC) of rodents, electron micrograph studies have shown that TC recipient Pyr neuron spines can be dually innervated by a recurrent inhibitory synapse (Dehay et al., 1991; Kubota et al., 2007). Dual innervation of Pyr neuron spines with TC axon terminals and excitatory recurrent terminals was not demonstrated in these studies. While it is highly unlikely that dual innervation of Pyr spines via TC and GABAergic synapses leads to a complete inhibitory veto of TC signaling (Dehay et al. 1991), the adjacent presence of inhibitory synapses may facilitate an increase in GABAergic tone at TC synapses.

This has a variety of implications for visual cortical function. The slow activation of presynaptic $GABA_B$ receptors on TC terminals has been suggested to reduce receptive field size in S1 (Chowdhury and Rasmusson, 2002; Kaneko and Hicks, 1990). *In vivo* experiments using naturalistic whole field visual stimulation found that cortical neurons become increasingly selective throughout the stimulation paradigm, and that this is mediated by suppressive surround interactions (Vinje and Gallant, 2000). Many theories have been postulated to explain this phenomenon, but recent work suggests that surround suppression in L4 does not depend on inhibition from the superficial layers of cortex (Self et al., 2014), but may instead be mediated at least in part by slow activating presynaptic $GABA_B$ receptors (Porter and Nieves, 2004). The presence of fast activating $GABA_A$ receptors, demonstrated here, may also play an important role in surround suppression in V1 during visual processing.

Cortical inhibition has a major role in regulating postnatal development in V1. The maturation of GABAergic inhibition signals the beginning of the critical period for visual cortical plasticity, which is a window of heightened sensitivity to changes in visual drive (Hensch 2004; 2005). During the critical period, thalamocortical and intracortical circuits are refined into their mature

states. Inhibition is necessary to organize TC axon branching, and segregate ocular dominance columns in V1 (Hensch, 2005). Because previous studies have only provided evidence for postsynaptic $GABA_A$ receptors, feedforward and intracortical inhibition have been thought to mediate this process. However, presynaptic $GABA_A$ receptors on TC terminals may also contribute to experience dependent plasticity.

$GABA_A$ receptors containing the α4 subunit have been shown to facilitate seizures in a model of epilepsy (Roberts et al., 2005; Sun et al., 2007; Mao et al., 2011). This may provide an important locus of study for seizure activity in the brain. $GABA_A$ α4 has also been implicated in autism (Fatemi et al., 2010). In addition, $GABA_A$ α4 subunits mediate the effects of anesthetics (Belelli et al., 2005; Garcia et al., 2010), neurosteroids (Belelli and Lambert, 2005), and alcohol (Hanchar et a., 2005; Jia et al., 2007; Rewal et al., 2009) on brain function. This may have important implications for the functional effects of alcohol specifically on the visual system, as well. As TC afferents provide a crucial gateway for sensory information to cortical circuits, presynaptic $GABA_A$ receptors containing the α4 subunit and located at TC terminals may play an important role in regulating neocortical circuit function under healthy and pathological conditions.

In addition to functional implications of this work, the results presented here have important implications for our current models of how inhibition modulates cortical function based on previously published studies. Intracortical muscimol infusions have been extensively used to assess the functional properties of TC inputs *in vivo*, under the assumption that it would silence cortical circuits, while leaving TC synapses unaffected. The presence of presynaptic $GABA_A$ receptors on TC terminals that we have demonstrated here compels further analysis of the effect of inhibition on thalamocortical and cortical activation and function.

References

Belelli D LJ (2005a) Neurosteroids: endogenous regulators of the GABA(A) receptor. Nature Reviews Neuroscience 6:565-575.

Belelli D PD, Rosahl TW, Wafford KA, Lambert JJ (2005b) Extrasynaptic GABAA receptors of thalamocortical neurons: a molecular target for hypnotics. The Journal of Neuroscience 25:11513-11520.

Brickley SG C-CS, Farrant M (1996) Development of a tonic form of synaptic inhibition in rat cerebellar granule cells resulting from persistent activation of GABAA receptors. The Journal of Physiology 497:753-759.

Chandra D HL, Linden AM, Procaccini C, Hellsten K, Homanics GE, Korpi ER (2010) Prototypic GABA(A) receptor agonist muscimol acts preferentially through forebrain high-affinity binding sites. Neuropsychopharmacology 35:999-1007.

Chandra D JF, Liang J, Peng Z, Suryanarayanan A, Werner DF, Spigelman I, Houser CR, Olsen RW, Harrison NL, Homanics GE (2006) GABAA receptor alpha 4 subunits mediate extrasynaptic inhibition in thalamus and dentate gyrus and the action of gaboxadol. Proceedings of the National Academy of Sciences 103:15230-15235.

Chowdhury SA RD (2002) Effect of GABAB receptor blockade on receptive fields of raccoon somatosensory cortical neurons during reorganization. Experimental brain research 145:150-157.

Cope DW HS, and Crunelli V (2005) GABAA Receptor-Mediated Tonic Inhibition in Thalamic Neurons The Journal of Neuroscience 25:11553-11563.

Cruikshank SJ, Lewis TJ, WConnors B (2007) Synaptic basis for intense thalamocortical activation of feedforward inhibitory cells in neocortex. Nature Neuroscience 10:462-468.

Dehay C DR, Martin KA, Nelson C (1991) Excitation by geniculocortical synapses is not 'vetoed' at the level of dendritic spines in cat visual cortex. The Journal of Physiology 440.

Eccles JC SR, Willis WD (1963) Pharmacological studies of presynaptic inhibition. The Journal of Physiology 168:500-530.

Fatemi SH RT, Folsom TD, Rooney RJ, Patel DH, Thuras PD (2010) mRNA and protein levels for GABAAalpha4, alpha5, beta1 and GABABR1 receptors are altered in brains from subjects with autism. The Journal of autism and developmental disorders 40:743-750.

Garcia PS KS, Jenkins A (2010) General anesthetic actions on GABA(A) receptors. Current Opinion in Neuropharmacology 8:2-9.

Hanchar HJ DP, Olsen RW, Otis TS, Wallner M (2005) Alcohol-induced motor impairment caused by increased extrasynaptic GABA(A) receptor activity. Nature Neuroscience 8:339-345.

JDerry JMC DS, Davies M (2004) Identification of a residue in the gamma-aminobutyric acid type A receptor a subunit that differentially affects diazepam-sensitive and -insensitive benzodiazepine site binding. The Journal of Neuroschemistry 88:1431-1438.

Jia F PL, Harrison NL (2007) GABAA receptors in the thalamus: alpha4 subunit expression and alcohol sensitivity. Alcohol 41.

Kaneko T HT (1990) GABA(B)-related activity involved in synaptic processing of somatosensory information in S1 cortex of the anaesthetized cat. British journal of pharmacology 100:689-698.

Kerr DI OJ (1995) GABAB receptors. Pharmacology and therapeutics 67:187-246.

Kim BG CJ, Choi IS, Lee MG, Jang IS (2011) Modulation of presynaptic GABA(A) receptors by endogenous neurosteroids. British journal of pharmacology 165:1698-1710.

Kubota Y HS, Kondo S, Karube F, Kawaguchi Y (2007) Neocortical inhibitory terminals innervate dendritic spines targeted by thalamocortical afferents. The Journal of Neuroscience 27:1139-1150.

Kullmann DM RA, Rusakov DM, Scott R, Semyanov A, Walker MC (2005) Presynaptic, extrasynaptic and axonal GABAA receptors in the CNS: where and why? Progress in Biophysics and Molecuar Biology 87:33-46.

Lee CC (2013) Thalamic and cortical pathways supporting auditory processing. Brain & Language 126:22-28.

Li L-y, Li Y-t, Zhou M, Tao HW, Zhang LI (2013) Intracortical multiplication of thalamocortical signals in mouse auditory cortex. Nature Neuroscience Brief Communications 16:1179-1183.

Mao X MP, Cao D, Sun C, Ji Z, Min D, Sun H, Xie N, Cai J, Cao Y (2011) Altered expression of GABAA receptors (α4, γ2 subunit), potassium chloride cotransporter 2 and astrogliosis in tremor rat hippocampus. Brain research bulletin 86:373-379.

Nahmani M EA (2005) VGluT2 Immunochemistry Identifies Thalamocortical Terminals in Layer 4 of Adult and Developing Visual Cortex. The Journal of Comparative Neurology 484:458-473.

Porter JT ND (2004) Presynaptic GABAB receptors modulate thalamic excitation of inhibitory and excitatory neurons in the mouse barrel cortex. The Journal of Neurophysiology 92:2762-2720.

Pouzat C MA (1999) Somatic recording of GABAergic autoreceptor current in cerebellar stellate and basket cells. The Journal of Neuroscience 19:1675-1690.

Rewal M JR, Gill TM, He DY, Ron D, Janak PH (2009) Alpha4-containing GABAA receptors in the nucleus accumbens mediate moderate intake of alcohol. The Journal of Neuroscience 29:543-549.

Roberts DS RY, Bandyopadhyay S, Lund IV, Budreck EC, Passini MA, Wolfe JH, Brooks-Kayal AR, Russek SJ (2005) Egr3 stimulation of GABRA4 promoter activity as a mechanism for seizure-induced up-regulation of GABA(A) receptor alpha4 subunit expression. Proceedings of the National Academy of Sciences 102:11894-11899.

Ruiz A CE, Scott RS, Rusakov DA, Kullmann DM (2010) Presynaptic GABAA receptors enhance transmission and LTP induction at hippocampal mossy fiber synapses. Nature Neuroscience 13:431-438.

Ruiz A KD (2013) Ionotropic receptors at hippocampal mossy fibers: roles in axonal excitability, synaptic transmission, and plasticity. Neural Circuits 6:1-12.

Schiff ML, Reyes AD (2012) Characterization of thalamocortical responses of regular-spiking and fast-spiking neurons of the mouse auditory cortex in vitro and in silico. The Journal of Neurophysiology 107:1476-1488.

Self MW LJ, Vangeneugden J, van Beest EH, Grigore ME, Levelt CN, Heimel JA, Roelfsema PR (2014) Orientation-tuned surround suppression in mouse visual cortex. The Journal of Neuroscience 34:9290-9304.

Sherman SM (2012) Thalamocortical interactions. Current Opinion in Neurobiology 22:1-5.

Stell BM MI (2002) Receptors with different affinities mediate phasic and tonic GABA(A) conductances in hippocampal neurons. The Journal of Neuroscience 22:RC223.

Stratford KJ, Tarczy-Hornoch K, Martin KAC, Bannister NJ, Jack JJB (1996) Excitatory synaptic inputs to spiny stellate cells in cat visual cortex. Nature Letters 382:258-261.

Sun C MZ, Erisir A, Kapur J (2007) Diminished neurosteroid sensitivity of synaptic inhibition and altered location of the alpha4 subunit of GABA(A) receptors in an animal model of epilepsy. The Journal of Neuroscience 27:12641-12650.

Vinje WE GJ (2000) Sparse coding and decorrelation in primary visual cortex during natural vision. Science 287:1273-1276.

Wang L KM, Gu, Y, Ge S, Maffei A (2013) Layer-Specific Experience-Dependent Rewiring of Thalamocortical Circuits. The Journal of Neuroscience 33:4181-4191.

Wang L MA (2014) Inhibitory Plasticity Dictates the Sign of Plasticity at Excitatory Synapses. The Journal of Neuroscience 34:1083-1093.

Yang W DJ, Lan, Nancy (1995) Cloning and characterization of the human GABA, receptor a4 subunit: identification of a unique diazepam-insensitive binding site. European Journal of Pharmacology 291:319-325.

Chapter V: Future directions – Thalamocortical plasticity during the critical period

Abstract

Thalamocortical (TC) plasticity during later postnatal development in primary sensory cortices is controversial. Plasticity refers to the ability of a given neuron to change the efficacy of its synapses depending on specific patterns of activation. This can lead either to the strengthening or weakening of inputs. Synaptic plasticity is critical for normal circuit development and function, and thalamocortical (TC) plasticity in V1 is poorly understood. In V1, plasticity at TC synapses may be important for the experience dependent refinement of inputs during the critical period. Here, we used optogenetics to selectively activate thalamocortical (TC) terminals combined with whole cell patch clamp stimulation to show that TC synapses can express plasticity during the critical period of development. Long term potentiation (LTP) and depression (LTD) could be successfully induced at TC synapses following specifically timed pre- and postsynaptic activation, known as spike timing dependent plasticity.

Authors: Michelle Kloc and Arianna Maffei

Author Contributions: M.K. and A.M. designed experiments, M.K. performed research and analyzed data; M.K. and A.M. wrote the chapter.

Introduction

When the sequential or simultaneous activation of a pre- or a post-synaptic leads to changes in the synaptic strength, the effect is known as synaptic plasticity (Hebb, 1949). The synaptic strength can either be potentiated (LTP) or depressed (LTD). The sign and magnitude of the change in synaptic efficacy is determined by the relative timing of pre- and postsynaptic activation, known as spike timing dependent plasticity (STDP; For review see Markram 2011; Feldman, 2012). During classic Hebbian STDP, when presynaptic activation occurs before

postsynaptic activation, synaptic strength is potentiated. When postsynaptic activation occurs before presynaptic activation, the synapse depressed (Fig 5.1). STDP depends heavily of the order of activation, and also can only occur within precise temporal windows of sequential activation (Markram 1997).

Specifically timed firing of connected neurons can strengthen or weaken synapses, which may be involved in sensory experience driven plasticity. Starting one week after eye opening, the visual system undergoes a period of maturation and refinement during a window of heightened sensitivity to changes in visual drive, known as the critical period for visual cortical plasticity (Hensch, 2004). During the critical period (CP), visual deprivation leads to profound changes in the intracortical circuits of V1 (Hubel and Wiesel, 1963; Fagiolini et al., 1994; Antonini et al., 1993; Frenkel and Bear, 2004; Maffei et al., 2006). There has been some evidence to suggest that TC synapses mediate these changes (Linden et al., 2009). Monocular deprivation (MD), which leads to an unbalanced activity from the two eyes, is a powerful tool to investigate experience dependent plasticity of visual cortical circuits. MD leads to decreased cortical responsiveness to the deprived eye, and eventually the deprived area of cortex will be taken over by inputs from the nondeprived eye. Whether TC transmission plays an active role in this process is poorly understood. Recent anatomical work shows that after short term (3 days) MD, TC synapses undergo significant remodeling (Coleman et al., 2010). Furthermore, the shift in ocular dominance (OD) in binocular V1 during MD is mediated by depression of TC synapses (Khibnik et al., 2010). MD can be induced either by eyelid suture, which decreases visual drive, or inactivation of the retina or optic nerve, which fully silences the input to the LGN. TC signaling drives visual cortical plasticity via distinct firing patterns depending on whether MD is induced by lid suture or inactivation (Linden et al., 2009).

This suggests that TC synapses may be plastic during the critical period, and may actively mediate intracortical plasticity. This would depend on how TC inputs are integrated with intracortical inputs, and whether or not coincidence activation of TC terminal fields and their postsynaptic targets affects synaptic efficacy. STDP at TC synapses may likely mediate TC involvement in experience dependent plasticity of intracortical circuits. To test this possibility, we determined whether or not STDP could be induced at TC-V1 synapses during the critical period. We selectively activated TC terminal fields using optogenetics, and stimulated TC-EPSCs from excitatory pyramidal (Pyr) neurons in L4 of V1 at P25 in mice. We show that the timing of TC activation and cortical activation can change synaptic efficacy. This compels an extensive study of TC plasticity during the CP, and how this may affect intracortical changes that occur during MD.

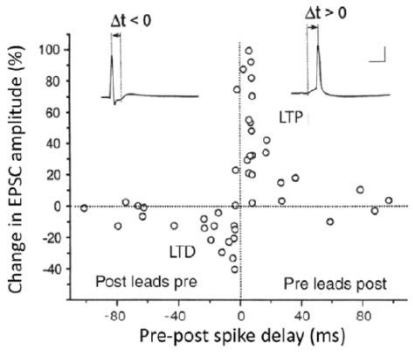

Figure 5.1. Hebbian STDP. Canonical STDP induced at an excitatory synapse, showing LTP when presynaptic activation leads postsynaptic activation; and LTD when postsynaptic activation leads presynaptic activation, Adapted from Feldman, 2002.

Results

LGN expression was verified and quantified as described previously (see Chapter II, III and VII; Fig. 2.1; Fig 3.1). Here, we induced STDP at TC synapses that changed synaptic efficacy. When postsynaptic activation of L4 neurons preceded TC terminal field activation by 35 ms, TC-EPSCs trend toward depression (Fig 5.3; -35 ms, -27±3% baseline TC-EPSC amplitude, n=6, p=0.08). When postsynaptic activation of L4 neurons preceded TC terminal field activation by 20 ms, TC-EPSC depression was less pronounced (Fig 5.3; -20 ms, -16±2% of baseline TC-EPSC amplitude, n=9). When pre-and postsynaptic activation occurred simultaneously, TC-EPSC amplitude was unchanged (Fig 5.3; 0 ms, -5±4% of baseline TC-EPSC amplitude, n=5). When TC terminal fields were activated 10 ms before L4 neuron activation, TC-EPSC amplitude was significantly potentiated (Fig 5.3; +10 ms, 20±2% of baseline, n=7, $p<0.05$). When TC terminal fields were activated 35 ms before L4 neuron activation, there was no change in TC-EPSC amplitude (Fig 5.3; +35 ms, 4±2%, n=17). This shows that Hebbian STDP (Fig 5.1) can be induced at TC-V1 synapses during the CP, within a narrow temporal window of pre- and postsynaptic activation. This may be important to mediate experience dependent plasticity of intracortical synapses. A great deal of study is necessary to determine how TC plasticity may affect V1 circuit activation, and what the possible functional consequences of TC plasticity may be.

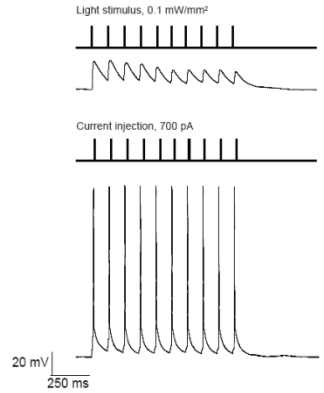

Figure 5.2. **STDP Induction paradigm**. Presynaptic activation by 2 ms pulses of blue light, at intensity of 0.1 mW/mm^2 precedes postsynaptic neuron activation via 700 pA current injection by 10 ms.

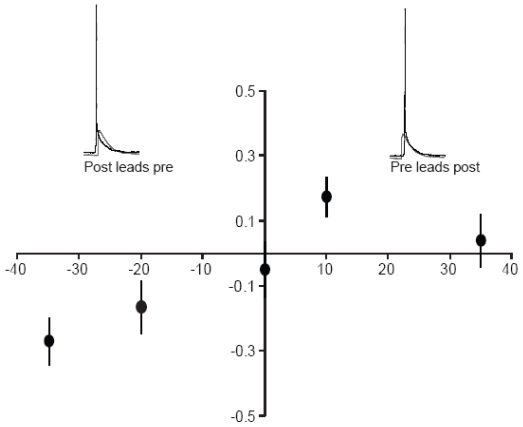

Figure 5.3. Hebbian STDP can be induced as TC-Pyr synapses. Percent change of TC-EPSCs recorded from L4 excitatory pyramidal neurons in mouse V1 following STDP induction. When postsynaptic firing came before presynaptic firing, TC synapses were depressed. When presynaptic firing came before postsynaptic firing, TC synapses were potentiated.

Discussion

Here, we combined specifically timed presynaptic optogenetic activation of TC terminal fields and postsynaptic activation of L4 neurons to induce spike timing dependent plasticity during the critical period. When TC terminal field stimulation preceded the L4 neuron activation, TC-EPSCs were potentiated. When pre- and postsynaptic activation occurred simultaneously, there was no change in TC-EPSC amplitude. When TC terminal field stimulation occurred after L4 neuron activation, the TC-EPSC was depressed. This is consistent with typical Hebbian STDP patterns. Hebbian STDP has been observed consistently at excitatory synapses onto neocortical neurons (Markram et al., 1997; Feldman, 2000; Nevian and Sakmann, 2006), as well as in many other subcortical brain regions.

The function of Hebbian STDP is to strengthen synapses when firing is correlated. When two neurons are connected, and presynaptic activation consistently leads to postsynaptic firing, it can be concluded that this synapse is functionally relevant and is potentiated. Conversely, if presynaptic firing and postsynaptic firing are decorrelated, the synapse is ineffective and is depressed. Developmentally, STDP contributes to the formation of receptive fields in primary sensory cortices (Song and Abbott, 2001; Clopath et al., 2010), and mediates competition between converging inputs (Zhang et al., 1998; Song et al., 2000). This has profound implications for both early and late postnatal development of TC inputs to V1.

Whether or not TC synapses can express LTP and LTD during the CP remains poorly understood and controversial. In rodents, TC synapses onto V1 neurons undergo significant changes in terminal size and number during the critical period (Erisir and Dreusicke, 2005), and TC transmission to V1 can be potentiated by environmental enrichment (Mainardi et al., 2010). However, this input has not been directly studied in a slice preparation in V1.

In S1, TC inputs are no longer plastic after the first week of development. In A1, which shares many similarities to S1 and V1, TC synapses were long considered incapable of plasticity following the first week of life. Instead, it was discovered that TC synapses can express LTP and LTD both as neonates and as adults, but becomes gated with age (Blundon et al., 2011; Chun et al., 2013). Here, we have provided some evidence to suggest that TC inputs may retain some mechanisms of plasticity. Taken together, we conclude that TC inputs of primary sensory cortices may be plastic during the critical period.

References

Antonella Antonini MF, Michael P Stryker (1999) Anatomical Correlates of Functional Plasticity in Mouse Visual Cortex. The Journal of Neuroscience 19:4388-4406.

Antonella Antonini MPS (1993) Rapid Remodeling of Axonal Arbors in the Visual Cortex. Science 260:1819-1821.

Blundon J IB, S Zakharenko (2011) Presynaptic gating of postsynaptically expressed plasticity at mature thalamocortical synapses. The Journal of Neuroscience 31:16012-16025.

Chun S IB, JA Blundon, SS Zakharenko (2013) Thalamocortical long-term potentiation becomes gated after the early critical period in the auditory cortex. The Journal of Neuroscience 33:7345-7357.

Clopath C BL, Vasilaki E, Gerstner W (2010) Connectivity reflects coding: a model of voltage-based STDP with homeostasis. Nature Neuroscience 13:344-352.

Coleman JE MN, Jeffrey P. Gavornik, Robert Haslinger, Arnold J. Heynen, Alev Erisir and Mark F. Bear (2010) Rapid Structural Remodeling of Thalamocortical Synapses Parallels Experience-Dependent Functional Plasticity in Mouse Primary Visual Cortex. The Journal of Neuroscience 30:9670-9682.

Erisir A, Dreusicke M (2005) Quantitative Morphology and Postsynaptic Targets of Thalamocortical Axons in Critical Period and Adult Ferret Visual Cortex. The Journal of Comparative Neurology 485:11-31.

Fagiolini M PT, Berardi N, Domenici L, Maffei L (1994) Functional postnatal development of the rat primary visual cortex and the role of visual experience: dark rearing and monocular deprivation. Vision Research 34:709-720.

Feldman DE (2000) Timing-Based LTP and LTD at Vertical Inputs to Layer II/III Pyramidal Cells in Rat Barrel Cortex. Neuron 27:45-56.

Feldman DE (2012) The Spike-Timing Dependence of Plasticity. Neuron 75:556-571.

Frenkel M BM (2004) How Monocular Deprivation Shifts Ocular Dominance in Visual Cortex of Young Mice. Neuron 44:917-923.

Gu Y A-CM, Wang J, Janoschka SR, Josselyn SA, Frankland PW, Ge S (2012) Optical controlling reveals time-dependent roles for adult-born dentate granule cells. Nature Neuroscience 15:1700-1706.

Hebb D (1949) The Organization of Behavior. New York: Wiley.

Hubel DH WT (1963) Single cell responses in striate cortex of kittens deprived of vision in one eye. The Journal of Neurophysiology 26:1003-1017.

Khibnik LA KKACaMFB (2010) Relative Contribution of Feedforward Excitatory Connections to Expression of Ocular Dominance Plasticity in Layer 4 of Visual Cortex. Neuron 66:493-500.

Linden ML AJH, Robert H Haslinger & Mark F Bear (2009) Thalamic activity that drives visual cortical plasticity. Nature Neuroscience Brief Communications 12:390-392.

Maffei A KN, Sacha B. Nelson & Gina G. Turrigiano (2006) Potentiation of cortical inhibition by visual deprivation. Nature Letters 443:81-84.

Mainardi M SL, Laura Gianfranceschi, Sara Baldini, Roberto De Pasquale, Nicoletta Berardi, Lamberto Maffei and Matteo Caleo (2010) Environmental Enrichment Potentiates Thalamocortical Transmission and Plasticity in the Adult Rat Visual Cortex. Journal of Neuroscience Research 88:3048-3059.

Markram H, Lubke, J., Frotscher, M., and Sakmann, B (1997) Regulation of synaptic efficacy by coincidence of postsynaptic APs and EPSPs. Science 275:213-215.

Nevian T SB (2006) Spine Ca2+ signaling in spike-timing-dependent plasticity. The Journal of Neuroscience 26:11001-11013.

Song S AL (2001) Cortical development and remapping through spike timing-dependent plasticity. Neuron 32:339-350.

Song S MK, Abbott LF (2000) Competitive Hebbian learning through spike-timing-dependent synaptic plasticity. Nature Neuroscience 3:919-926.

Wang L, Kloc M, Gu Y, Ge S, Maffei A (2013) Layer-Specific Experience-Dependent Rewiring of Thalamocortical Circuits. The Journal of Neuroscience 33:4181– 4191.

Zhang LI TH, Holt CE, Harris WA, and Poo M (1998) A critical window for cooperation and competition among developing retinotectal synapses. Nature 395:37-44.

Chapter VI: Discussion

Thalamocortical inputs from the LGN relay sensory information to primary visual cortex (V1), and drive cortical activity. Because of limitations in the available technical approaches to study thalamocortical inputs into V1, the synaptic organization and properties of this input remain poorly understood. Here, we have combined an optogenetic approach with acute slice electrophysiology to investigate TC input to V1 neurons using acute slice electrophysiology and optogenetics, which allowed for a detailed examination of synaptic properties.

Layer-specific properties of TC inputs onto V1

In Chapter II, we discussed the layer-specific synaptic properties, experience dependence, and organization of TC terminals in layers 4 and 6 on V1. TC terminal fields were selectively activated using light pulses, and excitatory postsynaptic currents (TC-EPSCs) were recorded via whole cell patch clamp of excitatory neurons in L4 and L6. TC-EPSCs onto L4 neurons were large and depressed following repeated stimuli, while TC-EPSCs recorded from L6 neurons were small, slower, and depressed less.

Thalamocortical inputs onto L4 and L6 of primary sensory cortices may play different roles. LGN inputs can act either as a driver (Type I) or modulator (Type II) of cortical activity; and these different functions relate to the synaptic properties (Sherman, 2007; 2012). Type I inputs are large, fast, and depress in response to repeated stimuli; and Type II inputs are smaller, slower, and depress less in response to repetitive stimuli. In primary auditory (A1) and somatosensory (S1) cortices, thalamic inputs to L4 are Type I inputs, or drivers; and thalamic inputs to L6 are Type II, or modulators (Viaene et al., 2010; Schiff and Reyes, 2012). The experiments and results described in Chapter II support this finding. The amplitude and short term depression observed at TC-EPSCs onto L4 neurons indicates a Type I TC input; and the

properties of TC-EPSCs onto L6 neurons was consistent with a Type II input.

The TC and intracortical circuits are also significantly different in L4 and L6. TC inputs form synapses with a much larger proportion of L4 neurons than L6 neurons, and a significantly larger number of TC recipient neurons were recurrently connected in L4 versus L6. TC-EPSCs recorded from recurrently connected neurons in L4 had a similar magnitude, suggesting that connected neurons are likely driven by the same TC axon.

In addition to differences in connectivity, there were also significant differences in the sensitivity to changes in visual experience of TC-EPSCs recorded from L4 and L6 neurons. After a short period of monocular deprivation, TC-EPSCs recorded from L4 neurons significantly decreased; but TC-EPSCs recorded from L6 were unaffected. This further suggests a different role for TC inputs onto L4 and L6 neurons.

TC inputs to L4 relay sensory information, and L4 then activates other layer of V1 in a feedforward manner. The function of L6 in the V1 circuit is less understood. Studies investigating L6 function have suggested that L6 acts as a coincidence detector of TC input (Usrey, Alonso, and Reid, 2000). Furthermore, L6 has been shown to affect cortical activity by modulating cortical gain following activation (DaCosta and Martin, 2009; Bortone et al., 2014). LGN axons that innervate V1 in principle carry the same information; however, the postsynaptic effects of LGN-V1 activation are layer specific. This supports the conclusion that LGN inputs to L4 and L6 in V1 may play different roles.

Target-specific properties of TC inputs to V1

The LGN drives the activity of L4, the main input layer of V1. L4 is composed of a highly interconnected network of excitatory and inhibitory neurons. In A1 and S1, TC inputs monosynaptically activate both excitatory and inhibitory circuits (Cruikshank et al., 2007; Schiff

and Reyes 2012). In V1, anatomical and functional evidence suggest that LGN inputs form synapses with both excitatory and inhibitory neurons (Freund et al., 1985; Ahmed et al., 1994; 1997), however the synaptic properties of this input remained unstudied. Chapter III describes the synaptic properties of Type I inputs from the LGN onto L4 neurons (see summary Fig 6.1). TC-EPSCs and TC-EPSPs were recorded from excitatory pyramidal (Pyr) and inhibitory L4 neurons following light activation of TC terminal fields. We found that L4 neurons have target cell-type specific properties. Two types of inhibitory neurons were tested in this study, the fast spiking (FS) and regular spiking non-pyramidal (RSNP) inhibitory neurons. Only FS neurons were monosynaptically activated by TC terminal field stimulation; therefore FS neurons mediate feedforward inhibition of V1 from the LGN. TC inputs activate FS neurons more strongly than the Pyr neurons, and this is mediated by both pre- and post-synaptic mechanisms. Presynaptically, TC inputs onto FS neurons have a larger number of release sites and a higher release probability than TC inputs onto Pyr neurons. Postsynaptically, TC-EPSCs onto FS neurons are mediated by GluA2-lacking AMPA receptors, and lack an NMDAR contribution to the current. TC-EPSCs onto Pyr neurons are mediated by GluA2-containing AMPAR and NMDAR current.

When LGN neurons relay sensory information to V1, they activate powerful feedforward excitation, and even more powerful feedforward inhibition. The pre- and postsynaptic differences noted in Chapter II likely underlie the differences in synaptic strength of TC inputs onto Pyr and FS neurons. However, these differences have many more implications for how the LGN activates L4. The differences in postsynaptic receptor composition indicate that Pyr and FS neurons compartmentalize calcium at LGN synapses differently. TC-EPSCs onto Pyr neurons mediated by both AMPAR and NMDAR mediated currents; so when the synapse is activated a

calcium current flows across the membrane. Although TC-EPSCs onto FS neurons is mediated by GluA2-lacking AMPARs, which pass some calcium, the magnitude of calcium ions flowing across the membrane is much smaller. This indicates that these synapses likely have a different capacity to induce plasticity, both short term and long term.

The difference in paired pulse ratio (PPR) and steady state ratio (SSR) of TC-EPSCs onto Pyr and FS neurons following repetitive stimulation of TC terminal fields further suggests a different capacity to induce plasticity at these synapses. TC-EPSCs onto Pyr neurons respond more efficiently to repetitive LGN activation, shown by a larger PPR and SSR. Differently, repetitively stimulation of TC inputs onto FS neurons resulted in greatly depressed TC-EPSCs. Despite this difference in depression, FS neurons still fired significantly more action potentials that Pyr neurons following TC terminal field stimulation. The direct activation of FS neurons by the LGN acts to clamp the circuit and prevent runaway excitation. Indeed, when inhibition is removed, Pyr neurons were consistently driven above threshold and fired action potentials. When the LGN activates V1, the large feedforward excitation and inhibition are precisely timed to control cortical activity. However, the fact that TC synapses onto Pyr neurons can still be reliably activated with repetitive stimulation suggests that while feedforward inhibition prevents the recurrent activation of the circuit from becoming epileptic, it does not impair sub- or suprathreshold signal processing by Pyr neurons. Recurrent excitation is critical for the processing of sensory information (DaCosta and Martin, 2011; Li et al., 2013), but must be controlled. Normal levels of excitation and inhibition are necessary for healthy circuit function, development, and plasticity; and direct LGN activation of Pyr and FS neurons is likely vital for maintaining a normally functioning L4 circuit; and consequently the entire visual cortical circuit.

Feedforward inhibition and corticothalamic feedback

Thalamocortical activation of V1 is complex. It activates both L4 and L6 in a feedforward manner, but TC inputs to L4 and L6 have layer specific properties and likely different functional roles. TC inputs onto Pyr and FS neurons also have target cell-type specific properties. In V1, inhibition is powerful and acts as a brake on the V1 circuit by preventing excessive recurrent excitation within L4. Runaway recurrent excitation would then propagate to other layers in V1; thus L4 inhibition is critical for normal activity levels of all V1 circuits. Feedforward activation of L4 FS neurons is not the only mechanism of inhibitory control over excessive TC activation. In Chapter III, we discuss a mechanism of cortical feedback control of TC inputs. Here, we have demonstrated the presence of presynaptic $GABA_A$ receptors containing the alpha 4 subunit on TC terminals using electrophysiology, immunohistochemistry, and electron microscopy (see summary Fig 6.1). TC synapses activate the inhibitory circuit more strongly than the excitatory circuit, as shown by a greater spike reliability ratio of FS neurons in L4. After repetitive activation of TC synapses, the overall GABAergic tone of L4 can increase as a result of FS neurons repetitively firing action potentials. An increased concentration of extracellular GABA in L4 could serve as a local feedback mechanism by binding to presynaptic $GABA_A$ receptors located on TC terminal fields. Thus, presynaptic $GABA_A$ receptors could act as a sensor for increased GABA in the extracellular space; and modulate the strength of TC inputs. Not only is inhibition controlling the excitability of the L4 circuit in V1, but it could also regulate the ability of TC terminal fields to activate TC-L4 synapses.

Role of TC transmission in cortical circuit function

The techniques and results presented here are only a small part of the work required to understand the properties and mechanisms of TC synapses onto V1 neurons. TC transmission to

V1, particularly L4, plays an important part in shaping cortical activity. During the critical period, TC transmission is the input that provides sensory information. In primary sensory cortices, whether TC inputs can maintain their capacity for plasticity after eye opening is controversial. Historically, it has been shown that TC synapses lose the capacity for plasticity following the first week of life. However, a different set of studies showed that TC inputs are still susceptible to decreased sensory input during windows of heightened sensitivity to changes in visual drive during the critical period for visual cortical plasticity (Antonini et al., 1999; Coleman et al., 2010). As shown in Chapter II, TC-EPSCs onto L4 neurons are sensitive to changes in visual drive during the critical period. Short monocular deprivation significantly reduces the amplitude of TC-EPSCs onto excitatory neurons (Wang et al., 2013). In functional experiments, TC activity drives experience dependent plasticity through different firing patterns. Short term monocular deprivation leads to the loss of TC-L4 synapses (Silver and Stryker, 1999; Coleman et al., 2010); and long term visual deprivation in V1 leads to the withdrawal of TC synapses from their targets (Antonini et al., 1993; 1999). Interestingly, then TC fibers withdraw from the cortex their synaptic density does not decrease, just their overall number of contacts with V1 neurons (Silver and Stryker, 1999). Furthermore, in V1, environmental enrichment led to the expression of LTP at TC synapses in the adult mouse (Mainardi et al., 1999). This suggests that TC synapses are in fact able to express plasticity, but plasticity can only be expressed under certain conditions.

Indeed, in A1, TC synapses onto L4 neurons underlie frequency-specific plasticity (Zhu et al., 2013). In A1, TC synaptic plasticity is not lost with maturity. Instead, the ability to express LTP and LTD becomes presynaptically gated by adenosine receptors (Blundon et al., 2011; Chun et al., 2013). This suggests that TC plasticity may in fact be induced at TC synapses during the

critical period in V1. The future directions of this project are to investigate the synaptic plasticity of TC inputs onto V1 neurons. Chapter IV shows that spike timing dependent plasticity (STDP) can be induced at TC synapses onto Pyr neurons in L4 during the critical period. Combined with controversial findings about TC plasticity in the primary sensory cortices, this compels the need for further study of synaptic plasticity of TC inputs onto excitatory and FS inhibitory neurons.

Together, these results add to and significantly enhance the current understanding of thalamocortical circuits in V1. For many years, it was unknown whether TC activation of the primary sensory cortices relied on the same mechanisms. The results presented here show that the properties of TC inputs to V1 share some similarities with input to other cortices, but perhaps not as many as were originally assumed. Thalamic input is fundamental to both sensory and nonsensory cortical function and development. Thalamic malfunction has been implicated in a number of neurological disorders such as schizophrenia (Behrendt, 2006; Cronenwett and Csernansky, 2010), epilepsy (Kanner, 2004; Avoli, 2012; Seneviratne, 2014), depression (Drevets, 2000; Clark et al., 2009), and sleep disorders (Germain et al, 2004; Brown et al., 2012). The potential effect of thalamic dysregulation is unlikely to be limited to only one system; therefore, understanding how TC inputs to L4 neurons drive cortical excitability and are integrated during development is crucial to understanding how abnormal TC activity may contribute to disease.

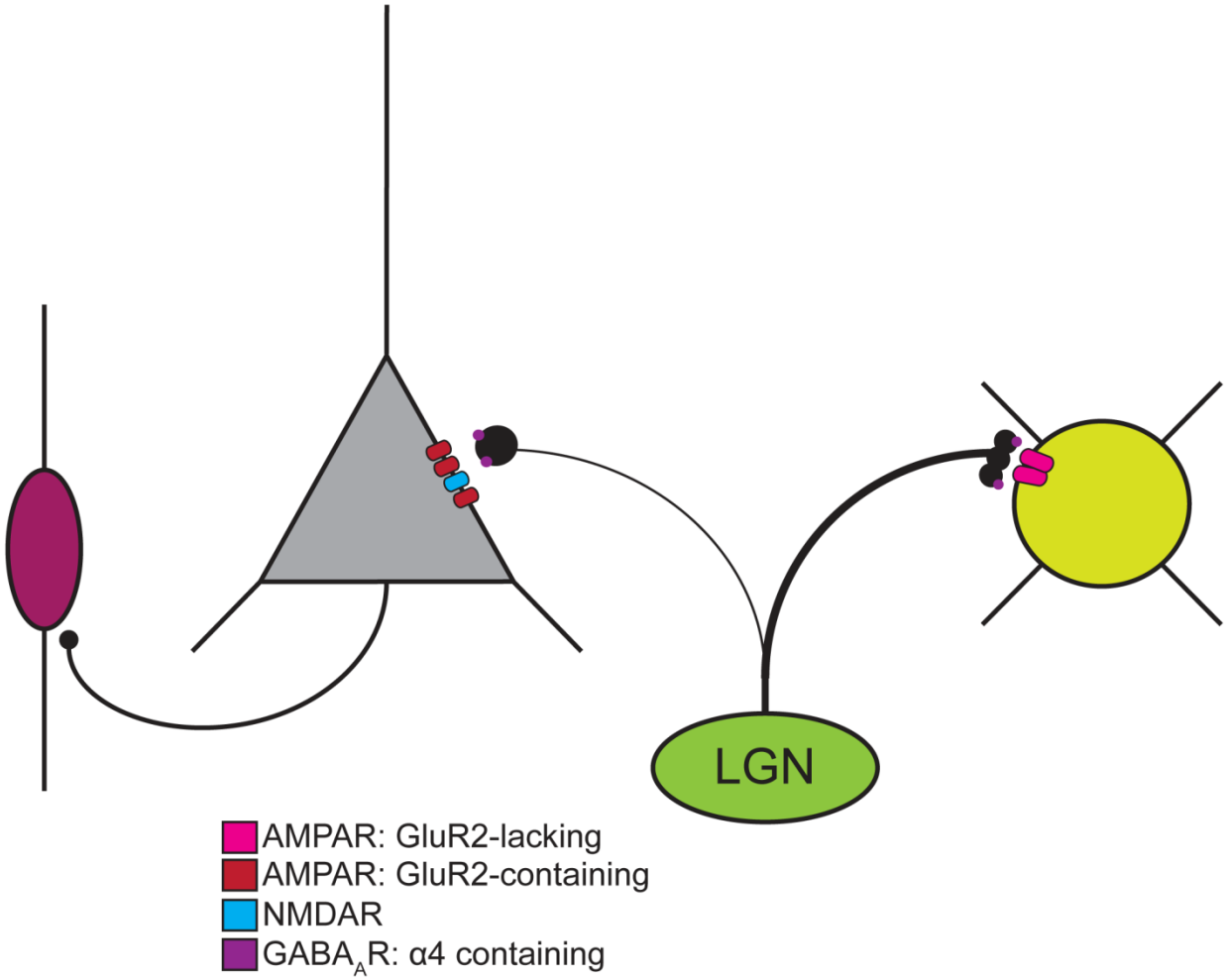

Fig 6.1: TC synapses onto L4 neurons in V1. TC inputs directly activate excitatory pyramidal and FS inhibitory neurons in L4.

References

Ahmed B, Anderson JC, Martin KAC (1997) Map of the Synapses Onto Layer 4 Basket Cells of the Primary Visual Cortex of the Cat. The Journal of Comparative Neurology 380:230–242.

Ahmed B, Anderson JC, Douglas RJ, Martin KAC, Nelson JC (1994) Polyneuronal Innervation of Spiny Stellate Neurons in Cat Visual Cortex. The Journal of Comparative Neurology 341:39-49.

Antonella Antonini MF, Michael P Stryker (1999) Anatomical Correlates of Functional Plasticity in Mouse Visual Cortex. The Journal of Neuroscience 19:4388-4406.

Antonella Antonini MPS (1993) Rapid Remodeling of Axonal Arbors in the Visual Cortex. Science 260:1819-1821.

Avoli M (2012) A brief history on the oscillating roles of thalamus and cortex in absence seizures. Epilepsia 53:779-789.

Blundon J IB, S Zakharenko (2011) Presynaptic gating of postsynaptically expressed plasticity at mature thalamocortical synapses. The Journal of Neuroscience 31:16012-16025.

Bortone D, Olsen SR, Scanziani M (2014) Translaminar inhibitory cells recruited by layer 6 corticothalamic neurons suppress visual cortex. Neuron 82:474-485.

Brown RE BR, McKenna JT, Strecker RE, McCarley RW (2012) Control of sleep and wakefulness. Physiological reviews 92:1087-1187.

Chun S IB, JA Blundon, SS Zakharenko (2013) Thalamocortical long-term potentiation becomes gated after the early critical period in the auditory cortex. The Journal of Neuroscience 33:7345-7357.

Clark L CS, Sahakian BJ (2009) Neurocognitive mechanisms in depression: implications for treatment. Annual Review of Neuroscience 32:57-74.

Coleman JE MN, Jeffrey P. Gavornik, Robert Haslinger, Arnold J. Heynen, Alev Erisir and Mark F. Bear (2010) Rapid Structural Remodeling of Thalamocortical Synapses Parallels Experience-Dependent Functional Plasticity in Mouse Primary Visual Cortex. The Journal of Neuroscience 30:9670-9682.

Cruikshank SJ, Lewis TJ, WConnors B (2007) Synaptic basis for intense thalamocortical activation of feedforward inhibitory cells in neocortex. Nature Neuroscience 10:462-468.

DaCosta NM MK (2009) The Proportion of Synapses Formed by the Axons of the Lateral Geniculate Nucleus in Layer 4 of Area 17 of the Cat. The Journal of Comparative Neurology 516:264-276.

DaCosta NM MK (2011) How Thalamus Connects to Spiny Stellate Cells in the Cat's Visual Cortex. The Journal of Neuroscience 31:2925-2937.

Drevets W (2000) Neuroimaging studies of mood disorders. Biological psychiatry 48:813-829.

Freund TF, Martin KAC, Somogyi P, Whitteridge D (1985) Innervation of Cat Visual Areas 17 and 18 by Physiologically Identified X- and Y- Type Thalamic Afferents. II. Identification of Postsynaptic Targets by GABA Immunocytochemistry and Golgi Impregnation. The Journal of Comparative Neurology 242:275-291.

Kanner A (2004) Thalamic Dysfunction in Idiopathic Generalized Epilepsy: New Findings of Old News. Epilepsy currents 4:57-58.

Lee CC (2013) Thalamic and cortical pathways supporting auditory processing. Brain & Language 126:22-28.

Lee CC, Imaizumi K (2013) Functional Convergence of Thalamic and Intrinsic Projections to Cortical Layers 4 and 6. Neurophysiology 45:396-406.

Li L-y, Li Y-t, Zhou M, Tao HW, Zhang LI (2013) Intracortical multiplication of thalamocortical signals in mouse auditory cortex. Nature Neuroscience Brief Communications 16:1179-1183.

Mainardi M SL, Laura Gianfranceschi, Sara Baldini, Roberto De Pasquale, Nicoletta Berardi, Lamberto Maffei and Matteo Caleo (2010) Environmental Enrichment Potentiates Thalamocortical Transmission and Plasticity in the Adult Rat Visual Cortex. Journal of Neuroscience Research 88:3048-3059.

Schiff ML, Reyes AD (2012) Characterization of thalamocortical responses of regular-spiking and fast-spiking neurons of the mouse auditory cortex in vitro and in silico. The Journal of Neurophysiology 107:1476-1488.

Seneviratne U CM, D'Souza W (2014) Focal abnormalities in idiopathic generalized epilepsy: a critical review of the literature. Epilepsia 55:1157-1169.

Sherman SM (2007) The thalamus is more than just a relay. Current Opinion in Neurobiology 17:417-422.

Sherman SM (2012) Thalamocortical interactions. Current Opinion in Neurobiology 22:1-5.

Silver MA Stryker M (1999) Synaptic density in geniculocortical afferents remains constant after monocular deprivation in the cat. The Journal of Neuroscience 19:10829-10842.

Viaene AN, Petrof I, Sherman SM (2011) Synaptic Properties of Thalamic Input to the Subgranular Layers of Primary Somatosensory and Auditory Cortices in the Mouse. The Journal of Neuroscience 31:12738-12747.

Wang L, Kloc M, Gu Y, Ge S, Maffei A (2013) Layer-Specific Experience-Dependent Rewiring of Thalamocortical Circuits. The Journal of Neuroscience 33:4181– 4191.

Zhu ZR XF, Wu JH, Ren SC, Zhang YH, Hu B, Zhang J, Han L, Xiong Y (2013) Frequency-specific plasticity of the auditory cortex elicited by thalamic stimulation in the rat. Neuroscience Letters 555:30-35.

Chapter VII: Methods and Materials

Surgerical Procedures. The surgery and experimental procedures were approved by the Stony Brook University Animal Use Committee and followed the guidelines of the National Institutes of Health. We developed an experimental approach for the direct investigation of TC synapses in acute slice preparation of V1. To allow for light activation of TC afferents in V1, adeno-associated virus serotype 9 (AAV9) (Gu et al., 2012) containing the ChR2-GFP gene (Zhang et al., 2010) was delivered with a Nanoject pressure injector in the LGN of postnatal day 14 (P14) rats anesthetized with a mixture containing 100 mg/kg Ketamine, 0.7 mg/kg Acepromazine, and 10 mg/kg Xylazine. For all experiments, both male and female rodents were included in the study. The location of the injection site and the titration of the number of viral particles required for reliable and successful expression were analyzed using histological analysis of fixed tissue. For experiments investigating the layer-specific properties of TC inputs in rats, the coordinates of injection at P14 were 3.6 mm posterior from bregma, 3.05 mm lateral from midline, 3.8 mm below the pia. This resulted in positive expression of channelrhodopsin2 (ChR2)-GFP in the location expected for the LGN 14 d after surgery at P28. It should be noted that the position of the injection site at 14 d is 2–3 mm rostral to the location of V1, making it highly unlikely for the construct to leak in V1 during injection. Furthermore, no leak of the construct occurred in the cortical region above the injection site; therefore, nonspecific infection of corticocortical axons from other cortical areas cannot account for the ChR2-GFP-expressing axons in V1. The subtype of AAV used in this study did not show retrograde labeling of neuron somata in V1, indicating specific expression of the light-gated conductance in LGN terminal fields.

For experiments investigating the target cell-type specific properties of L4 neurons in mice, the construct was injected into the LGN of postnatal day (P) 15 mice anesthetized with a cocktail of

100 mg/kg ketamine and 10 mg/kg xylazine using a Nanoject pressure injection system ($50*10^{12}$ viral particles/nl; Wang et al 2013). The coordinates of injection were 2.0 mm posterior from bregma, 1.9 mm lateral from the midline, and 2.9 mm below the pia. This procedure resulted in expression of ChR2-GFP localized in the LGN following a 10 days incubation period. The construct did not leak into the cortical area above the injection site, so there was no aspecific expression of the construct in the structures above the LGN. The subtype of AAV was chosen for its preferred anterograde transport. To further confirm the lack of retrograde transport we quantified the possible presence of backfilled somata across the entire cortical mantle in each slice used for this study. None of the preparations showed backfilled somata in any layer of V1, similar to what we reported in our previous study (Wang et al, 2013).

Assessment of reliable expression. To assess the reliability of the levels of expression of the ChR2-GFP construct in the LGN and in LGN terminal fields in V1 across preparations, two cohorts of mice and rats were perfused transcardially with 4% paraformaldehyde in phosphate buffer 10 (mice) and 14 (rats) days after injection. The brain was dissected and postfixed in 30% sucrose solution. Slices (100 μm thick) from fixed brains were cut with a Vibroslicer (Leica VT1000). Coronal slices containing either LGN (to verify the location of the injection site) or V1 (100 μm) were visualized with confocal microscopy. The location, spread and intensity of the GFP signal was quantified using ImageJ. Once the most effective concentration was assessed (300 nl volume containing $50*10^{12}$ particles/nl), it was used throughout the study. In slices containing V1 the intensity profile of the GFP signal was quantified in regions of interest (ROIs) spanning the cortical mantle (ROI: 40 μm wide and extending from the pial surface to the border between layer 6 and the white matter). A calibration curve of the levels of GFP fluorescence across layers was calculated as the average ± standard deviation of the GFP intensity measured

in 15 slices from 6 animals (Figure 1C, green line: average; black lines: ± standard deviation). To determine the success of each injection, the profile of GFP expression was quantified for each acute slice used for patch-clamp recordings, and the intensity of the GFP signal of all subsequent preparations was compared against this curve. This allowed for comparisons of recordings obtained from slices with similar levels of ChR2 expression in the LGN terminal fields in V1. Recordings were excluded from the analysis if obtained from slices in which the GFP signal deviated more than one standard deviation from the calibration curve.

Electrophysiological Recordings. Animals were deeply anesthetized by placing them in a closed jar saturated with isofluorane vapors. They were then decapitated and the brain was dissected out to prepare acute coronal slices containing LGN or the monocular portion of V1 as described previously (Maffei et al., 2006). For experiments investigating layer specific differences of TC input and experiments investigating presynaptic $GABA_A$ receptors, rats were used fourteen days after injection of AAV9 containing the ChR2-GFP construct; mice were used ten days after injection. To verify the localization of the effectiveness of ChR2 expression in the injection site, coronal slices containing the LGN were also prepared from each brain. Before recording in V1, patch-clamp recordings were performed in LGN slices to verify sufficient levels of expression of the light-sensitive protein (Fig. 2.1A*;* 3.1B). To further test that action potentials in LGN neurons were driven by light pulses and not by synaptic activity, the experiments were repeated in the presence of 20 μM DNQX and 50 μM APV to block AMPA and NMDA receptors (Fig. 3.1B). After verification of successful injections, patch-clamp recordings were obtained from visually identified neurons in L4 and/or L6 of coronal slices containing monocular V1. Triple simultaneous recordings were obtained from visually identified L4 and L6 neurons to allow for direct comparison of TC-EPSC properties in L4 and L6 of the same slice. Different neuron

subtypes in L4 were identified visually.

Brief light pulses (1-2 ms) to activate the LGN terminal field (or LGN neurons in slices containing the LGN) were delivered using an LED blue optic fiber (470 nm) mounted on the fluorescence pathway of an upright microscope (Olympus BX51WI) through a 40X water-immersion objective. The intensity of the light was regulated with a power generator connected to the optic fiber (power: 0.1– 0.3mW/mm^2). Duration and frequency of light pulses were synchronized with electrophysiological data acquisition through the analog output of a Multi-Patch clamp amplifier (HEKA). The power of light stimulation for our LED fiber was measured with an optical power meter (Coherent Inc.) placed in the recording chamber. For each recorded neuron a minimum of 50 repetitions of light pulses were delivered at a frequency of 0.05 Hz. Offline, light-evoked TC-EPSCs were aligned at 10–90% of rise time, to obtain the average synaptic response for each neuron and allow quantification of the TC-EPSC.

Simultaneous triple patch-clamp recordings were obtained within L4 or L6 of slices from the same animal to test for differences in recurrent IC connectivity and TC responsiveness. The angle of slicing was adjusted to preserve the full extent of the neuronal processes in both L4 and L6 (Zarrinpar and Callaway, 2006). Patch clamp recordings were routinely performed 75–100 µm below the slice surface to ensure well preserved neuronal morphology and connectivity in both layers. Identification of connected pairs was as previously described (Maffei et al., 2004, 2006; Maffei and Turrigiano, 2008). While we did not intentionally target a specific L6 neuron type, the *post hoc* morphological reconstruction of our recorded neurons indicated that most, if not all, L6 neurons we recorded corresponded to L6 pyramidal neurons with apical dendrites extending to the superficial layers. These neurons are similar in morphology to those described by Bannister et al. (2002) as extending their axonal projections mainly in the infragranular

layers.

Light activation of LGN terminal fields were used to evoke TC-EPSCs onto cortical neurons (recorded in voltage-clamp mode) while the amplitude of recurrent EPSPs (recorded in current-clamp mode) was obtained for each triplet recorded. Recorded neurons in the LGN and in V1 were filled with biocytin, and their morphology and location were verified *post hoc* with immunohistochemical procedures.

Criteria to define L4 neuron responses as monosynaptic. TC-EPSCs were considered monosynaptic if their delay from stimulus onset was below 2.5 ms and did not show any additional peak on the decay phase of the postsynaptic current. A group of Pyr (17%) and FS (34%) neurons showed di-synaptic currents detected as additional peaks on the decay phase of the evoked response. The delay from stimulus onset of those later peaks was on average 11.4 ± 0.2 ms. As the theoretical reversal potential in our internal solution is -50 mV, even inhibitory di-synaptic events are detectable as inward currents on the decay phase of the evoked TC-EPSC. All recorded neurons showing di-synaptic responses were excluded from the analysis, therefore the number of samples reported in the manuscript indicates selectively neurons whose responses fit our definition of monosynaptic TC-EPSC. Non-stationary peak scaled noise analysis and analysis of release properties were performed on TC-EPSCs evoked with minimal light intensity to activate putative single axons. While minimal light intensity evoked TC-EPSCs with amplitude comparable to those evoked by focal laser stimulation (Cruikshank et al., 2010) and those evoked by minimal electrical stimulation in thalamocortical slices in the somatosensory cortex (Beierlein et al., 2003) onto both Pyr and FS neurons, in our preparations we did not observe failures. The absence of failures likely depends on the depolarization of terminals evoked by direct activation of the light-gated sodium conductance expressed by LGN axons.

Visual deprivation. Visual deprivation with monocular eyelid suture (MD) was started at P24 and maintained for 3 d. Briefly, the animals were anesthetized with a mixture of Ketamine (70 mg/kg) Xylazine (5 mg/kg), and Acepromazine (0.3 mg/kg). Once the animals were deeply anesthetized, the area surrounding one of the eyes was thoroughly cleaned with isopropanol and coated with lidocaine gel to provide local analgesia. The eye was moisturized with eye drops and 4 mattress sutures were placed using polyester suture thread (Ethicon 6-0). After the procedure the animals were allowed to recover on a heating pad and brought back to the animal facility only when fully alert. The experimentalist was blind to the eyelid suture and slice preparation.

Non-stationary noise analysis. Non stationary noise analysis (Sigworth, 1980; Traynelis and Jaramillo, 1998; Hartveit and Veruki, 2007) was applied to determine the single channel conductance and number of open channels of excitatory postsynaptic currents (TC-EPSCs). The analysis was performed on TC-EPSCs recorded at -70 mV in the presence of the NMDA receptor blocker APV (50 μM) to determine differences in the properties of the AMPA receptor mediated component of the TC-EPSC. For each neuron 10 light-evoked TC-EPSCs were averaged, and each individual trace was scaled to the mean. The variance of the TC-EPSCs during the decay phase was averaged into 1 ms bins, and plotted against the mean current. This plot was fitted to a polynomial equation $\sigma^2 = iI - (I^2 / N)$ to calculate unitary current (i_u) and number of open channels (N_o).

Analysis of release properties. Strontium chloride ($SrCl_2$) is known to produce delayed asynchronous release (Goda and Stevens, 1994) and has a long lifetime in the presynaptic terminal (Xu-Friedman, 2000). Bath application of $SrCl_2$ was shown to decrease the amplitude of an evoked response down to that driven by release at a single release site (Morishita and Alger, 1997; Bartley et al., 2008). The amplitude of a single release site-evoked response varies

depending on the presynaptic cell (Daw et al., 2009). The remaining desynchronized release sites produce synaptic events that can be detected in decay phase of the first evoked response (up to 200 ms from stimulus onset). In a set of experiments 10 mM $SrCl_2$/ 0 mM $CaCl_2$ was bath applied following the acquisition of a 10 min baseline TC-EPSC. The effect of $SrCl_2$ on the amplitude of the evoked TC-EPSC was quantified, and the number of subsequently activated release sites was inferred by assessing 180 the number of events detected across the 200 ms time window from the light stimulus.

Quantal analysis. To assess the site of action of $SrCl_2$, quantal analysis was performed on the first evoked response before and after application of $SrCl_2$ (Wang et al., 2012; Sola et al. 2004). A binomial model (Wernig, 1975) was fit to the data to calculate the probability of release (p) and number of release sites (n) from the average TC-EPSC amplitude and coefficient of variation (CV). Statistical comparisons of CVs before and after applications of $SrCl_2$ were also provided for each neuron type.

Post hoc neuron identification. After recording, slices were fixed in 4% paraformaldehyde for 1 week. After that, they were washed in PBS, permeabilized with 1% TritonX for 2 h, and then incubated overnight at 4°C in a solution containing Streptavidin-Alexa Fluor 594 1:2000 in PBS and 0.1% Triton X. After a final wash in PBS, slices were mounted with Fluoromount and imaged with a fluorescent microscope (Zeiss Axioskop). Only neurons with pyramidal morphology localized in L4 (Chapter II and III) and L6 (Chapter II) of the monocular portion of V1 were included in the analysis.

STDP Induction. In order to express STDP at TC synapses, pre- and postsynaptic activation were specifically timed in current clamp. Prior to STDP induction, a ten minute baseline was recorded. STDP was induced by delivering 10 2ms light pulses at 25 Hz. L4 neurons fired action potentials

by delivering 10 2 ms pulses of 700 pA. TC terminal fields were stimulated at 35 ms or 20 ms before L4 neuron activation; simultaneously with L4 neuron activation; or 10 ms or 35 ms after neuron activation. Following the STDP induction paradigm, TC-EPSC amplitude was measured for a minimum of 40 minutes.

Statistical analysis for electrophysiology data. Normality of data distributions was verified with the Kolmogorov–Smirnov test. Statistical significance was determined with two-tailed unpaired *t tests*. To test for differences across conditions, one-way ANOVAs were applied and followed by *post hoc* unpaired *t tests*. χ^2 for contingency, Pearson correction, was applied to test for significant differences in IC connection probability or in the proportion of TC-responsive neurons. Spearman rank-order correlation analysis was performed on the amplitude of TC-EPSCs onto a population of recurrently connected and non-recurrently connected neurons in L4 and L6; and to determine possible correlations of the magnitude of the effect of $SrCl_2$ on the first evoked TC EPSC with the baseline amplitude of the TC-EPSC. Where appropriate, data are presented as mean ± SE. For all statistical tests, *P* values < 0.05 were considered significant.

Solutions. Artificial cerebro-spinal fluid (ACSF) contained (in mM): 126 NaCl, 3 KCl, 2 $MgSO_4$, 1 $NaHPO_4$, 25 $NaHCO_3$, 2 $CaCl_2$, 14 Dextrose. The internal solution contained (in mM): 20 KCl, 100 K-Glu, 10 K-HEPES, 4 Mg-ATP, 0.3 Na-GTP, 10 Na-Phosphocreatine, and 0.4% Biocytin. The pH of the internal solution was adjusted to 7.35 with KOH, and the osmolarity was adjusted to 295 mOsm with sucrose. In all pharmacological experiments, drugs were bath-applied. In experiments designed to quantify the NMDA / AMPA ratio, 3 μM QX-314 (Tocris) was added to the internal solution. All other drugs were bath applied. For isolating AMPA and NMDA receptor mediated components 20 μM DNQX (Tocris) and 50 μM APV (Tocris) were applied sequentially and additively. To desynchronize release sites 10 mM $SrCl_2$ (Sigma-Aldrich) was

added to a $CaCl_2$ free ACSF following acquisition of a 10 minute baseline. The physiological properties of presynaptic $GABA_A$ receptors were tested with 1 mM muscimol (Tocris) and 10 μM diazepam (Tocris). $GABA_A$ receptors were blocked with 20 μM picrotoxin (Tocris).

Immunohistochemical detection of presynaptic $GABA_A$ Receptors. Fourteen days after surgery at P28, animals were anesthetized with 100 mg/kg ketamine, 0.7 mg/kg Acepromazine, and 10 mg/kg Xylazine and perfused intracardially with ice cold phostphate buffered saline (pH 7.2, PBS) followed by paraformaldehyde (4%, Electron Microscopy Sciences) in PBS. The brain was dissected, post-fixed for 24 hours in the same fixative and transferred to a 30% sucrose solution. Slices (100 μm thick) containing monocular V1 were sectioned using a freezing microtome, washed in PBS, and permeabilized for 1 hour in 0.4% Triton-X 100. Slices were then transferred into primary antibody solution containing mouse anti-VGlut2 (1:200, Synaptic Systems), rabbit anti-Gephyrin (1:200, Invitrogen), and 0.1% Trition-X 100 in PBS. After incubating 48 – 60 hours at 4°C, sections were washed in PBS and incubated in secondary antibody solution containing anti-rabbit TexasRed (1:500, GeneTex) and anti-mouse DyLight 405 (1:100, Jackson Laboratories) in PBS for 1 hour at room temperature. Stained sections were mounted on glass slides and coverslipped with Vectashield fluorescent mounting medium (Vecta Labs).

Imaging and Data Analysis of presynaptic $GABA_A$ Receptors. Tissue sections were imaged using an Olympus Fluoview FV-1000 confocal microscope. Lower magnification images to visualize the layers of V1 were taken using a 5X objective. To show colocalization of antibody markers, images of layer 4 were taken using a 60X objective; ImageJ was used for image analysis. Four slices were imaged per animal, and analysis was limited to a region of interest of 100x100 μm. To detect colocalization of secondary antibodies, the Colocalization Finder plugin (author: Christophe Laummonerie) was used to detect overlap of fluorescent signal, and analysis was

restricted to pixels with the maximum intensity (signal to noise ratio) using the correlation scatterplot. Next, the fluorescence profile of each colocalized puncta that was identified using the colocalization finder method was measured by drawing a line (6 μm) and plotting the signal intensity (arbitrary units, A.U.). Areas of colocalization of gephyrin and TC axons (GFP) were included in the analysis if the peak of fluorescent signal (at least 50% greater than background) plotted by area was the same ± 0.1 μm. The angle of the line was determined by the researcher for optimum signal to noise ratio. The ratio of cells with detectable fluorescent colocalization was computed using the total number of cells in the ROI.

Tissue preparation and immunogold labeling for electron microscopy. All EM staining procedures were performed by Dr. Alev Erisir at the University of Virginia, Charlottesville VA. Animals were deeply anesthetized with 100 mg/kg ketamine, 0.7 mg/kg Acepromazine, and 10 mg/kg Xylazine and perfused through the ascending aorta with 4% paraformaldehyde and 1% glutaraldehyde in 0.1 M phosphate buffer, pH 7.3. The brain was dissected and postfixed in the perfusion fixative overnight, then rinsed thoroughly in 0.1 M PB. A vibrotome was used to cut 40 μm thick slices of V1. Prior to embedding, slices were incubated in anti-GFP antibodies, and then a DAB staining protocol was used to label the GFP expressing TC terminals. Slices were were immersed in 4% uranyl acetate (Electron Microscopy Sciences), dissolved in anhydrous methanol for 24 h at 90°C, rinsed in methanol at 45°C, and infiltrated with resin (Electron Microscopy Sciences) for 48 h at 45°C. Monocular V1 was carefully dissected and sliced ultra-thin, picked up on mesh grids, and blocked in fetal goat serum for 10 minutes. Sections were then incubated in anti-$GABA_A$ alpha 4 primary antibody, followed by an appropriate secondary antiserum conjugated to 10 nm colloidal gold particles.